

Utah State University

DigitalCommons@USU

---

All Graduate Theses and Dissertations

Graduate Studies

---

5-2020

## Improvement of Ultraviolet Digital Image Correlation (UV-DIC) at Extreme Temperatures

Thinh Quang Thai  
*Utah State University*

Follow this and additional works at: <https://digitalcommons.usu.edu/etd>



Part of the [Mechanical Engineering Commons](#)

---

### Recommended Citation

Thai, Thinh Quang, "Improvement of Ultraviolet Digital Image Correlation (UV-DIC) at Extreme Temperatures" (2020). *All Graduate Theses and Dissertations*. 7770.  
<https://digitalcommons.usu.edu/etd/7770>

This Dissertation is brought to you for free and open access by the Graduate Studies at DigitalCommons@USU. It has been accepted for inclusion in All Graduate Theses and Dissertations by an authorized administrator of DigitalCommons@USU. For more information, please contact [digitalcommons@usu.edu](mailto:digitalcommons@usu.edu).



IMPROVEMENT OF ULTRAVIOLET DIGITAL IMAGE CORRELATION (UV-DIC)

AT EXTREME TEMPERATURES

by

Thinh Quang Thai

A dissertation submitted in partial fulfillment  
of the requirements for the degree

of

DOCTOR OF PHILOSOPHY

in

Mechanical Engineering

Approved:

---

Ryan B. Berke, Ph.D.  
Major Professor

---

Tadd T. Truscott, Ph.D.  
Committee Member

---

Barton L. Smith, Ph.D.  
Committee Member

---

Thomas H. Fronk, Ph.D.  
Committee Member

---

Marvin W. Halling, Ph.D.  
Committee Member

---

Richard S. Inouye, Ph.D.  
Vice Provost for Graduate Studies

UTAH STATE UNIVERSITY  
Logan, Utah

2020

Copyright © Think Quang Thai 2020

All Rights Reserved

## ABSTRACT

Improvement of Ultraviolet Digital Image Correlation (UV-DIC)

at Extreme Temperatures

by

Thinh Quang Thai, Doctor of Philosophy

Utah State University, 2020

Major Professor: Ryan B. Berke, Ph.D.

Department: Mechanical and Aerospace Engineering

For the purposes of designing mechanical structures in challenging environments such as extreme temperatures and vibration, it is essential to adopt non-contacting, full-field strain measurements. Non-contacting methods are preferable because, unlike strain gauges, they are less vulnerable to damage in extreme environments. Full-field measurements are preferable because, unlike point-based methods, they convey a greater sense of the overall thermo-mechanical environment. To meet these two requirements, Digital Image Correlation (DIC) is one of the most popular and versatile methods for non-contacting and full-field strain measurement. In brief, DIC is performed by recording images with a digital camera before and after deformation, from which full-field displacements are computed by correlating the relative deformation between the two images. In some high temperature applications like hot-fire testing and hypersonic flight, the images acquired from cameras tend to saturate due to light emitted from high temperature objects according to blackbody radiation. It is well known that the emitted

light is brighter at longer wavelengths (i.e. red and infrared) compared to shorter wavelengths (i.e. blue and ultraviolet (UV)). Therefore, a novel variation of DIC named UV-DIC was introduced to extend the temperature limit when performing DIC at extreme temperatures. Thanks to its shorter wavelengths when compared to other common wavelengths, especially blue light, UV-DIC is potentially the highest temperature DIC.

When performing high temperature DIC, it is required to maintain a good contrast of the acquired images throughout testing. One of the significant factors in determining contrast, particularly in quasi-static testing, is exposure time. This dissertation will examine the importance of exposure time on DIC measurement uncertainty, thereby giving a normalized metric which helps DIC users select an appropriate exposure time (likely to extend to other factors such as aperture and amplified gain) not only at the start of the test but during mid-test. In addition, the dissertation will investigate a novel phenomenon of speckle pattern inversion which is occasionally reported during high temperature DIC testing. Based on explanations of the physical mechanism, recommended solutions are introduced to evade the inversion. Furthermore, a method to help salvage data in cases of inversion is also presented. With all its contributions, this dissertation is expected to improve the capabilities of UV-DIC, thereby greatly improving strain measurements at extreme temperatures.

(121 pages)

## PUBLIC ABSTRACT

### Improvement of Ultraviolet Digital Image Correlation (UV-DIC) at Extreme Temperatures

Thinh Quang Thai

Extreme temperature has increasingly played an essential role in design and operation of various engineering applications including spacecraft re-entry, hypersonic flight, next-generation nuclear reactors, and hot-fire rocket testing. To protect instruments against the harsh environments, it is preferable to use non-contacting measurements when monitoring the integrity of those mechanical structures. Digital Image Correlation (DIC) is a popular method which uses digital cameras in order to track motion thanks to images acquired before and after deformation. Displacements and strains are plotted over a full-field region which is conducive to identify highly risky zones. At high temperature, objects emit light which interferes with image acquisition. It is known that the emitted light is considerably suppressed when images are taken at very short wavelengths such as ultraviolet (UV). This dissertation will investigate the importance of exposure time, which is a significant factor when determining the camera sensitivity, on the uncertainty of UV-DIC measurements. Through examining the exposure time, this dissertation is intended to give insights for users when performing DIC at high temperature in both pre-testing conditions and on-going testing. In addition, the dissertation will discuss a specific phenomenon of pattern inversion which is occasionally reported in high temperature DIC measurement. Under this phenomenon, due to differences in emissivity of refractory paint

and the background material, portions of the object which appear dark at room temperature instead appear bright at high temperature, and vice versa. The dissertation will explain the physical principle behind pattern inversion and introduce alternative solutions to evade the pattern inversion. With the aforementioned contributions, the dissertation is expected to improve the UV-DIC technique intensively and extensively.

To my parents and my older brother



## ACKNOWLEDGEMENTS

First and foremost, I would like to express my deepest gratitude to my advisor, Dr. Ryan Berke for his continual support, immense insights and fervent mentorship throughout this dissertation. Doctoral study is a grueling journey and he is an integral part of my accomplishment.

I would like to acknowledge the research funding from the Utah State University Office of Research and Graduate Studies and NASA's Marshall Space Flight Center.

My special appreciation goes to all committee members, especially Dr. Smith and Dr. Truscott for their innovative insights on my first two papers. I also would like to thank the MAE department staff for paperwork assistance. Many thanks go to Terry Zollinger for machining specimens.

Next, I would like to thank all my fellow labmates. It is my great honor to be a part of the large group in order to have productive meetings, helpful discussion and thorough revision on my papers from all of them.

A profound gratitude is extended to Dino Celli, an intern at Air Force Research Laboratory (AFRL) for assistance in securing thermocouples on non-weldable specimens. The idea marked a turning point in my research.

Lastly, I am deeply indebted to my dearest family: my parents and my older brother in Vietnam for their mental support and ceaseless encouragement. All of them are permanently influential persons in my life.

Thinh Quang Thai

## CONTENTS

	Page
ABSTRACT.....	iii
PUBLIC ABSTRACT .....	v
ACKNOWLEDGEMENTS .....	viii
LIST OF TABLES .....	xi
LIST OF FIGURES .....	xii
CHAPTER	
1 INTRODUCTION .....	1
1.1 Motivation.....	1
1.2 Research Background .....	3
1.2.1 Brief Overview of DIC .....	3
1.2.2 High Temperature DIC Measurement .....	8
1.2.3 Literature Gaps.....	9
1.3 Objectives .....	12
1.4 Dissertation Outline .....	13
1.5 References.....	14
2 IMPORTANCE OF EXPOSURE TIME ON DIC MEASUREMENT UNCERTAINTY AT EXTREME TEMPERATURES .....	19
2.1 Prologue .....	19
2.2 Abstract .....	19
2.3 Introduction.....	20
2.4 Methods.....	23
2.5 Results.....	31
2.6 Discussion .....	39
2.7 Conclusions.....	44
2.8 Acknowledgements.....	45
2.9 References.....	45
3 CHANGE OF EXPOSURE TIME MID-TEST IN HIGH TEMPERATURE DIC MEASUREMENT.....	48
3.1 Prologue .....	48
3.2 Abstract .....	48
3.3 Introduction.....	49
3.4 Methods.....	51
3.5 Results.....	58

3.6	Discussion .....	69
3.7	Conclusions.....	73
3.8	Acknowledgements.....	74
3.9	References.....	74
4	SPECKLE PATTERN INVERSION IN HIGH TEMPERATURE DIC MEASUREMENT.....	76
4.1	Prologue .....	76
4.2	Abstract.....	76
4.3	Introduction.....	77
4.4	Methods.....	79
4.5	Results.....	84
4.6	Discussion.....	88
4.7	Conclusions.....	93
4.8	Acknowledgements.....	94
4.9	References.....	94
5	DISCUSSION.....	97
6	CONCLUSIONS.....	99
	CURRICULUM VITAE.....	102

## LIST OF TABLES

Table		Page
1.1	Lighting manipulation methods.....	9
2.1	Mean and variance of displacement and strain field .....	34
3.1	Summary of image pairs used in correlations .....	55
3.2	Raw data of $\Delta$ calculation at RT and 1600°C.....	57
4.1	Test matrix with an explanation of light coming to the camera sensor.....	82
5.1	$\Delta$ calculation of RT, 1300°C, 1450°C and 1600°C at multiple exposure times .....	98

## LIST OF FIGURES

Figure		Page
1.1	Schematic illustration of reference subset and deformed subset .....	5
2.1	Schematic of square gauge region test specimen (left), a photo of specimens with speckled gauge region (middle) and a close-up of the speckle pattern (right) .....	24
2.2	Schematic of the 2-thermocouple placement (left) and temperature relationship of the two thermocouples (right).....	25
2.3	The temperature map from FLIR IR camera at 1600°C, data bar shows temperature (°C) map inside dashed rectangle .....	26
2.4	Photograph of the fixture with experimental setup.....	27
2.5	Transmissivity of UV camera and related optics .....	28
2.6	Mean u displacement at room temperature, compared between case 1 (no applied motion) and case 2 (non-zero rigid motion) with the Gleeble on or off as indicated. Each uncertainty band is the 95% confidence interval .....	32
2.7	Mean strain $\epsilon_{xx}$ at room temperature, compared between case 1 (no applied motion) and case 2 (non-zero rigid motion) with the Gleeble on or off as indicated. Each uncertainty band is the 95% confidence interval .....	33
2.8	Raw speckle images of specimen surface at different temperatures (increasing from left to right) and exposure times (increasing from top to bottom) respectively, and histograms of the greyscale values corresponding to the images. Images which are too saturated to perform DIC are indicated with a red cross .....	35
2.9	Comparison of $\epsilon_{xx}$ at room temperature and (a) 1300°C, (b) 1450°C and (c) 1600°C when there is no applied displacement.....	36
2.10	(a) The thermal strain $\epsilon_{xx}$ (pixel/pixel) map at 1600°C obtained with Vic-2D from comparing a reference image at room temperature and a deformed image at 1600°C, (b) The $\epsilon_{xx}$ (pixel/pixel) strain map at 1600°C obtained with Vic-2D from two images with no applied temperature or displacement. All images were recorded at an exposure time of 20,000 $\mu$ s .....	37
2.11	Thermal expansion strain at multiple temperatures over the gauge length	38
2.12	Example of 90% confidence interval approach, using room temperature data at exposure time of a) 2,500 $\mu$ s, b) 20,000 $\mu$ s and c) 61,000 $\mu$ s .....	41

2.13	Relationship between exposure time and $\Delta$ at different temperatures.....	42
2.14	Strain $\epsilon_{xx}$ vs $\Delta$ at (a) RT, (b) 1300°C, (c) 1450°C, and (d) 1600°C when there is no applied displacement.....	43
3.1	(a) A specimen schematic, (b) a photograph of testing specimen, (c) a magnification of speckle pattern, (d) experimental setup of UV optics imaging system.....	52
3.2	The thermal map at 1600°C taken by FLIR IR camera, vertical color bar displays temperature (°C) scale inside white dashed rectangle.....	54
3.3	Example of 90% confidence interval approach with respective speckle pattern, using room temperature data at exposure time of 20,000 $\mu$ s.....	56
3.4	Image pairs which successfully correlated at room temperature.....	58
3.5	95% uncertainty band when changing exposure time at room temperature illustrated by (a) u displacement and (b) strain $\epsilon_{xx}$ .....	60
3.6	Influence of changing exposure time on uncertainty band at RT illustrated via $\Delta$ .....	61
3.7	Relationship of 95% uncertainty band and $\Delta$ variation at various exposure times.....	62
3.8	Investigation of slope with respect to $\Delta$ of reference images.....	62
3.9	Image pairs which successfully correlated at 1600°C.....	63
3.10	95% uncertainty band when changing exposure time at 1600°C illustrated by (a) u displacement and (b) strain $\epsilon_{xx}$ .....	65
3.11	Influence of changing exposure time on uncertainty band at 1600°C illustrated via $\Delta$ .....	66
3.12	Image pairs which successfully correlated at RT vs 1600°C.....	67
3.13	95% uncertainty band when changing exposure time during mid test illustrated by (a) u displacement and (b) strain $\epsilon_{xx}$ .....	68
3.14	Non-uniform thermal strain from correlation of 45,000 $\mu$ s at room temperature against 30,000 $\mu$ s at 1600°C.....	69
3.15	Correlation of image pairs at RT vs 1600°C when investigating via (a) $Z_1$ , (b) $Z_2$ and (c) $\Delta$ .....	72
4.1	(a) Graphite specimen used in the experiments including a magnification of the speckle region (right), (b) a photograph of the experimental setup and related optics and (c) a photograph of the Gleeble 1500D system.....	81
4.2	Flowchart to map Test A and Test B.....	84

4.3	Speckle images recorded at low temperature and high temperature when there is no UV filter and a UV filter, respectively. For legibility, the images from test B in this figure have been artificially brightened by multiplying all pixel values by 2, but image B.4 still remains uniformly dark. No artificial brightening was used in DIC calculations.....	85
4.4	Graphical depiction of the subtraction-based method for excluding inversion at high temperature when a UV bandpass filter has not been used .....	87
4.5	Thermal strain map from Vic-2D of Test A (a) and Test B (b) along with its differences (c).....	88
4.6	Reflected and emitted speckle patterns at low and high temperature under small depth of field. The lens is initially focused based on the reflected pattern (top row), and re-focused based on the emitted pattern (bottom row) .....	92
4.7	Reflected and emitted speckle patterns at low and high temperature under large depth of field. All images are captured in a fixed focal length. Refocus of the lens is not necessary since the difference of focal length is negligible when compared to the large depth of field.....	93

# CHAPTER 1

## INTRODUCTION

### **1.1. Motivation**

In recent years, extreme temperature has played an important role in the design and operation of various engineering applications including nuclear reactors [1], spacecraft reentry [2], gas turbines [3] and hot-fire rocket engine testing [4,5]. A host of highly promising materials have been introduced and developed for those increasing demands. For example, Carbon-Carbon (C-C) and Ceramic Matrix Composite (CMC) materials are used for high temperature uncooled nozzle extensions on liquid rocket engines [6]. Nevertheless, information and understanding in terms of mechanical performance of those candidate materials remains limited. This places the integrity of the mechanical structures in jeopardy when working under combined thermo-mechanical environments. Therefore, in order to improve the safety, reliability and performance of high temperature mechanical structures, it is essential to get a better understanding regarding thermo-mechanical behaviors of candidate materials.

Since these extreme environments include conditions like high temperature or vibration, it is preferable to adopt non-contacting and full field strain measurement methods rather than contacting or point-wise techniques. Digital Image Correlation (DIC) [7] is a versatile method that is popular in the scientific mechanics community to obtain full-field strains. In brief, DIC uses high resolution cameras to capture images before and after deformation. A computer program is then employed to compare the captured images, thereby exporting the full-field displacement map. Strains are then computed by taking



derivatives of displacement. Based on its working principles, DIC has a host of advantages [8] when comparing to other traditional techniques like strain gages including (1) it is non-contacting thus can survive the full duration of the test provided a sufficient standoff distance is supplied [9], (2) it is able to collect full field data and (3) it can be applied in a broad range of length scales from nanoscale [10] to meter-scale [11] as long as appropriate cameras and lenses are used.

At high temperatures, objects emit light in accordance with the black body radiation of Planck's law. Therefore, images acquired from cameras at high temperature tend to saturate due to the increased intensity of light coming to the camera sensor. It is known that the objects emit more light at longer wavelengths (i.e. red and infrared) in comparison with shorter wavelengths (i.e. blue and ultraviolet) [12]. For this reason, many researchers [13,14] implemented a low-wavelength optical bandpass filter (i.e. blue bandpass filter) to screen out the brightest glowing. In this work, we use ultraviolet (UV) optics to extend the temperature limit even further. Thanks to its shorter wavelength when compared to blue light, UV-DIC has been demonstrated for its superior capability in restricting the oversaturation in high temperature DIC measurement. Specifically, in Reference [15], blue-filtered DIC was saturated at 900°C whereas under the same camera settings UV-DIC remained non-saturated to at least 1125°C. UV-DIC has since been demonstrated to at least 1600°C [16,17] but its upper temperature limit remains unknown.

Given the high potential of UV-DIC, the overall objective of this dissertation is to develop a comprehensive and robust technique which can perform DIC at extreme

temperatures based on UV-DIC. The outcomes of this dissertation are expected to enhance the implementation of UV-DIC.

## **1.2. Research Background**

### **1.2.1. Brief Overview of DIC**

Digital Image Correlation (DIC) is one of the most popular and versatile methods in the scientific mechanics community due to its simplicity of experimental setup and its capability to perform full-field non-contact measurements. The technique was first introduced by Peters and Ranson [18] in 1982. In that work, from the principle of tracking of speckle images, they were able to produce a displacement and strain map. Michael Sutton, another member of their group [19], improved DIC to obtain the full-field planar displacement of a cantilever beam subjected to an end load. Throughout the 1980's, additional research papers were published by their group as improvements of the DIC method [20,21]. DIC can be performed either in 2D using a single camera or in 3D using multiple cameras.

In principle, DIC requires three fundamental steps so that a meaningful measurement is performed, particularly (1) sample preparation, (2) acquiring images during loading and (3) analyzing the images using a correlation algorithm [22].

For the first step (sample preparation), the minimum requirement is to create a random speckle pattern on the sample surface if there is no inherent speckle. Generally, a good speckle pattern has features of high contrast, randomness, isotropy and stability [23]. In order to meet these requirements, various assessment methods of speckle pattern quality have been introduced and developed [24,25]. In practice, there are many ways to make a

good speckle pattern depending on desired length scales. Such methods include airbrush spraying [26], lithography [27], focused ion beam [28] and spin coating [29].

For the second step (image acquisition during loading), in 2D DIC the camera sensor is required to be parallel to the flat surface of a specimen. This alleviates any out of plane displacement. If the sensor is not parallel, it makes magnification non-uniform, resulting in artificial in-plane deformation. Also, geometric distortion should be mitigated, especially in high-resolution imaging systems, because it is likely to interfere with correlation in image matching. In an effort to remove optical distortion, Yoneyama et al. [30] calculated a correction coefficient from displacement distribution in rigid motion test.

For the third step (analyzing images with a correlation algorithm), DIC employs a collection of pixel values called a subset to track the motion of points from the reference image to the deformed images. The subset is chosen because it includes a wide distribution of greyscale levels which gives more information in searching for its position in the deformed image. In other words, a subset has a unique signature to differentiate from other subsets in a deformed image.

Figure 1.1 shows the displacement mapping in 2D-DIC between a reference subset and a deformed subset. The square reference subset has a size of  $(2M+1) \times (2M+1)$  pixels and is centered at point  $A(x_0, y_0)$ . Relative to the center of the reference subset, the center of the deformed subset is displaced in the  $x$  and  $y$  directions by  $u$  and  $v$ , respectively resulting in the coordinates of point  $A'(x'_0, y'_0)$ . Relative to point  $A$ , a point  $B(x, y)$  in the reference subset has coordinates  $\Delta x$  and  $\Delta y$  compared to the center of the reference subset. Assuming continuity of the solid object, a set of neighboring points in a reference subset

remains as neighboring points in the deformed subset. Therefore, point B in the reference subset is mapped to point B'(x', y') in the deformed subset.

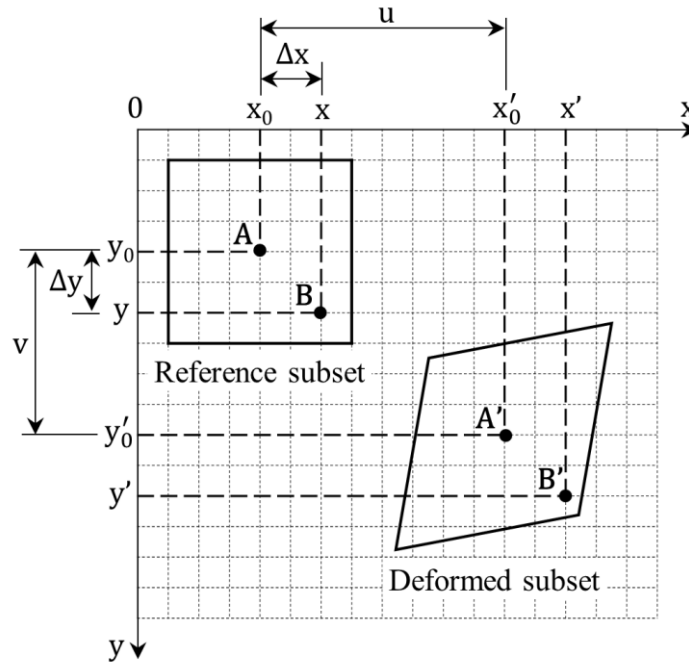


Figure 1.1. Schematic illustration of reference subset and deformed subset

The displacement mapping function is given as [31]:

$$\begin{aligned} x' &= x_0 + \Delta x + u + u_x \Delta x + u_y \Delta y \\ y' &= y_0 + \Delta y + v + v_x \Delta x + v_y \Delta y \end{aligned} \quad (1.1)$$

where  $u_x = \partial u / \partial x$ ,  $u_y = \partial u / \partial y$ ,  $v_x = \partial v / \partial x$ ,  $v_y = \partial v / \partial y$  are the displacement gradients. The terms  $(x_0 + \Delta x + u)$  and  $(y_0 + \Delta y + v)$  represent translation while  $(u_x \Delta x + u_y \Delta y)$  and  $(v_x \Delta x + v_y \Delta y)$  account for normal strain, shear strain, and rotation.

To compare between the reference subset and the deformed subset, it is required to introduce a correlation criterion. Let  $f(x, y)$  and  $g(x', y')$  characterize the distribution of grey intensity of the reference and deformed subsets, respectively. The three most commonly

used correlation functions are based on the method of sum of squared differences, as follows: [32]

**1/ Sum of squared differences (SSD):**

$$C_{SSD}(\vec{p}) = \sum_{i=-M}^M \sum_{i'=-M}^M [f(x_i, y_i) - g(x'_i, y'_i)]^2 \quad (1.2)$$

**2/ Normalized sum of squared differences (NSSD):**

$$C_{NSSD}(\vec{p}) = \sum_{i=-M}^M \sum_{i'=-M}^M \left[ \frac{f(x_i, y_i)}{\bar{f}} - \frac{g(x'_i, y'_i)}{\bar{g}} \right]^2 \quad (1.3)$$

where

$$\bar{f} = \sqrt{\sum_{i=-M}^M \sum_{i'=-M}^M [f(x_i, y_i)]^2} \quad (1.4)$$

$$\bar{g} = \sqrt{\sum_{i=-M}^M \sum_{i'=-M}^M [g(x'_i, y'_i)]^2}$$

**3/ Zero-normalized sum of squared differences (ZNSSD):**

$$C_{ZNSSD}(\vec{p}) = \sum_{i=-M}^M \sum_{i'=-M}^M \left[ \frac{f(x_i, y_i) - f_m}{\Delta f} - \frac{g(x'_i, y'_i) - g_m}{\Delta g} \right]^2 \quad (1.5)$$

where

$$f_m = \frac{1}{(2M+1)^2} \sum_{i=-M}^M \sum_{i'=-M}^M f(x_i, y_i) \quad (1.6)$$

$$g_m = \frac{1}{(2M+1)^2} \sum_{i=-M}^M \sum_{i'=-M}^M g(x'_i, y'_i)$$

$$\Delta f = \sqrt{\sum_{i=-M}^M \sum_{i=-M}^M [f(x_i, y_i) - f_m]^2}$$

$$\Delta g = \sqrt{\sum_{i=-M}^M \sum_{i=-M}^M [g(x'_i, y'_i) - g_m]^2}$$
(1.7)

It should be noted that the SSD correlation criterion is sensitive to fluctuations in lighting. The NSSD criterion is insensitive to linear scaling in lighting (for example, changes in camera sensitivity) but remains sensitive to offsets in lighting (for example, additional light sources). The ZNSSD criterion is insensitive to both linear scaling and offsets in lighting.

Taking into account the shape change of subsets during deformation, the correlation function turns to a nonlinear function with respect to the mapping parameters vector  $\vec{p} = (u, u_x, u_y, v, v_x, v_y)^T$ . In order to find solution of six parameters vector  $\vec{p}$ , it is common to use Newton-Raphson method which is called Iterative Spatial Domain Cross-Correlation Algorithm. The solution can be written as:

$$\vec{p} = \vec{p}_0 - \frac{\nabla C(\vec{p}_0)}{\nabla \nabla C(\vec{p}_0)}$$
(1.8)

where  $\vec{p}_0$  is the initial guess,  $\vec{p}$  is the next solution in the iteration,  $\nabla C(\vec{p}_0)$  is the first-order gradient of the correlation function,  $\nabla \nabla C(\vec{p}_0)$  is the second-order gradient of the correlation function, also known as the Hessian matrix [33].

### 1.2.2. High Temperature DIC Measurement

Theoretically, DIC is able to work at any temperature as long as the acquired images are still in good contrast. Nonetheless, there are three major challenges that necessarily demand to be tackled [34]:

(1) A speckle pattern must be stable and keep consistent contrast during heating. Particularly, the speckle must not flake off or discolor at high temperatures. In order to circumvent this challenge, some solutions were suggested such as refractory coatings [35], cobalt oxide [36] or sandblasting [37]. In this work, a refractory paint which is rated to 1760°C was used.

(2) Any optical distortion due to thermal turbulence and heat haze between camera and specimen need to be minimized. In order to tackle this issue, Novak and Zok [38] suggested using an air knife to blow off the heat haze. In this work, specimens were tested in a vacuum chamber, thus removing any warping due to variation of the refraction index of air.

(3) The emitted light from specimen due to black body radiation of Planck's law needs to be suppressed. The intensity of emitted light is more significant at higher temperatures and deteriorates the speckle contrast. The emitted light is also known to be brighter at longer wavelengths. Some researchers suggest using blue light illumination and a blue bandpass filter to screen out the brightest glow [39,40], but eventually the glow in the range of blue wavelengths becomes bright as well. More recently, Berke and Lambros [15] demonstrated that UV optics, which operates at an even shorter wavelength than blue, can potentially extend the temperature range of DIC even further. Their method is

potentially the highest-temperature DIC capability, which enables recording more information of heterogeneous material behavior at extreme temperatures. Thus, UV-DIC was used as optical imaging in this work.

### 1.2.3. Literature Gaps

In order to improve UV-DIC, the first step is to investigate the camera settings at the start of the test. In DIC, it is instrumental for images to have good contrast [41], especially when performing DIC at high temperature. Contrast can be improved by manipulating the light sensitivity of the cameras. There are five main ways to control the light [16], but each comes with its own drawbacks as summarized in Table 1.1.

Table 1.1. Lighting manipulation methods

Lighting Method	Drawbacks
(1) Use a brighter light source	<ul style="list-style-type: none"> <li>• Costs money to buy new equipment</li> <li>• Safety concerns (especially lasers or UV)</li> </ul>
(2) Increase exposure time on camera	<ul style="list-style-type: none"> <li>• More prone to motion blur</li> </ul>
(3) Increase aperture on lens	<ul style="list-style-type: none"> <li>• Reduced depth of field</li> </ul>
(4) Increase gain on camera	<ul style="list-style-type: none"> <li>• Amplify noise along with signal</li> </ul>
(5) Post-process dark images	<ul style="list-style-type: none"> <li>• Very easy to corrupt measurement</li> </ul>

Assuming (i) that one uses the brightest lights that they have safely available, and (ii) that loading is sufficiently slow such that motion blur is negligible, exposure time is the easiest method to manipulate the light without introducing significant errors. Exposure



time can be varied digitally via a computer user interface without disrupting the lens, whereas apertures must be physically adjusted by manually twisting the lens, thus displacing optical alignment while also refocusing the lens. Gain and post-processing techniques can also be varied digitally, but should be generally avoided unless small apertures and exposure times are critical to obtaining a meaningful measurement. For these reasons, the initial objective of this dissertation is to investigate the influence of exposure time on uncertainty of DIC measurement.

Moreover, exposure time is a dimensional unit which varies from camera to camera. Accordingly, in order to apply recommendations about exposure time universally to any camera, it is helpful to develop a normalized metric. My first published paper in *Experimental Techniques* (presented in Chapter 2) has solved that challenge. In literature, other authors have attempted to address this topic, yet their solutions are generally cumbersome when applied in practice. Wang et al. and Ke et al. [42–44] introduced a robust and thorough framework to ensure sufficient contrast which is considerably beneficial to readers who are greatly interested in designing a DIC code, but is cumbersome and time-consuming in practice in comparison with my metric. More simply, P. Reu [45,46] suggested that given “typical” dark and bright speckles and he recommended the difference between them should be at least 50 counts. However, he did not define explicitly what a “typical” dark and bright speckle was. For this reason, my paper in Chapter 2 developed a metric based on Reu’s recommendation which is simple, quick and easy to apply. In short, I propose that the metric called Delta ( $\Delta$ ) which defines dark and bright speckles by computing the span of the median 90% of data in the greyscale histogram. If  $\Delta > 50$  and

the upper threshold of the span does not equal 255 for an 8-bit monochromatic camera, it is a good indicator to let DIC users know that they had good contrast images.

The metric from the first paper presented an easy, quick and reliable method to assess the contrast of images. Consequently, this gives DIC users a reference point to choose an appropriate exposure time prior to testing. In some cases, objects at high temperature may emit more light than anticipated at the beginning of the test. Accordingly, holding exposure time fixed throughout the test may be unfeasible and can lead to data being completely lost. To the best of my knowledge, most research investigating the importance of camera configurations mainly emphasizes pre-testing conditions or doing some post-processing. However, by changing exposure time mid-test, one can potentially salvage data that would otherwise be lost due to over-exposure of the camera. My second paper published in *Measurement Science and Technology* (presented in Chapter 3) examined whether exposure time can be changed during mid-test, what conditions are necessary and its effects on DIC measurement uncertainty. Suggestions were introduced regarding evaluation of images at room temperature and then extrapolated to exposure at extreme temperature, thus giving a comprehensive picture about setting exposure time not only prior to testing but modification during the test if needed. That paper is believed to be the first research to focus on the change of camera settings (in this case, exposure time) during a DIC test.

Speckle pattern inversion is an interesting phenomenon which is occasionally reported when performing DIC at high temperature. One of primary factors contributing to this phenomenon is the difference in emissivity between the dark and light materials of the

speckle pattern. In particular, all objects at high temperature emit light according to black body radiation. In some cases, the background emits more light than the speckle leading to an image which is inverted when compared to the same speckle pattern at room temperature. Correlations are unable to be completed if there exist substantial differences of the speckle pattern between room temperature and high temperature. The paper presented in Chapter 4 introduces an optical method using the UV bandpass filter to eliminate the speckle inversion at high temperature DIC testing. Unlike other research using the post-processing like grey level corrections to eliminate inversion digitally [47], my technique is based on the optical principles to evade or at least postpone inversion physically. Furthermore, that paper presents a subtraction method to salvage data from inverted images in some cases where DIC users did not follow my initial recommendations.

### **1.3. Objectives**

The primary objectives of this dissertation are as follows:

1. Investigate the influence of exposure time on DIC measurement uncertainty, thereby giving a normalized metric to let DIC users know how to choose an appropriate camera setting prior to testing. The metric is likely to apply to any cameras thus having a wide range of applications.
2. Examine the conditions which exposure time can be changed during mid test and its influence on DIC uncertainty. Thanks to that, a comprehensive recommendation is given to help DIC users set a suitable exposure time not only at the start of the test but during mid test.

3. Investigate the physical mechanism behind speckle pattern inversion, and develop strategies to mitigate it. Thereby, we introduce a method to avoid inversion when performing DIC at high temperature. Additionally, we present a post-processing technique to help DIC users remove inversion from inverted images.

#### **1.4. Dissertation Outline**

The dissertation is organized in multi-paper format. The dissertation has total of six chapters including this Introduction chapter. Chapter 2 through Chapter 4 refer to individual papers which were published or to be submitted to peer-reviewed scientific journals. References are placed at the end of each chapter. Here is the brief summary of each chapter:

- Chapter 1 provides the overview of the dissertation including motivation, research background, objectives and this outline.
- Chapter 2 is a full-length paper which was published in *Experimental Techniques*. The paper presents the importance of exposure time when performing DIC at extreme temperatures.
- Chapter 3 is also a full-length paper which was published in *Measurement Science and Technology*. The paper is a continuation of the Chapter 2 paper and discusses the change of exposure time mid-test in high temperature DIC measurement.
- Chapter 4 is another full-length paper which is in preparation to be submitted to a peer-reviewed journal. That paper focuses on the explanation of speckle pattern inversion and introduces an optical method by using the UV bandpass filter to evade the inversion of speckle pattern in high temperature DIC measurement.

- Chapter 5 presents further discussion about relationship of  $\Delta$  with respect to exposure time and temperature.
- Chapter 6 is the conclusion which summarizes the contributions of the dissertation and also gives some future works.

### 1.5. References

- [1] Abdou, M. A., Gierszewski, P. J., Tillack, M. S., Nakagawa, M., Reimann, J., Sze, D. K., Bartlit, J., Grover, J., R. Puigh, and McGrath, R. T., 1987, “Technical Issues and Requirements of Experiments and Facilities for Fusion Nuclear Technology,” *Nucl. Fusion*, **27**(4), p. 619.
- [2] Duda, P., and Nakamura, T., 2017, “Identification of the Transient Temperature and Stress Distribution in an Atmospheric Reentry Capsule Assuming Temperature-Dependent Material Properties,” *Aerosp. Sci. Technol.*, **67**, pp. 265–272.
- [3] Berg, R. A., Tan, C. S., Ding, Z., Laskowski, G., Palafox, P., and Miorini, R., 2018, “Experimental and Analytical Assessment of Cavity Modes in a Gas Turbine Wheelspace,” *J. Eng. Gas Turbines Power*, **140**(6), pp. 062502-062502–11.
- [4] Gradl, P. R., and Valentine, P. G., 2017, “Carbon-Carbon Nozzle Extension Development in Support of In-Space and Upper-Stage Liquid Rocket Engines,” *53rd Annual AIAA/SAE/ASEE Joint Propulsion Conference 2017*, Atlanta, GA, United States.
- [5] Valentine, P. G., and Gradl, P. R., 2019, “Extreme-Temperature Carbon- and Ceramic-Matrix Composite Nozzle Extensions for Liquid Rocket Engines,” *70th International Astronautical Congress*, Washington, DC, United States.
- [6] Schmidt, S., Beyer, S., Knabe, H., Immich, H., Meistring, R., and Gessler, A., 2004, “Advanced Ceramic Matrix Composite Materials for Current and Future Propulsion Technology Applications,” *Acta Astronaut.*, **55**(3), pp. 409–420.
- [7] Sutton, M. A., Orteu, J. J., and Schreier, H. W., 2009, *Image Correlation for Shape, Motion and Deformation Measurements: Basic Concepts, Theory and Applications*, Springer US.
- [8] Gradl, P. R., 2016, “Digital Image Correlation Techniques Applied to Large Scale Rocket Engine Testing,” *AIAA Propulsion and Power 2016 Conference*, Salt Lake City, UT, United States.

- [9] Hansen, R. S., Bird, T. J., Voie, R., Burn, K. Z., and Berke, R. B., 2019, "A High Magnification UV Lens for High Temperature Optical Strain Measurements," *Rev. Sci. Instrum.*, **90**(4), p. 045117.
- [10] Wang, X., Pan, Z., Fan, F., Wang, J., Liu, Y., Mao, S. X., Zhu, T., and Xia, S., 2015, "Nanoscale Deformation Analysis with High-Resolution Transmission Electron Microscopy and Digital Image Correlation," *J. Appl. Mech.*, **82**(12), pp. 121001-121001–9.
- [11] Rizo-Patron, S., and Sirohi, J., 2017, "Operational Modal Analysis of a Helicopter Rotor Blade Using Digital Image Correlation," *Exp. Mech.*, **57**(3), pp. 367–375.
- [12] Pan, B., Wu, D., Wang, Z., and Xia, Y., 2011, "High-Temperature Digital Image Correlation Method for Full-Field Deformation Measurement at 1200 °C," *Meas. Sci. Technol.*, **22**(1), p. 015701.
- [13] Grant, B. M. B., Stone, H. J., Withers, P. J., and Preuss, M., 2009, "High-Temperature Strain Field Measurement Using Digital Image Correlation," *J. Strain Anal. Eng. Des.*, **44**(4), pp. 263–271.
- [14] Wang, S., Yao, X. F., Su, Y. Q., and Ma, Y. J., 2015, "High Temperature Image Correction in DIC Measurement Due to Thermal Radiation," *Meas. Sci. Technol.*, **26**(9), p. 095006.
- [15] Berke, R. B., and Lambros, J., 2014, "Ultraviolet Digital Image Correlation (UV-DIC) for High Temperature Applications," *Rev. Sci. Instrum.*, **85**(4), p. 045121.
- [16] Thai, T. Q., Hansen, R. S., Smith, A. J., Lambros, J., and Berke, R. B., 2019, "Importance of Exposure Time on DIC Measurement Uncertainty at Extreme Temperatures," *Exp. Tech.*, **43**(3), pp. 261–271.
- [17] Thai, T. Q., Smith, A. J., Rowley, R. J., Gradl, P. R., and Berke, R. B., 2020, "Change of Exposure Time Mid-Test in High Temperature DIC Measurement," *Meas. Sci. Technol.*
- [18] Peters, W. H., and Ranson, W. F., 1982, "Digital Imaging Techniques in Experimental Stress Analysis," *Opt. Eng.*, **21**(3), p. 213427.
- [19] Sutton, M., Wolters, W., Peters, W., Ranson, W., and McNeill, S., 1983, "Determination of Displacements Using an Improved Digital Correlation Method," *Image Vis. Comput.*, **1**(3), pp. 133–139.
- [20] Sutton, M., Mingqi, C., Peters, W., Chao, Y., and McNeill, S., 1986, "Application of an Optimized Digital Correlation Method to Planar Deformation Analysis," *Image Vis. Comput.*, **4**(3), pp. 143–150.

- [21] Peters, W. H., Sutton, M. A., Ranson, W. F., Poplin, W. P., and Walker, D. M., 1989, "Whole-Field Experimental Displacement Analysis of Composite Cylinders," *Exp. Mech.*, **29**(1), pp. 58–62.
- [22] Pan, B., 2018, "Digital Image Correlation for Surface Deformation Measurement: Historical Developments, Recent Advances and Future Goals," *Meas. Sci. Technol.*, **29**(8), p. 082001.
- [23] Dong, Y. L., and Pan, B., 2017, "A Review of Speckle Pattern Fabrication and Assessment for Digital Image Correlation," *Exp. Mech.*, **57**(8), pp. 1161–1181.
- [24] Pan, B., Lu, Z., and Xie, H., 2010, "Mean Intensity Gradient: An Effective Global Parameter for Quality Assessment of the Speckle Patterns Used in Digital Image Correlation," *Opt. Lasers Eng.*, **48**(4), pp. 469–477.
- [25] Hua, T., Xie, H., Wang, S., Hu, Z., Chen, P., and Zhang, Q., 2011, "Evaluation of the Quality of a Speckle Pattern in the Digital Image Correlation Method by Mean Subset Fluctuation," *Opt. Laser Technol.*, **43**(1), pp. 9–13.
- [26] Hu, Z., Xu, T., Luo, H., Gan, R. Z., and Lu, H., 2016, "Measurement of Thickness and Profile of a Transparent Material Using Fluorescent Stereo Microscopy," *Opt. Express*, **24**(26), pp. 29822–29829.
- [27] Scrivens, W. A., Luo, Y., Sutton, M. A., Collette, S. A., Myrick, M. L., Miney, P., Colavita, P. E., Reynolds, A. P., and Li, X., 2007, "Development of Patterns for Digital Image Correlation Measurements at Reduced Length Scales," *Exp. Mech.*, **47**(1), pp. 63–77.
- [28] Sabaté, N., Vogel, D., Gollhardt, A., Marcos, J., Gràcia, I., Cané, C., and Michel, B., 2006, "Digital Image Correlation of Nanoscale Deformation Fields for Local Stress Measurement in Thin Films," *Nanotechnology*, **17**(20), p. 5264.
- [29] Zhu, J., Yan, G., He, G., and Chen, L., 2016, "Fabrication and Optimization of Micro-Scale Speckle Patterns for Digital Image Correlation," *Meas. Sci. Technol.*, **27**(1), p. 015203.
- [30] Yoneyama, S., Kikuta, H., Kitagawa, A., and Kitamura, K., 2006, "Lens Distortion Correction for Digital Image Correlation by Measuring Rigid Body Displacement," *Opt. Eng.*, **45**(2), p. 023602.
- [31] Pan, B., Xie, H., Guo, Z., and Hua, T., 2007, "Full-Field Strain Measurement Using a Two-Dimensional Savitzky-Golay Digital Differentiator in Digital Image Correlation," *Opt. Eng.*, **46**(3), p. 033601.

- [32] Pan, B., Qian, K., Xie, H., and Asundi, A., 2009, "Two-Dimensional Digital Image Correlation for In-Plane Displacement and Strain Measurement: A Review," *Meas. Sci. Technol.*, **20**(6), p. 062001.
- [33] Vendroux, G., and Knauss, W. G., 1998, "Submicron Deformation Field Measurements: Part 2. Improved Digital Image Correlation," *Exp. Mech.*, **38**(2), pp. 86–92.
- [34] Thai, T. Q., 2018, "Importance of Exposure Time on Digital Image Correlation (DIC) at Extreme Temperatures," All Graduate Theses and Dissertations. 7067, Utah State University.
- [35] Wang, W., Xu, C., Jin, H., Meng, S., Zhang, Y., and Xie, W., 2017, "Measurement of High Temperature Full-Field Strain up to 2000 °C Using Digital Image Correlation," *Meas. Sci. Technol.*, **28**(3), p. 035007.
- [36] Chen, X., Xu, N., Yang, L., and Xiang, D., 2012, "High Temperature Displacement and Strain Measurement Using a Monochromatic Light Illuminated Stereo Digital Image Correlation System," *Meas. Sci. Technol.*, **23**(12), p. 125603.
- [37] Blaber, J., Adair, B. S., and Antoniou, A., 2015, "A Methodology for High Resolution Digital Image Correlation in High Temperature Experiments," *Rev. Sci. Instrum.*, **86**(3), p. 035111.
- [38] Novak, M. D., and Zok, F. W., 2011, "High-Temperature Materials Testing with Full-Field Strain Measurement: Experimental Design and Practice," *Rev. Sci. Instrum.*, **82**(11), p. 115101.
- [39] Pan, B., Wu, D., and Yu, L., 2012, "Optimization of a Three-Dimensional Digital Image Correlation System for Deformation Measurements in Extreme Environments," *Appl. Opt.*, **51**(19), pp. 4409–4419.
- [40] Meyer, P., and Waas, A. M., 2015, "Measurement of In Situ-Full-Field Strain Maps on Ceramic Matrix Composites at Elevated Temperature Using Digital Image Correlation," *Exp. Mech.*, **55**(5), pp. 795–802.
- [41] Yoneyama, S., 2016, "Basic Principle of Digital Image Correlation for In-Plane Displacement and Strain Measurement," *Adv. Compos. Mater.*, **25**(2), pp. 105–123.
- [42] Wang Y. Q., Sutton M. A., Bruck H. A., and Schreier H. W., 2009, "Quantitative Error Assessment in Pattern Matching: Effects of Intensity Pattern Noise, Interpolation, Strain and Image Contrast on Motion Measurements," *Strain*, **45**(2), pp. 160–178.



- [43] Wang, Y.-Q., Sutton, M. A., Ke, X.-D., Schreier, H. W., Reu, P. L., and Miller, T. J., 2011, “On Error Assessment in Stereo-Based Deformation Measurements,” *Exp. Mech.*, **51**(4), pp. 405–422.
- [44] Ke, X.-D., Schreier, H. W., Sutton, M. A., and Wang, Y. Q., 2011, “Error Assessment in Stereo-Based Deformation Measurements,” *Exp. Mech.*, **51**(4), pp. 423–441.
- [45] Reu, P., 2013, “Stereo-Rig Design: Lighting—Part 5,” *Exp. Tech.*, **37**(3), pp. 1–2.
- [46] Reu, P., 2015, “All about Speckles: Contrast,” *Exp. Tech.*, **39**(1), pp. 1–2.
- [47] Archer, T., Beauchêne, P., Huchette, C., and Hild, F., 2019, “Global Digital Image Correlation up to Very High Temperatures with Grey Level Corrections,” *Meas. Sci. Technol.*, **31**(2), p. 024003.

CHAPTER 2  
IMPORTANCE OF EXPOSURE TIME ON DIC MEASUREMENT UNCERTAINTY  
AT EXTREME TEMPERATURES

### **2.1. Prologue**

This chapter presents a full-text paper which was published in *Experimental Techniques*, volume 43, issue 3, pages 261-271 on February 15, 2019 under the title “Importance of Exposure Time on DIC Measurement Uncertainty at Extreme Temperatures”. The experiment and data were performed and processed at Utah State University, Logan, UT. The author list is Think Q. Thai, Robert S. Hansen, Adam J. Smith, John Lambros, and Ryan B. Berke. The original paper is entirely presented below.

### **2.2. Abstract**

Digital Image Correlation (DIC) is a popular optical method for deformation and strain measurement. At extreme temperatures, it is known that materials emit light in addition to reflecting the light supplied by a light source, and the emitted light can saturate a camera sensor. More recently, a novel variation of DIC, named ultraviolet (UV) DIC, extended the range of temperature further by using a UV bandpass filter to screen out some of the brightest glowing and external UV illumination to provide additional reflected lighting. In principle, for a given optical set-up the temperature range can be extended further by reducing the camera’s sensitivity to light, and exposure time is an instrumental parameter when setting such camera configurations. In this paper, we examine the influence of multiple exposure times on the uncertainty of UV-DIC correlation

measurements. Rigid-motion experiments were performed at four different temperatures: room temperature, 1300°C, 1450°C, and 1600°C. At each temperature level, UV images were recorded for DIC at exposure times ranging from 500  $\mu\text{s}$  to 61,000  $\mu\text{s}$  – a range of over two orders of magnitude. The results showed abrupt increases of error at extremely dark or bright exposure times, but at intermediate exposure times the errors of UV-DIC were minimal. A normalized metric was presented in order to give a general guideline when choosing exposure time for camera sensitivity. It is recommended that cameras should be set at a suitable range of exposure time (between 10,000  $\mu\text{s}$  and 40,000  $\mu\text{s}$  for the camera used in this paper) in order to perform meaningful DIC up to 1600°C.

Keywords: DIC, extreme temperature, exposure time, ultraviolet light, graphite, Gleeble.

### **2.3. Introduction**

Digital Image Correlation (DIC) [1, 2] is one of the most popular and versatile methods for obtaining full field strain maps. In brief, DIC employs high-resolution cameras to record images of a speckle pattern applied to the sample surface in an undeformed and deformed state. A computer algorithm is then used to track the deformation of the speckle pattern between the two images, respectively, within a selected region. Strains are usually calculated by taking derivatives of displacement fields. In comparison with strain gauges [3], DIC has gained popularity since (1) it is able to collect full-field data (as opposed to point-wise or specimen-averaged techniques), (2) it is non-contacting (except for a thin layer of paint), and (3) having no inherent length scale, it can be used at any time or length scale if appropriate cameras and lenses are used. DIC has been demonstrated at lengths from sub-micrometer [4, 5] to tens of meters [6, 7] and from room temperature to 2000°C [8].

In order to perform a meaningful DIC analysis, it is essential to have an appropriate amount of light reach the camera sensor when images are acquired [9]. When there is too much light on the camera sensor, the image can become overly saturated. Conversely, the image is underexposed if there is not enough light. There are four main ways that the amount of light reaching the camera sensor can be amplified:

(1) **Using a brighter light source.** This could be more expensive and can introduce some safety hazards such as those presented by lasers [10] and/or UV lights [11].

(2) **Using a wider aperture on the lens.** It is noted that a wider aperture gives a smaller depth of field, but also yields brighter images [12].

(3) **Setting the camera to a longer exposure time.** This works well for quasi-static testing but a longer exposure time is more prone to motion blur, especially for vibration and dynamic loading experimentation [13].

(4) **Increasing the gain on the camera amplifier.** This is usually the worst option since it makes images become noisy and grainy [14].

Theoretically, DIC should work independently of temperature as long as the contrast of speckle pattern is within an acceptable range [15, 16]. However, at extreme temperatures, the specimen emits its own light in addition to reflecting the light supplied. This results in the degradation of speckle contrast making the cross correlations weaker [11, 17]. It is known that the glow is much brighter at longer wavelengths (i.e., red and infrared) than it is at shorter wavelengths (i.e., blue), and this can be mitigated using blue optical bandpass filters [18–20]. More recently, our group introduced an adapted technique called ultraviolet digital image correlation [11] (UV-DIC), which uses a UV filter to extend

the temperature range of DIC even farther while simultaneously providing sufficient lighting through UV illumination, as needed.

In each study where blue or UV filtering was used, various investigators have reported different upper temperature limits for DIC depending on their camera settings. For example, Novak and Zok [20] estimated that the maximum temperature for blue-filtered DIC was around 1500°C. However, Wang et al. [8] reported being able to perform blue-filtered DIC at temperatures as high as 2000°C. Conversely, we showed when comparing blue-filtered DIC against UV-DIC that, under the (fixed) camera settings used in that study, blue-filtered DIC instead saturated as low as 900°C [11]. It is clear that a limiting factor in performing DIC at extreme temperatures is not only the wavelength of light that images are recorded at, but also the sensitivity of the camera to the light at those wavelengths.

In this paper, the influence of exposure time is examined on DIC measurements at extreme temperatures. Exposure time is chosen as the parameter to study since, of the four ways listed to control light, it is the easiest to manipulate while introducing minimal errors into the measurement. All tests are quasi-static to avoid motion blur from the specimen. Although the specimen is quasi-static, we still get minimal motion blur due to the movement of air, which is largely negated by performing the test in vacuum. Experiments were performed at four different temperature levels: room temperature, 1300°C, 1450°C and 1600°C. Three sets of measurements were made: (i) baseline noise calculations, in which no motion or deformation is applied between two DIC images; (ii) isothermal rigid motion experiments, in which DIC results were computed from pairs of images taken at fixed temperatures; and (iii) thermal expansion measurements, in which DIC was

performed using a reference image at room temperature and deformed images at elevated temperature. The isothermal measurements were performed over exposure times ranging from 500  $\mu\text{s}$  to 61,000  $\mu\text{s}$  in order to assess the error of UV-DIC. The thermal expansion measurements demonstrated the ability for UV-DIC to span a broad temperature range when the emitted light was sufficiently filtered. Finally, in our discussion section, we evaluate a simple metric for assessing whether a speckle image had sufficient contrast to perform DIC, and made further recommendations to promote good contrast when performing DIC at extreme temperatures.

## **2.4. Methods**

Experiments were performed using graphite rods purchased from GraphiteStore.com [21]. The graphite has a melting point of 3000°C in vacuum but oxidizes aggressively in air, and thus all high temperature tests were performed in vacuum. For all experiments, the level of vacuum in the test chamber is on the order of  $10^{-9}$  torr. Specimens were machined from graphite rods with a length of 152.4 mm (6 in) and diameter of 12.7 mm (0.5 in) by using a manual knee mill. The gauge region was a square cross section of 7.62 mm (0.3 in) in order to provide a flat, planar surface on which to perform DIC. Figure 2.1 shows a schematic and photograph of the machined specimens. The graphite, which is naturally dark, provides the dark background on which to create a speckle pattern for DIC. A white speckle pattern was then applied directly onto the surface of the square cross-section gauge region of the sample using a splattering method. This splattering method consisted of flicking the bristles of a toothbrush dipped in paint to splash white paint onto the flat surface of the specimen. The speckle size created by this method is relatively coarse; however, for the scale of millimeters

used in this work it offers sufficient accuracy to perform DIC. The paint was Pyro-Paint 634-AL from Aremco Products Inc. (Valley Cottage, NY, USA) which has melting point of 1760°C. The paint was dried at room temperature for 2 hours and then cured for 2 hours in a box furnace at 93°C (200°F), per the manufacturer's instructions.

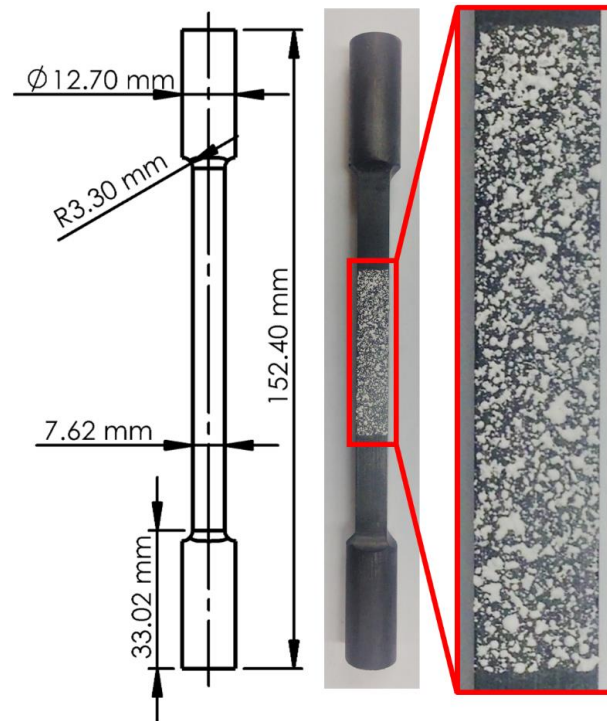


Figure 2.1. Schematic of square gauge region test specimen (left), a photo of specimens with speckled gauge region (middle) and a close-up of the speckle pattern (right)

The specimen was then tested in a Gleeble 1500D thermo-mechanical system which consists of a load frame inside of a vacuum chamber, and which can heat a specimen up to 3000°C. Heating is accomplished by running a high voltage through the electrically-conducting specimen. In order to heat the specimen in the Gleeble, a K-type thermocouple is required as a feedback control. The highest temperature level employed in this paper is 1600°C occurring in the middle of specimen. However, a K-type thermocouple is only rated

to 1250°C [22]. Therefore, a method was devised to extend the range of available testing temperatures beyond the K-type thermocouple range. Two K-type thermocouples (called TC1 and TC2) recorded temperatures at two different locations 35 mm apart, as shown in Figure 2.2. A thermal gradient was then applied along the length of the specimen, resulting in the temperature recorded by TC1 in the middle always being higher than temperature recorded by TC2 towards one end. The temperature relationship between TC1 and TC2 is also shown in Figure 2.2. In subsequent experiments, TC1 was removed so as not to obscure the view of the speckle pattern from the cameras. TC2 was then used to provide temperature control by assigning temperatures which corresponded to the desired temperature in the middle. In this fashion the controller K-type thermocouple (TC2) always remained below its limit of 1250°C, while in the middle of the gauge section a higher temperature was achieved.

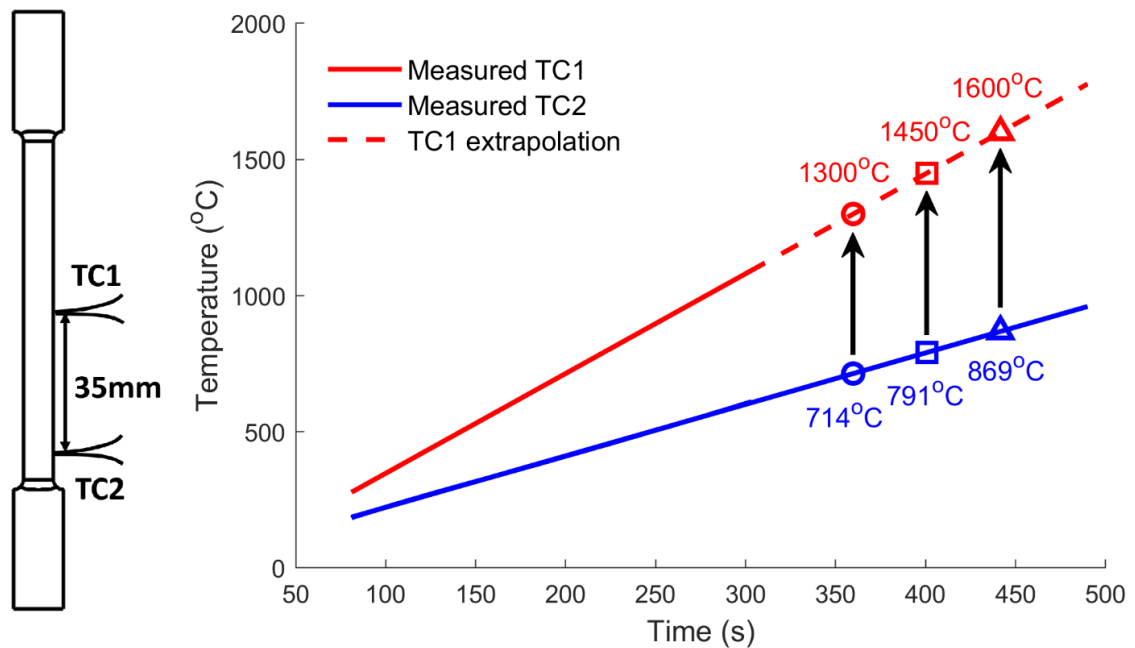


Figure 2.2. Schematic of the 2-thermocouple placement (left) and temperature relationship of the two thermocouples (right)



To further support the validity of the 2-thermocouple method, Figure 2.3 shows a temperature map captured from a FLIR A6751sc IR camera. The temperature varies in the horizontal direction and is hottest in the middle of specimen, which agrees with the temperatures measured by TC1 and TC2 in Figure 2.2. There is of course a temperature gradient in the sample as seen in Figure 3, which is the basis of using the 2-thermocouple method. However, since the present work is concerned with determining the influence of exposure time on DIC results, uniformity of temperature is not required. Note that it was not possible to use the FLIR measurement as a temperature control variable. Only a K-type thermocouple can be used as a control signal with the Gleeble 1500D.

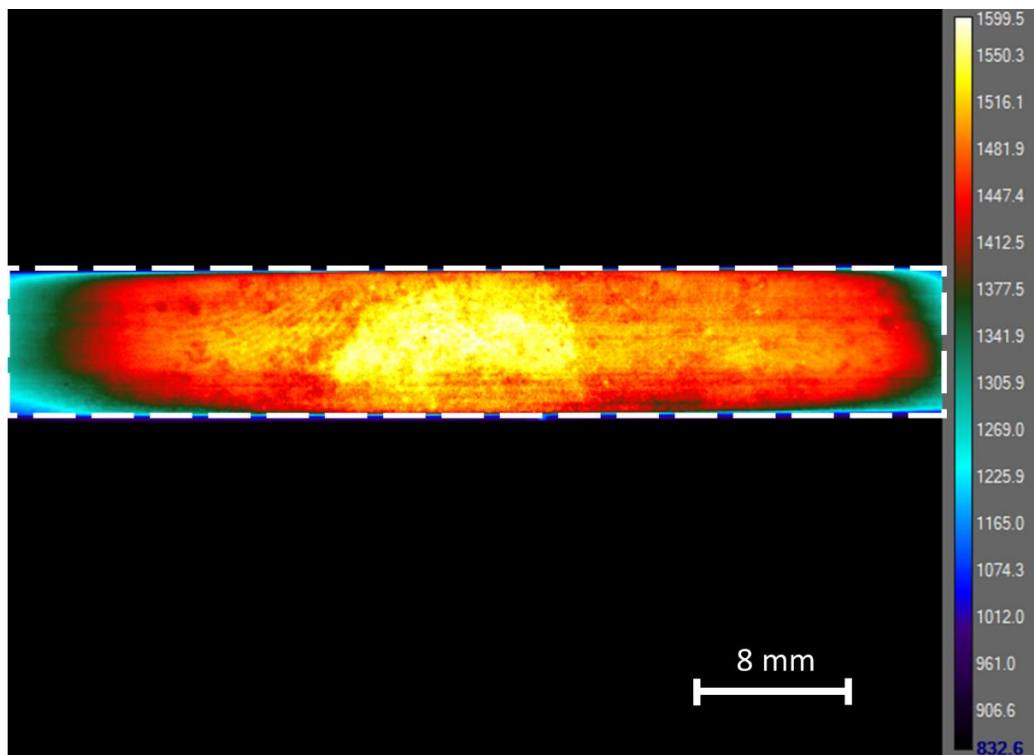


Figure 2.3. The temperature map from FLIR IR camera at 1600°C, data bar shows temperature (°C) map inside dashed rectangle

A fixture was designed using aluminum T-slot framing to appropriately mount the UV camera, UV lights and UV filter above the Gleeble, as shown in Figure 2.4. The specimen was monitored through a borosilicate glass window, which transmits both UV and visible light. The thickness of the window is 16.40 mm. The window is held in position by an aluminum frame and it is sealed by a rubber O-ring to keep vacuum pressure. The camera model was a CM-140GE-UV camera manufactured by JAI, which detects both visible and ultraviolet light. The camera was equipped with a UV lens from Universe Kogaku Inc. with a focal length of 50 mm and was fitted with an XNite 330C M58 ultraviolet bandpass filter from LDP LLC. The UV lights, which emit at a peak wavelength of 365 nm, were purchased from CCS Inc. Figure 2.5 shows the transmissivity of the UV camera and related optics, as provided by the manufacturers.

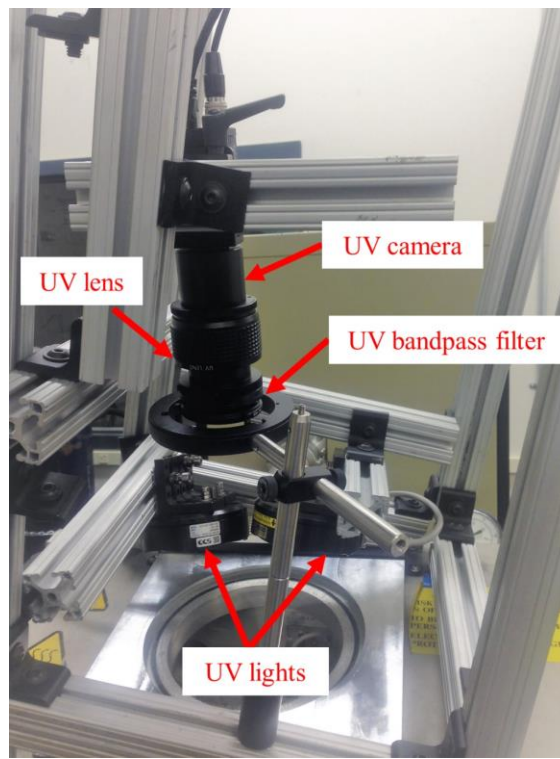


Figure 2.4. Photograph of the fixture with experimental setup

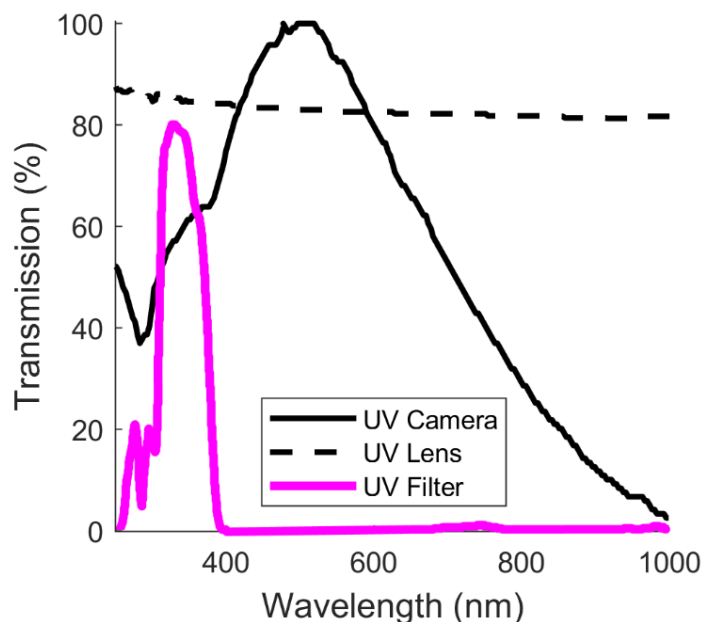


Figure 2.5. Transmissivity of UV camera and related optics

At high temperature, the temperature of the window could potentially cause errors to DIC measurement due to air heating outside the window and curvature of the window. However, this issue is expected to be minimal. Since the specimen is heated via an electrical current, only the specimen is directly heated, not the entire volume of the chamber. The tests are in vacuum to minimize the heat transfer from conduction and convection. Although the radiation can be transmitted in vacuum, it is expected to be small. Even when the specimen is at 1600°C, the window is safe to touch.

The specimen was heated to temperatures corresponding to room temperature (RT) and multiple extreme temperatures (1300°C, 1450°C and 1600°C) at the middle of the specimen. The loading condition is purely static. Since the goal of this paper is to examine the influence of exposure times, any other factors contributing to camera sensitivity (i.e., UV light intensity, aperture, and gain) were kept fixed. Specifically, the aperture of the

lens was set to an f-number of 4 and the gain of the camera was set to 0. The brightness of the UV source was not measured, but is given as  $20.4 \text{ mW/cm}^2$  corresponding to a working distance of 116.5 mm, which is significantly shorter than the working distance in this paper. In general, the brightness of the UV source decreases with longer working distance. In this paper, both the working distance and the intensity of the lights are kept constant throughout the test. Therefore, the brightness of UV light, though unmeasured, is unchanged during the test. Images were taken at multiple exposure times ranging from the shortest exposure time that the camera is capable of ( $500 \mu\text{s}$ ) to the longest exposure time ( $61,000 \mu\text{s}$ ).

Even at room temperature, when the Gleeble is on, the vacuum pump causes the unit to vibrate. To explore the possible relative motion between the camera (outside the vacuum chamber) and the specimen (inside the chamber), an investigation was performed, which confirmed that there is such relative motion caused by the vacuum pump, but the motion is small in comparison to the precision of the measurements. At room temperature, the two following cases were tested, and at extreme temperatures a third case was also tested:

- **Case 1**: No motion applied to the specimen. For each value of exposure time, two images at the same state were taken in succession.

- **Case 2**: A rigid motion was applied. The camera was moved away from the reference state in mostly the horizontal direction, producing a relative motion in the recorded images. A third image was then recorded at each exposure time.

- **Case 3**: Thermal expansion measurements. Case 1 images at high temperature are correlated against case 1 reference images at room temperature. No new images are recorded.

Additionally, in the tests at high temperatures, another factor limiting the precision of the measurements is out of plane thermal expansion which is proportional to  $\Delta z/z = t\alpha\Delta T/z$  where  $\Delta z$  is the out of plane thermal expansion,  $z$  is the distance between the lens and the front of specimen (for this test  $z=44.5$  cm),  $t$  is the thickness of the specimen ( $t = 7.62$  mm),  $\alpha$  is coefficient of thermal expansion (varies with temperature) and  $\Delta T$  is the temperature change in the test. For example, if the test is at  $1300^{\circ}\text{C}$ ,  $\alpha = 2.6020 (10^{-6}\text{K}^{-1})$  (taken from Results section), so the precision of the measurements is proportional to  $\Delta z/z = 58\mu\epsilon$ .

A commercial DIC software from Correlated Solutions Inc. named Vic-2D (version 2009) was employed to compute displacement and strain distributions over the gauge length region. The subset size was  $61 \times 61$  pixels, the step size was 25 pixels, and the strain window was 15 subsets. The calculation was performed separately for each temperature and exposure time, such that each use of the software involved only three images at room temperature (Case 1 and Case 2 with the same reference image) or two images at high temperatures (Case 1 only). The same images were later used to compute thermal expansion strains (i.e., Case 3) by assigning a reference image at room temperature and deformed images at the elevated temperatures.

After all data was collected, the data was post-processed using MATLAB to find the mean and 95% confidence interval. The 95% confidence interval was computed by sorting the data in ascending order, then finding the thresholds which indicate values between 2.5% and 97.5% of the data. In Figure 2.6, only  $u$  displacement is presented while in Figure 2.7, Figure 2.9, and Figure 2.14 only strains are presented.

## 2.5. Results

### A. Room temperature

The mean displacement and axial normal strain are presented in Figure 2.6 and Figure 2.7, respectively, with uncertainty bands showing the 95% confidence intervals. Since displacements were mostly applied in the axial direction, only the axial components are included. Each figure contains three datasets: case 1 (no applied motion) with the Gleeble turned off, case 1 with the Gleeble turned on, and case 2 (applied rigid motion) with the Gleeble turned on. For clarity, the first and last dataset have been staggered horizontally slightly by adding  $\pm 500 \mu\text{s}$  to exposure time in order to avoid excessive overlapping of the uncertainty bands. Each dataset also features a horizontal line to indicate the combined mean of all points in the set, which should be nominally zero (for case 1 displacements and all strains) and non-zero (for case 2 displacements). The left vertical axis (written in pink) refers to Case 1 including Gleeble turned off and Gleeble turned on whereas the right axis (written in blue) is used for Case 2.

As can be seen in Figure 2.6, when the Gleeble is on, it imposes a small relative motion between the cameras and specimens according to the mean line. However, when comparing to Figure 2.7, strains are all consistently around zero over the whole range of exposure time. This justifies that the relative motion is purely rigid-body motion, which we believe may be due to the vibration of the vacuum pump. Accordingly, at high temperatures only the strains (not the displacements) will be reported in later figures.

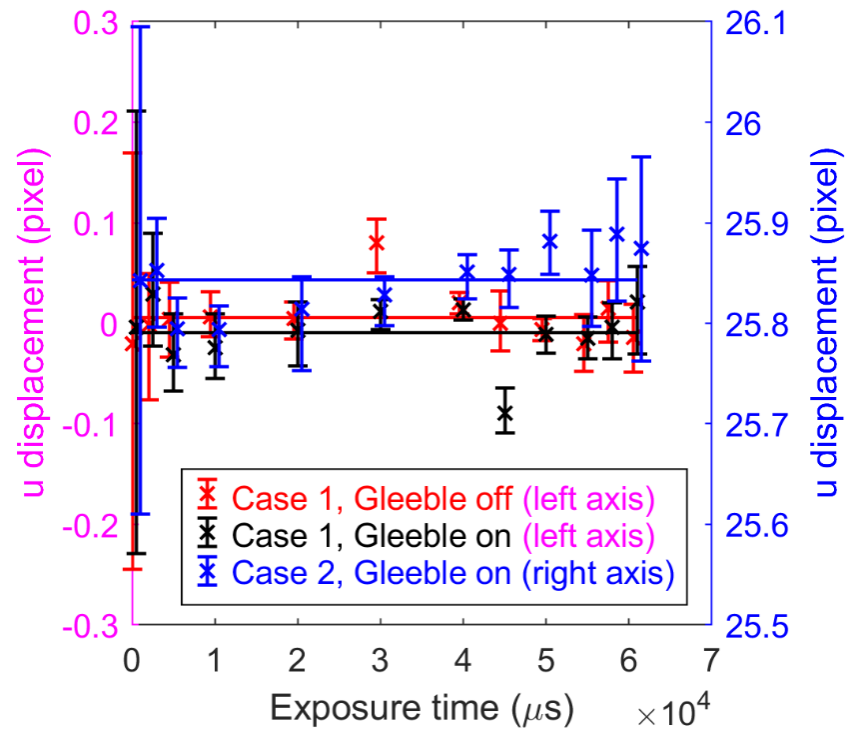


Figure 2.6. Mean u displacement at room temperature, compared between case 1 (no applied motion) and case 2 (non-zero rigid motion) with the Gleeble on or off as indicated. Each uncertainty band is the 95% confidence interval

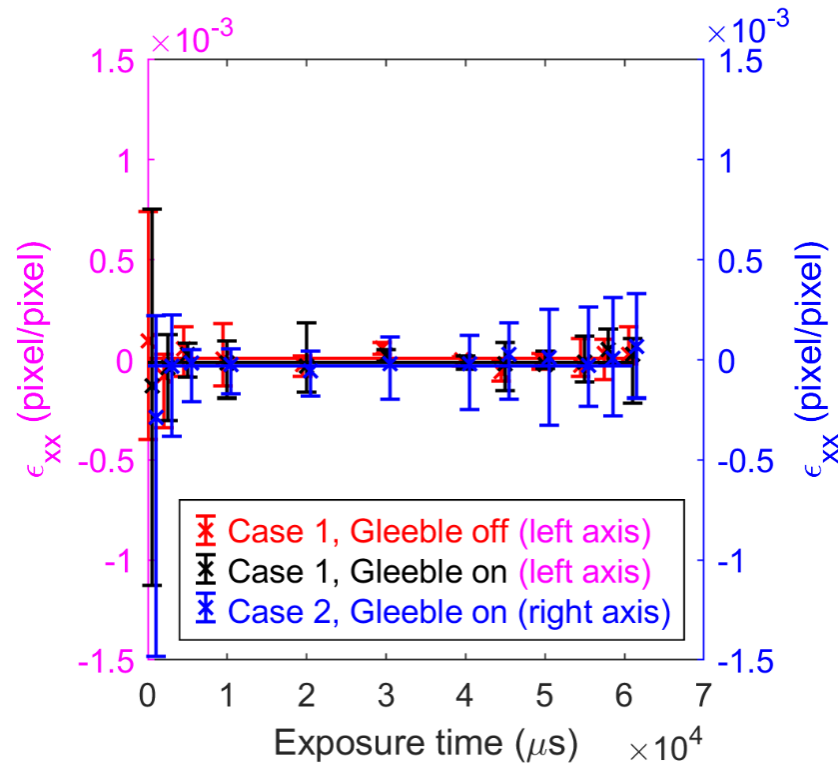


Figure 2.7. Mean strain  $\epsilon_{xx}$  at room temperature, compared between case 1 (no applied motion) and case 2 (non-zero rigid motion) with the Gleeble on or off as indicated. Each uncertainty band is the 95% confidence interval

Since the displacement and strain fields are not uniform, Table 2.1 shows the mean and variance of displacement and strain field in Figure 2.6, Figure 2.7 and Figure 2.9. The mean value represents the bias error and the variance shows how far a set of data points spread out from their mean value.



Table 2.1. Mean and variance of displacement and strain field

Figure		Temperature	Mean	Variance	Collected data
Figure 2.6	Case 1, Gleeble off	Room temperature	0.0057	7.0652e-04	Horizontal displacement (pixel)
	Case 1, Gleeble on		-0.0092	9.5563e-04	
	Case 2, Gleeble on		25.8432	9.7073e-04	
Figure 2.7	Case 1, Gleeble off	Room temperature	7.1348e-06	2.4994e-09	Horizontal strain
	Case 1, Gleeble on		-1.2978e-05	2.1891e-09	
	Case 2, Gleeble on		-3.0635e-05	7.5206e-09	
Figure 2.9		(a) 1300°C	-3.8209e-05	1.8446e-08	Horizontal strain
		(b) 1450°C	1.9566e-05	5.5766e-09	
		(c) 1600°C	-7.1006e-05	1.0632e-08	

## B. Extreme temperatures

A series of images showing the speckled surface of the specimen are arranged in Figure 2.8 at different temperatures (room temperature, 1300°C, 1450°C and 1600°C) and select exposure times (20,000  $\mu$ s, 30,000  $\mu$ s, 50,000  $\mu$ s and 61,000  $\mu$ s) along with histograms of the corresponding greyscale values. As both temperature and exposure time increase, the images become visibly brighter. Eventually, some images became so saturated that Vic-2D could no longer perform a correlation. The speckle images where Vic-2D was unable to correlate are marked with red crosses.

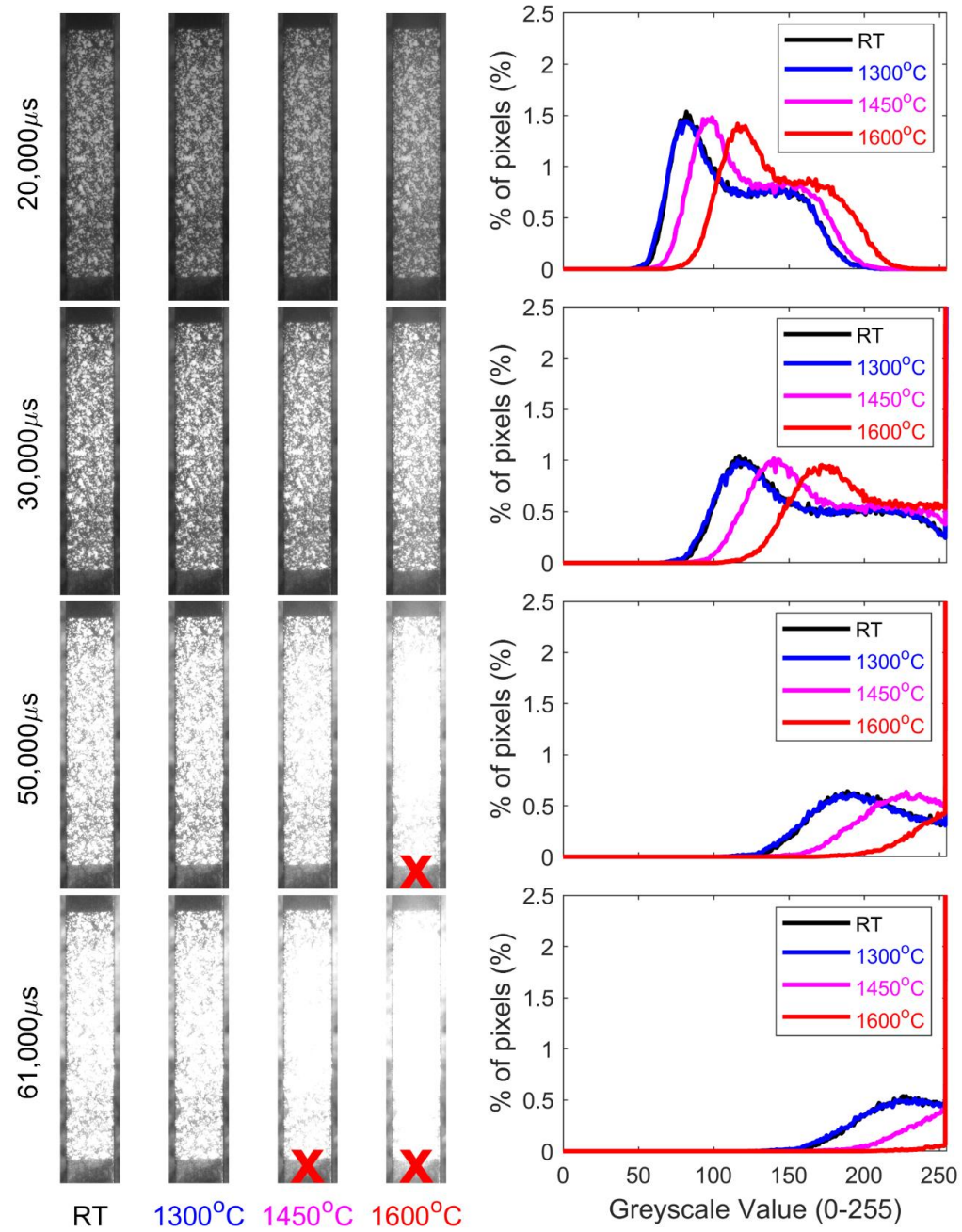


Figure 2.8. Raw speckle images of specimen surface at different temperatures (increasing from left to right) and exposure times (increasing from top to bottom) respectively, and histograms of the greyscale values corresponding to the images. Images which are too saturated to perform DIC are indicated with a red cross

Figure 2.9 shows comparisons of  $\epsilon_{xx}$  at room temperature (RT) vs 1300°C (a), 1450°C (b) and 1600°C (c) respectively when there are no applied displacements (i.e., Case 1). At the highest temperatures and longest exposure times (including the cases indicated by red crosses in Figure 2.8), data is unavailable because the images were too saturated for Vic-2D to perform its correlation.

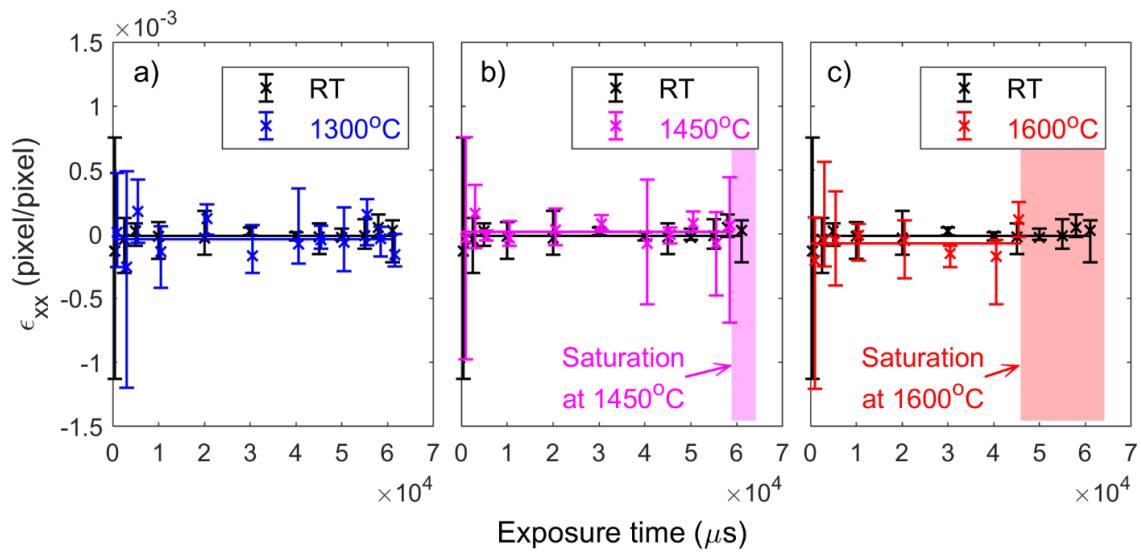


Figure 2.9. Comparison of  $\epsilon_{xx}$  at room temperature and (a) 1300°C, (b) 1450°C and (c) 1600°C when there is no applied displacement

Figure 2.10(a) shows the non-uniform thermal strain distribution over the gauge length due to the thermal gradient in Figure 2.3. The thermal strain (i.e., Case 3) is computed by comparing a reference image at room temperature and a deformed image at 1600°C. Figure 2.10(b) presents the  $\epsilon_{xx}$  strain contour at 1600°C when there is no applied change in temperature or displacement. The exposure time is 20,000  $\mu\text{s}$  since generally it gives a small uncertainty band at high temperatures. The data is overall centered around zero which is in good agreement with the condition of no applied displacement. Note that

the data in Figure 2.10(a) is of thermal strain at 1600°C while data in Figure 2.10(b) is nominally of zero-strain at 1600°C when there is no applied temperature or displacement.

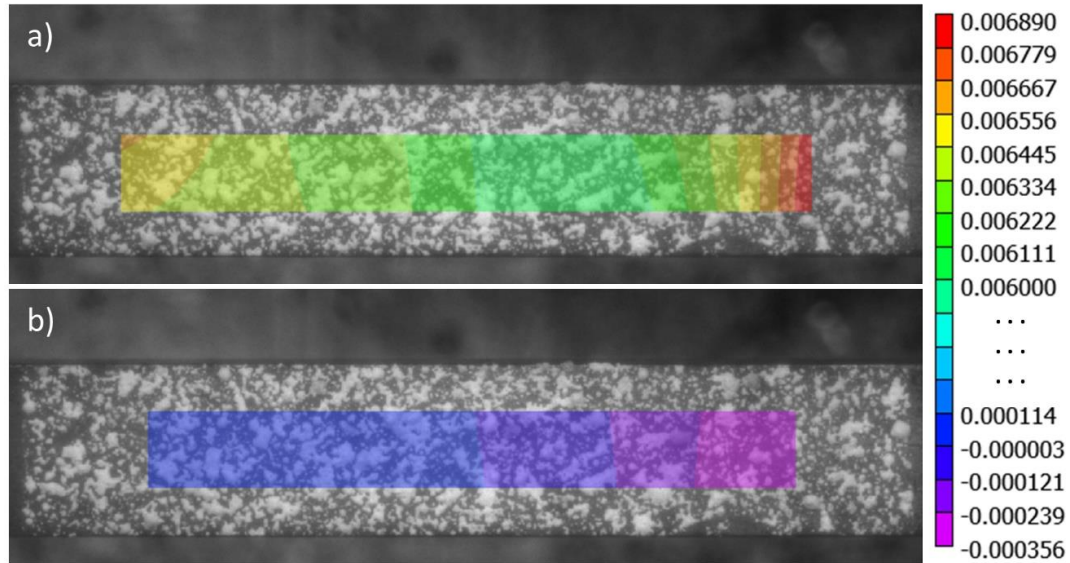


Figure 2.10. (a) The thermal strain  $\varepsilon_{xx}$ (pixel/pixel) map at 1600°C obtained with Vic-2D from comparing a reference image at room temperature and a deformed image at 1600°C, (b) The  $\varepsilon_{xx}$ (pixel/pixel) strain map at 1600°C obtained with Vic-2D from two images with no applied temperature or displacement. All images were recorded at an exposure time of 20,000  $\mu$ s

Figure 2.11 shows thermal strains (i.e., Case 3) at 1300°C, 1450°C and 1600°C as a function of position along the gauge length. Unlike the strains in the previous figures, the thermal strain was computed by correlating between a reference image at room temperature and corresponding deformed images at high temperature. The exposure time was set to 20,000  $\mu$ s. As can be seen in Figure 2.11, thermal strain becomes larger and less uniform at higher temperature. The dashed horizontal lines are the mean thermal strains. They are calculated by taking average of all thermal strain points along gauge length. The solid

horizontal lines are 95% confidence interval of mean thermal strain. The coefficient of thermal expansion (CTE) is computed by the formula:  $CTE = \varepsilon_{avg}/T_{max}$  where  $\varepsilon_{avg}$  is the mean thermal strain and  $T_{max}$  is the maximum temperature occurring in the middle of specimen. Particularly, the mean thermal strain (dashed horizontal lines in Figure 2.11) is 0.0034, 0.0055, and 0.0063 at 1300°C, 1450°C and 1600°C, respectively, which corresponds to mean coefficients of thermal expansion (CTE) of  $2.6020 (10^{-6}K^{-1})$ ,  $3.8087 (10^{-6}K^{-1})$  and  $3.9362 (10^{-6}K^{-1})$ , respectively. For a temperature of 1600°C, the standard deviation of CTE is  $0.1367 (10^{-6}K^{-1})$  which is relatively small when compared to its mean value (around 5%). The CTE from the manufacturer is  $2 (10^{-6}K^{-1})$  [21]. Although it is unknown over which temperatures the manufacturer measured CTE, our results are generally of the same order of magnitude as the specifications of the manufacturer. In addition, Figure 2.11 shows that thermal strains over the gauge length become less uniform at higher temperatures due to thermal gradients.

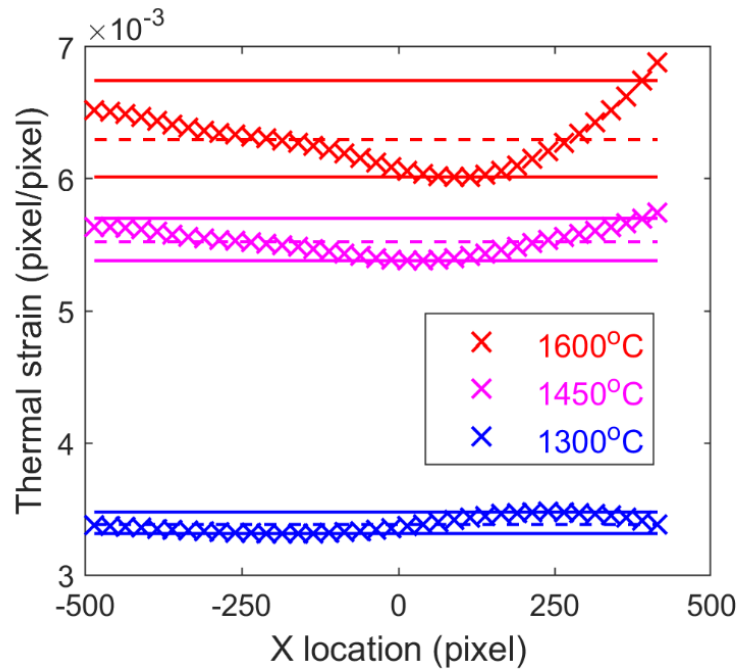


Figure 2.11. Thermal expansion strain at multiple temperatures over the gauge length

## 2.6. Discussion

In general, results at room temperatures from Figure 2.6 and Figure 2.7 showed that the uncertainty bands are much wider in Case 2 compared to Case 1. Any error caused by the vibration of the Gleeble (i.e., the difference between the two grand mean lines in Case 1) is well within the precision of the system (i.e., the size of the uncertainty bands of Case 2). Therefore, the influence of Gleeble vibration is expected to be negligible in a real experiment with non-zero motion. Another observation is that the uncertainty bands are wider at extreme exposure times and narrower at moderate exposure times. This is reasonable since the contrast of images at extreme exposure times is degraded, resulting in deteriorating the correlation.

The upper temperature limit of DIC depends on the light sensitivity of the camera system. As can be seen in Figure 2.9, when an exposure time of 61,000  $\mu\text{s}$  was used, the upper temperature limit of UV-DIC was 1300°C, whereas when it was reduced to 58,000 $\mu\text{s}$ , the limit was 1450°C and by using 45,000  $\mu\text{s}$  and below it was able to reach 1600°C. In other words, the variation of exposure time alters the contrast of the image resulting in a change of the upper temperature limit.

For a given exposure time, the uncertainty bands are wider at extreme temperatures compared to room temperature as shown in Figure 2.9. This is reasonable since images get brighter at higher temperatures resulting in weaker correlation. Additionally, as temperature increases, images tend to saturate at progressively lower exposure times than they saturated at lower temperatures, resulting in dropped data points (at the very highest exposure times) and larger uncertainty bands (at less high exposure times).

The above observations are based upon camera settings which are specific to the particular model of camera. Thus, to provide more robust recommendations, it is preferable to adopt a metric that can be applied to other cameras. One notable metric was proposed by Phillip Reu [23], who suggested that the best minimum contrast (for an 8 bit camera) is when the difference between the greyscale value of a typical dark pixel and typical bright pixel is at least 50 counts. He later presented a similar recommendation, where he plotted a histogram comparable to those in Figure 2.8 and recommended that the maximum value to appear in that histogram should be at least 50 counts [14]. While the latter suggestion makes for a very convenient metric to calculate quickly, it is very susceptible to outliers if one pixel happens to be much brighter or darker than the overall speckle pattern. Also, in the case of extreme temperature measurements involving over-saturation, the maximum count is often limited by the camera sensor (255 for an 8 bit camera) but the minimum count will continue to increase with temperature, resulting in poor contrast due to over-saturation.

Reverting to Reu's earlier metric [23], the following discussion presents a more quantitative approach to determine which dark pixels and which bright pixels should be considered "typical" by computing the 90% confidence interval. In this new approach, we integrate the histogram from 0 until we reach 5% of the total pixels, and that greyscale value would represent a "typical dark pixel" which we call  $Z_1$ . Similarly, we integrate the histogram from 0 until we reach 95% of the total pixels, and that greyscale value would represent a "typical bright pixel" which we call  $Z_2$ . The contrast, given the symbol  $\Delta$ , is defined as the difference in grey values between the typical dark speckles and the typical bright speckles [14]. In other words,  $\Delta = Z_2 - Z_1$  such that 90% of all pixels lie within the span of  $\Delta$ . An

example of this approach is shown in Figure 2.12 at three different exposure times which represents (a) low exposure time, (b) intermediate exposure time and (c) high exposure time. Figure 2.12(a) illustrates a bad contrast ( $\Delta < 50$ ) while Figure 2.12(b) presents a good contrast ( $\Delta > 50$ ). In Figure 2.12(c),  $\Delta$  is higher than 50 but is still considered as a bad case due to saturation of the camera sensor ( $Z_2 = 255$ ). So in addition to a requirement that  $\Delta$  should be at least 50 counts, an additional constraint should be  $Z_2 \neq 255$ .

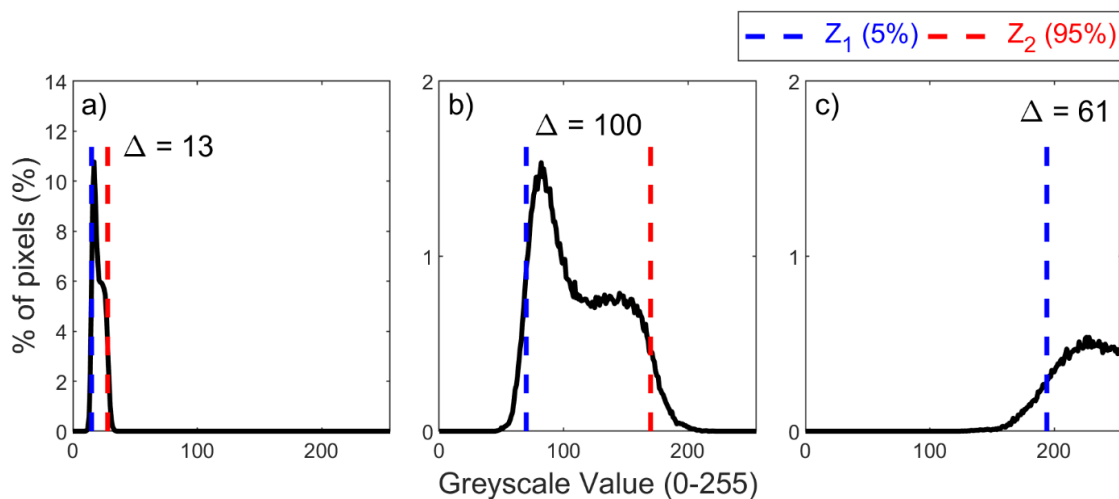


Figure 2.12. Example of 90% confidence interval approach, using room temperature data at exposure time of a) 2,500  $\mu\text{s}$ , b) 20,000  $\mu\text{s}$  and c) 61,000  $\mu\text{s}$

Figure 2.13 presents the relationship between exposure time and  $\Delta$  at four different temperature levels. The figure shows that low  $\Delta$  happens not only when exposure time is too low, but also when exposure time is too high. Under the camera settings used in this study,  $\Delta$  is linearly proportional to exposure time if exposure time is below 30,000  $\mu\text{s}$  and inversely proportional if exposure time is above 30,000  $\mu\text{s}$ . In addition, when exposure time is below 30,000  $\mu\text{s}$ , there is no remarkable difference in  $\Delta$  at multiple temperature



levels whereas when exposure time is above 30,000  $\mu\text{s}$ , higher temperatures lead to lower  $\Delta$  (low contrast) when compared at the same value of exposure time. In other words, high temperature greatly affects the contrast of images when camera sensitivity is above a certain limit. In this case, the difference between various temperatures is clearly noticeable when exposure is beyond 30,000  $\mu\text{s}$ .

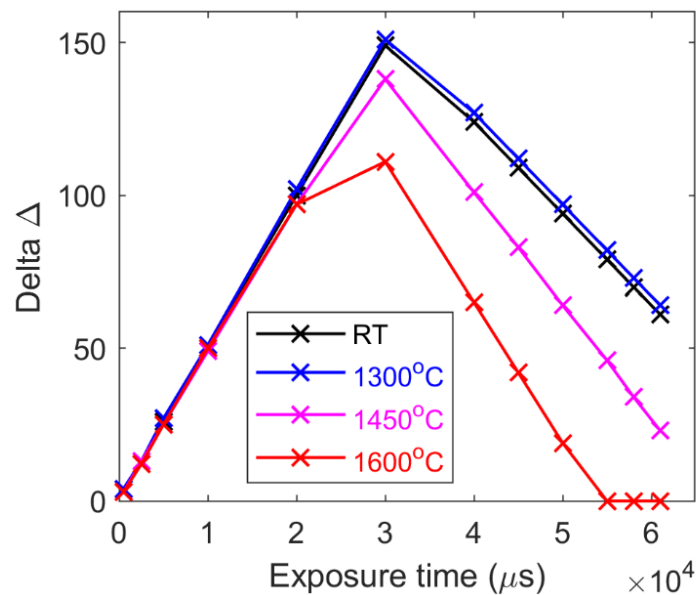


Figure 2.13. Relationship between exposure time and  $\Delta$  at different temperatures

Figure 2.14 shows the relationship between strain  $\epsilon_{xx}$  and  $\Delta$  at four different temperature levels, using the data presented in Figure 2.9. Data was recorded at multiple exposure times ranging from 500  $\mu\text{s}$  to 61,000  $\mu\text{s}$ . The vertical black dashed line is at  $\Delta=50$ , which is the boundary of good camera sensitivity recommended by Reu [23]. It is noticeable that when  $\Delta$  is bigger than 50, uncertainty bands tend to be smaller whereas if  $\Delta$  is much smaller than 50, uncertainty bands are larger.

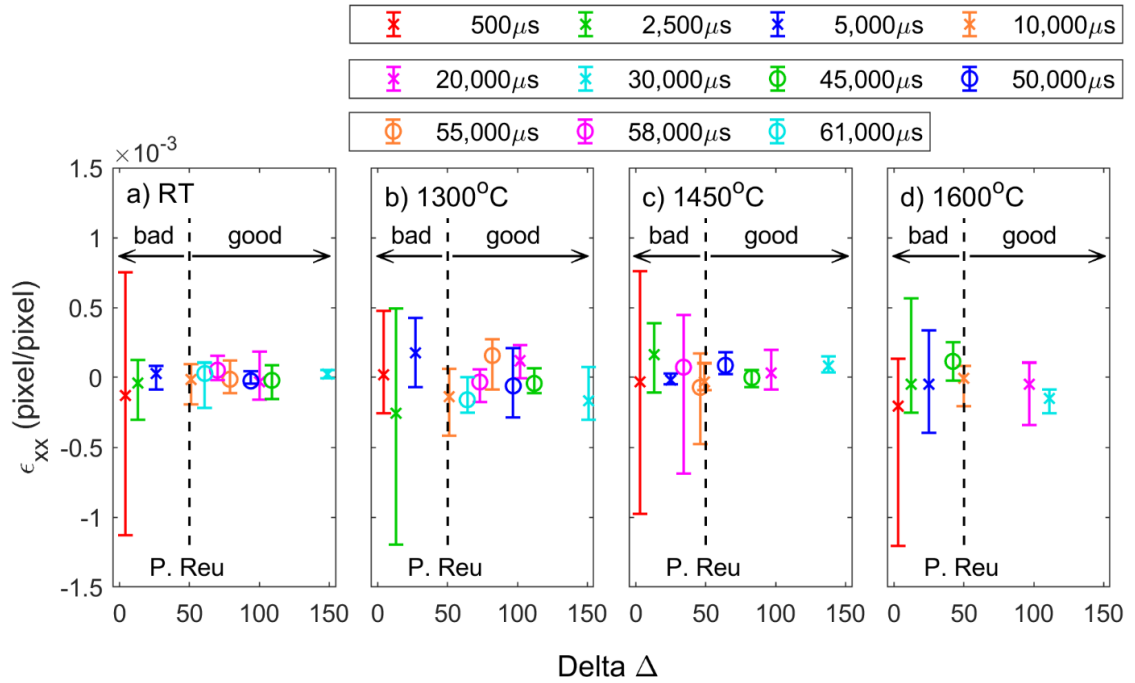


Figure 2.14. Strain  $\epsilon_{xx}$  vs  $\Delta$  at (a) RT, (b) 1300°C, (c) 1450°C, and (d) 1600°C when there is no applied displacement

Based on our definition of  $\Delta$ , it is therefore recommended that before heating a sample and performing DIC at high temperature, an initial image should be recorded at room temperature and  $\Delta$  should be higher than 50. For the conditions used in this study, this recommendation consistently covers all images recorded at exposure times of 10,000  $\mu s$  and above. As can be inferred from Figure 2.14, data is unavailable at 61,000  $\mu s$ , 58,000  $\mu s$ , 55,000  $\mu s$ , 50,000  $\mu s$  for 1600°C and 61,000  $\mu s$  for 1450°C while we have full data for 1300°C and room temperature. It is thus further recommended that before testing at higher temperatures, the exposure time should be kept as low as possible while maintaining sufficient  $\Delta$  to avoid over-saturation in the higher temperature images.

The metric of  $\Delta$  is intended as a quick and convenient metric for DIC users to quickly assess the quality of a DIC speckle pattern at high temperature. Readers who desire a more meticulous method of error assessment are referred to three works by Wang et al. In the first work, Wang et al. [24] considered various sources of error including interpolation method, subpixel motion, intensity noise, image contrast, level of uniaxial normal strain and subset size. They then constructed a mathematical framework for considering those errors for 1D and 2D motion. The next paper [25] extends the consideration of error to 3D motion. Extensive numerical simulations were performed to verify the capability of the developed framework in estimation of bias and variance for a 3D motion measurement. The last paper [26] is an experimental validation of the theoretical framework presented in [24] and [25]. Between these three papers, the authors introduced a thorough and robust framework for error assessment of DIC measurement that is essential for designing a DIC code. However, for readers who just want a convenient metric to assess saturation at high temperature, we have presented  $\Delta$  which can be obtained relatively quickly.

## **2.7. Conclusions**

In summary, the influence of exposure time on DIC at extreme temperatures was investigated thoroughly in this paper. Since the uncertainty bands on displacement and strain measurements are wider at extreme exposure times, it is recommended to avoid setting the exposure time too short (5,000  $\mu\text{s}$  and below for the camera settings used in this paper) at all temperatures. Additionally, at high temperatures, it is advised to avoid setting the exposure time too long to avoid overexposing the images. For the example used in this

study, exposure times of between 10,000  $\mu\text{s}$  to 40,000  $\mu\text{s}$  are a good range for this camera system to test from room temperature up to 1600°C. To better apply results from this paper to other cameras, a normalized metric called Delta ( $\Delta$ ) is presented to ensure that 90% of all pixels span a sufficiently broad range of greyscale values. Exposure time should be selected to allow as low light sensitivity as possible while maintaining  $\Delta > 50$ . Most importantly, the upper temperature limit of DIC depends on the light sensitivity of the camera system which depends on multiple factors – including exposure time – and can be effectively extended by reducing the sensitivity of the system.

## **2.8. Acknowledgements**

This work was funded in part by a grant from NASA's Marshall Space Flight Center (award # 80MSFC18M0009) and by the Utah State University Office of Research and Graduate Studies. JL also wishes to acknowledge the support of the Air Force Office of Scientific Research (AFOSR) through grant number FA9550-16-1-0055.

## **2.9. References**

- [1] Sutton MA, Orteu JJ, Schreier H (2009) Image Correlation for Shape, Motion and Deformation Measurements: Basic Concepts, Theory and Applications. Springer US
- [2] Chu TC, Ranson WF, Sutton MA (1985) Applications of digital-image-correlation techniques to experimental mechanics. *Exp Mech* 25:232–244. <https://doi.org/10.1007/BF02325092>
- [3] Ramos T, Braga DFO, Eslami S, et al (2015) Comparison Between Finite Element Method Simulation, Digital Image Correlation and Strain Gauges Measurements in a 3-Point Bending Flexural Test. *Procedia Eng* 114:232–239. <https://doi.org/10.1016/j.proeng.2015.08.063>

- [4] Berfield TA, Patel JK, Shimmin RG, et al (2007) Micro- and Nanoscale Deformation Measurement of Surface and Internal Planes via Digital Image Correlation. *Exp Mech* 47:51–62. <https://doi.org/10.1007/s11340-006-0531-2>
- [5] Carroll J, Abuzaid W, Lambros J, Sehitoglu H (2010) An experimental methodology to relate local strain to microstructural texture. *Rev Sci Instrum* 81:083703. <https://doi.org/10.1063/1.3474902>
- [6] Gradl PR (2016) Digital Image Correlation Techniques Applied to Large Scale Rocket Engine Testing. In: *AIAA Propulsion and Power 2016 Conference*. Salt Lake City, UT, United States
- [7] Carr J, Baqersad J, Niezrecki C, Avitabile P (2016) Full-Field Dynamic Strain on Wind Turbine Blade Using Digital Image Correlation Techniques and Limited Sets of Measured Data From Photogrammetric Targets. *Exp Tech* 40:819–831. <https://doi.org/10.1007/s40799-016-0082-0>
- [8] Wang W, Xu C, Jin H, et al (2017) Measurement of high temperature full-field strain up to 2000 °C using digital image correlation. *Meas Sci Technol* 28:035007. <https://doi.org/10.1088/1361-6501/aa56d1>
- [9] Yoneyama S (2016) Basic principle of digital image correlation for in-plane displacement and strain measurement. *Adv Compos Mater* 25:105–123. <https://doi.org/10.1080/09243046.2015.1129681>
- [10] Meyer P, Waas AM (2015) Measurement of In Situ-Full-Field Strain Maps on Ceramic Matrix Composites at Elevated Temperature Using Digital Image Correlation. *Exp Mech* 55:795–802. <https://doi.org/10.1007/s11340-014-9979-7>
- [11] Berke RB, Lambros J (2014) Ultraviolet digital image correlation (UV-DIC) for high temperature applications. *Rev Sci Instrum* 85:045121. <https://doi.org/10.1063/1.4871991>
- [12] Reu P (2013) Stereo-rig Design: Lens Selection – Part 3. *Exp Tech* 37:1–3. <https://doi.org/10.1111/ext.12000>
- [13] Reu P (2013) Calibration: A good calibration image. *Exp Tech* 37:1–3. <https://doi.org/10.1111/ext.12059>
- [14] Reu P (2015) All about speckles: Contrast. *Exp Tech* 39:1–2. <https://doi.org/10.1111/ext.12126>
- [15] Lyons JS, Liu J, Sutton MA (1996) High-temperature deformation measurements using digital-image correlation. *Exp Mech* 36:64–70. <https://doi.org/10.1007/BF02328699>

- [16] Grant BMB, Stone HJ, Withers PJ, Preuss M (2009) High-temperature strain field measurement using digital image correlation. *J Strain Anal Eng Des* 44:263–271. <https://doi.org/10.1243/03093247JSA478>
- [17] Chen X, Xu N, Yang L, Xiang D (2012) High temperature displacement and strain measurement using a monochromatic light illuminated stereo digital image correlation system. *Meas Sci Technol* 23:125603. <https://doi.org/10.1088/0957-0233/23/12/125603>
- [18] Blaber J, Adair BS, Antoniou A (2015) A methodology for high resolution digital image correlation in high temperature experiments. *Rev Sci Instrum* 86:035111. <https://doi.org/10.1063/1.4915345>
- [19] Pan B, Wu D, Wang Z, Xia Y (2011) High-temperature digital image correlation method for full-field deformation measurement at 1200 °C. *Meas Sci Technol* 22:015701. <https://doi.org/10.1088/0957-0233/22/1/015701>
- [20] Novak MD, Zok FW (2011) High-temperature materials testing with full-field strain measurement: Experimental design and practice. *Rev Sci Instrum* 82:115101. <https://doi.org/10.1063/1.3657835>
- [21] GraphiteStore.com, Inc. Fine Extruded Graphite Rod, 0.5"OD x 12"L. <http://www.graphitestore.com/fine-extruded-graphite-rod-0-5od-x-12l-nc001325>. Accessed 9 Apr 2018
- [22] OMEGA Engineering, Inc. Thermocouple Type K Reference Table. In: Thermocouples. <https://www.omega.com/prodinfo/thermocouples.html>. Accessed 11 Mar 2018
- [23] Reu P (2013) Stereo-rig Design: Lighting—Part 5. *Exp Tech* 37:1–2. <https://doi.org/10.1111/ext.12020>
- [24] Wang Y. Q., Sutton M. A., Bruck H. A., Schreier H. W. (2009) Quantitative Error Assessment in Pattern Matching: Effects of Intensity Pattern Noise, Interpolation, Strain and Image Contrast on Motion Measurements. *Strain* 45:160–178. <https://doi.org/10.1111/j.1475-1305.2008.00592.x>
- [25] Wang Y-Q, Sutton MA, Ke X-D, et al (2011) On Error Assessment in Stereo-based Deformation Measurements. *Exp Mech* 51:405–422. <https://doi.org/10.1007/s11340-010-9449-9>
- [26] Ke X-D, Schreier HW, Sutton MA, Wang YQ (2011) Error Assessment in Stereo-based Deformation Measurements. *Exp Mech* 51:423–441. <https://doi.org/10.1007/s11340-010-9450-3>

CHAPTER 3  
CHANGE OF EXPOSURE TIME MID-TEST IN HIGH TEMPERATURE  
DIC MEASUREMENT

### **3.1. Prologue**

This chapter presents a full-text paper which was accepted in *Measurement Science and Technology* in March 2020 under the title “Change of Exposure Time Mid-Test in High Temperature DIC Measurement”. The paper is currently in press and will be published shortly. The experiment and data were performed and processed at Utah State University, Logan, UT. The author list is Think Q. Thai, Adam J. Smith, Robert J. Rowley, Paul R. Gradl, and Ryan B. Berke. The original paper is entirely presented below.

### **3.2. Abstract**

Performing Digital Image Correlation (DIC) at extreme temperatures has been greatly challenging due to the radiation which saturates the camera sensor. At such high temperatures, the light intensity emitted from an object is occasionally so powerful that acquired images are overwhelmingly saturated. This induces data loss, potentially ruining the test, thus requiring the user to restart the test. For this reason, selection of an appropriate camera sensitivity plays a crucial role prior to beginning the test. Exposure time is a factor contributing to camera sensitivity and it is the easiest setting to manipulate during the test since it introduces minimal errors when comparing to other factors, especially in quasi-static tests. This paper examines the influence of changing exposure time mid-test on DIC measurement uncertainty. The investigation was conducted by rigid body motion

experiments at room temperature and 1600°C, respectively. Thereby, some recommendations are given to help DIC users assess their images at room temperature to extrapolate the exposure at extreme temperatures along with accompanying solutions to salvage data at high temperature.

Keywords: DIC, extreme temperature, exposure time, ultraviolet light, graphite, Gleeble.

### **3.3. Introduction**

Acquisition of deformation and strain measurements is an important step in designing engineering applications, but deformation and strain are frequently non-uniform. In such cases, it is necessary to get a full field strain map for the purpose of material characterization. Digital Image Correlation (DIC) [1,2] is a non-contacting method which is widely used to obtain full field strain maps by comparing images acquired from high resolution cameras before and after deformation. DIC has many advantages [3,4], including (1) it is non-contacting, (2) it is able to collect full field data and (3) it can be applied in a broad range of length scales from nanoscale [5,6] to meter-scale [7,8] as long as appropriate camera and lenses are provided.

To make meaningful image comparisons, it is pivotal to acquire images with sufficient monochromatic grayscale contrast [9]. There are four main methods to control image contrast [10] including: (i) the aperture on the lens, (ii) the exposure time of the camera, (iii) the intensity of the supplied light source and (iv) the gain of the camera amplifier. Each method has its own pros and cons and, depending on testing conditions, one method could be technically superior to others. For example, during a dynamic test,



exposure time must be kept short to avoid motion blur, but during a quasi-static test, exposure time is allowed to be variable [11].

When performing DIC at temperatures above 550°C, one of the primary challenges is the glowing of objects from black body radiation which deteriorates image contrast [12,13]. It is known that the radiation is much brighter at longer wavelengths (i.e. red and infrared) than it is at shorter wavelengths (i.e. blue and ultraviolet (UV)). Researchers [14–16] have used a blue band-pass filter and external blue illumination to screen out some of the brightest glow, raising the temperature limit at which DIC can be applied without oversaturation to as high as 2000°C [17]. Berke and Lambros introduced a novel variation of DIC named UV-DIC [18], which utilizes UV optics in order to increase the temperature limit even further compared to blue. Under the camera settings used in that study, blue-filtered DIC saturated at as low as 900°C while UV-DIC remained minimally saturated to at least 1125°C. UV-DIC has since been demonstrated to at least 1600°C [19] but its upper temperature limit remains unknown. Thanks to its shorter wavelength, UV-DIC can potentially perform to even higher temperatures than the 2000°C reported for blue-filtered DIC.

Recently, Thai et al. [19] recognized that the upper temperature limit of DIC depends on the camera's sensitivity to light. In that paper, he proposed a normalized metric called Delta ( $\Delta$ ) as a general guideline for setting the exposure time of cameras with different sensitivity. However, his recommendation only considered how to select exposure time at the beginning of a test, which is then left constant for the duration of the test. High temperature tests are expensive and unpredictable, and in some cases, the specimen may emit more light than anticipated prior to testing. The image contrast is thus degraded by

powerful radiation, so maintaining the initial exposure time during the whole test becomes unfeasible. By changing the exposure time during mid-test, DIC users may still be able to get some meaningful data instead of being presented with no data or restarting the experiment.

In this paper, we investigate the influence on DIC measurement uncertainty when changing exposure time during a test. Compared to paper [19], in which camera settings (e.g. exposure time) were selected prior to performing high temperature tests and remained constant, this paper emphasizes changing exposure time in situ during the course of measurement. The effect on DIC measurement is then examined (A) when both images are taken at room temperature; (B) when both images are taken at high temperature; and (C) when the reference image is at room temperature but the deformed image is at high temperature. Experiments were performed at room temperature (RT) and 1600°C, respectively. Having done so, some suggestions are given to DIC users about the alteration of exposure time during a test.

### **3.4. Methods**

Specimens as shown schematically in Figure 3.1(a) were machined from super fine grain, high density, extruded graphite rods purchased from Graphtek LLC. The rods had a length of 152.4 mm (6 in) and diameter of 12.7 mm (0.5 in). A square cross section of 7.62 mm (0.3 in) was machined in order to provide a flat, planar surface on which to perform DIC. The graphite was chosen as the material since it is inexpensive, easily machinable, and has a melting point of 3000°C in vacuum which is beyond the highest temperature in this work (1600°C). A white speckle pattern as shown in Figure 3.1(b) and (c) was applied

using Pyro-Paint 634-AL from Aremco Products Inc. which has a maximum temperature rating of 1760°C, also above the highest temperature explored in this work. The white speckle pattern was applied directly on the graphite's naturally dark background by a splattering method. Prior to testing, the paint was dried at room temperature for 2 hours and then cured at 93°C (200°F) for 2 hours according to the manufacturer's manual. Additionally, an optical imaging system including a UV camera, UV lens, UV lights and UV filter was mounted on a T-slot fixture as shown in Figure 3.1(d). More information on the camera system and related optics can be found in Reference [19].

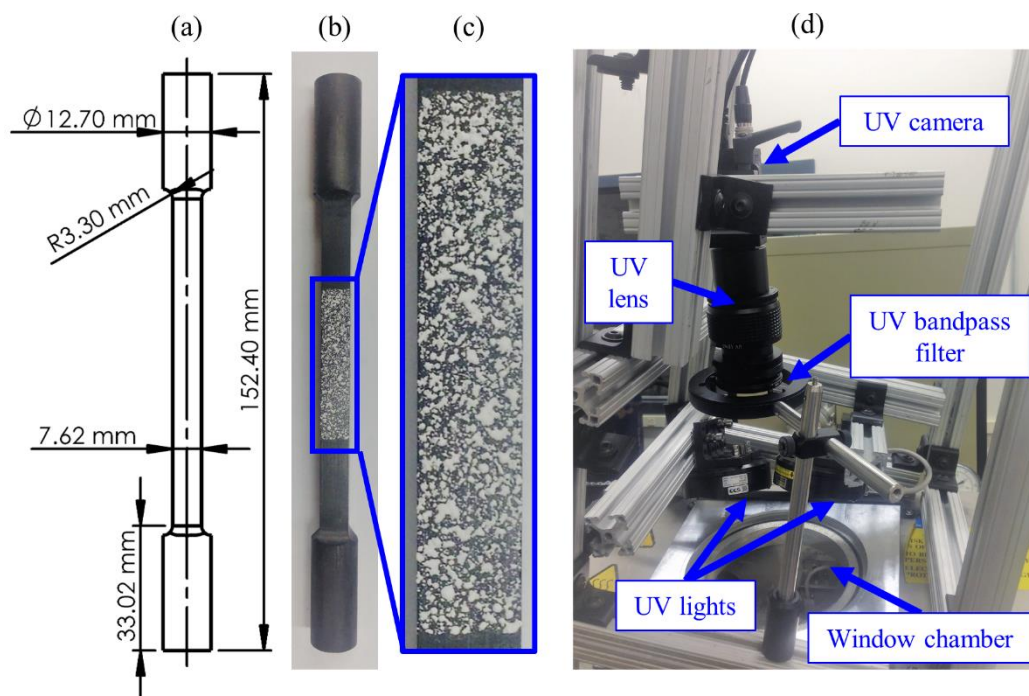


Figure 3.1. (a) A specimen schematic, (b) a photograph of testing specimen, (c) a magnification of speckle pattern, (d) experimental setup of UV optics imaging system

Due to the aggressive oxidation of graphite in air environments, all high temperature testing was performed in vacuum using a Gleeble 1500D thermo-mechanical

system, which heats electrically-conducting specimens via joule heating. A K-type thermocouple was used as feedback control during temperature heating. However, K-type thermocouples are only rated to 1250°C [20] while tests were performed up to 1600°C. For this reason, a modified method was introduced to heat beyond the range of the K-type thermocouple. Since the two ends of specimen were held by cooled grips, a thermal gradient results along the axis of the specimen, with the hottest temperature occurring in the middle of specimen. The specimen was heated twice: first with two thermocouples, TC1 in the middle and TC2 at one end, until TC1 reached a maximum temperature of 1250°C. This established a linearly proportional relationship between the temperatures recorded by the two thermocouples. TC1 was then removed so to not block any cameras' view of the surface for DIC, and TC2 was used for feedback control. More details were presented in [19]. Figure 3.2 shows a thermal image of a heated specimen captured from a FLIR A6751sc IR camera. As can be seen from the figure, the temperature is highest in the middle at 1600°C and decreases steadily towards two ends. Temperatures are linearly proportional to those observed at lower temperatures by both thermocouples.

In order to investigate the effect of only exposure time, all other parameters contributing to camera sensitivity (i.e. UV light intensity, aperture, and gain) remained unchanged. Specifically, the UV light intensity was set to around 60%, the aperture of the lens was 4 and the gain of the camera was 0. The specimen was tested at two different temperature levels: room temperature (RT) and 1600°C. No loads were applied throughout testing. At each temperature level (RT and 1600°C) and at each of value of exposure time (totaling 12 values spanning the full capability of the camera from 500  $\mu$ s to 61,000  $\mu$ s),

two consecutive images at the same state were taken. In total,  $12 \times 2 = 24$  images were captured at room temperature and 24 more at high temperature corresponding to Experiment A and Experiment B in the Results Section.

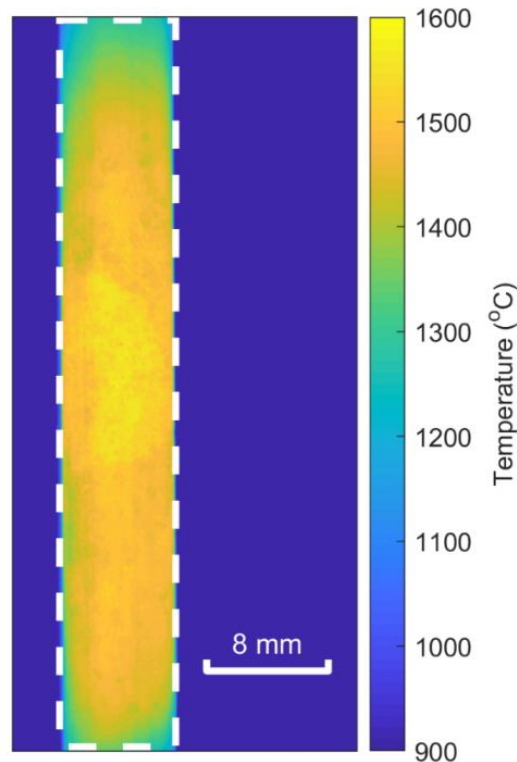


Figure 3.2. The thermal map at 1600°C taken by FLIR IR camera, vertical color bar displays temperature (°C) scale inside white dashed rectangle

Images were then processed using Vic-2D (version 2009), a commercial DIC algorithm from Correlated Solutions Inc. As summarized in Table 3.1, an image at each of the 12 exposure times was correlated against a second image at each of the 12 exposure times, such that each use of Vic-2D involved only 2 images and the analysis was performed  $12 \times 12 = 144$  times for a given temperature. Three cases were studied: (A) both images at room temperature (144 image pairs), (B) both images at 1600°C (144 more image pairs),

and (C) a reference image at room temperature correlated with a deformed image at 1600°C (144 more image pairs). In every correlation, the subset size was 61x61 pixels, the step size was 25 pixels, and the strain window was 15 subsets. The majority of the image pairs did not correlate, and are excluded from the presented data.

Table 3.1. Summary of image pairs used in correlations

	Reference Image		Deformed Images		Image Pairs
A	12 Exposure Times at RT	x	12 Exposure Times at RT	=	144 Image Pairs
B	12 Exposure Times at 1600°C	x	12 Exposure Times at 1600°C	=	144 Image Pairs
C	12 Exposure Times at RT	x	12 Exposure Times at 1600°C	=	144 Image Pairs

Next, the output from Vic-2D was post-processed by MATLAB to compute the mean strain and 95% confidence interval. Since no load was applied, all strain should be nominally zero at any fixed temperature. The mean strain is an indicator of the accuracy of DIC under changing exposure times, while the confidence interval is an indicator of precision. The 95% confidence interval was computed by sorting the strain data in ascending order, then calculating the distance between the 2.5% and 97.5% thresholds of the data.

Exposure time varies from camera to camera. For example, high speed cameras have short exposure time while the slower-speed UV cameras used in this study lean towards longer exposure time. For this reason, a metric of image contrast,  $\Delta$ , was

introduced in order to let DIC users know how to choose an appropriate exposure time value which can be applied to any camera. A detailed computing procedure was presented in [19], but is summarized as follows. The contrast  $\Delta = Z_2 - Z_1$  is the difference in grey values between a “typical” dark speckle ( $Z_1$ ) and a “typical” bright speckle ( $Z_2$ ), as recommended by Phillip Reu [21]. In this case,  $Z_1$  and  $Z_2$  are selected by the range of the median 90% of pixels in the image. As illustrated in Figure 3.3, the histogram is integrated from 0 until reaching 5% of the total pixels, and that greyscale value represents a “typical dark pixel” which is called  $Z_1$ . Similarly, the histogram is integrated from 0 until reaching 95% of the total pixels, and that greyscale value represents a “typical bright pixel” called  $Z_2$ . A “good” contrast is when  $\Delta \geq 50$  [22] and  $Z_2 < 255$  (less than 5% of saturated pixels) for an 8-bit camera.

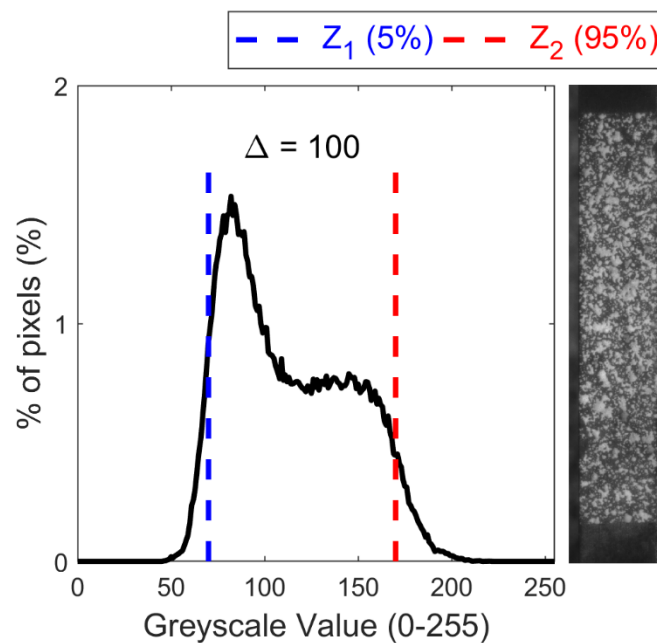


Figure 3.3. Example of 90% confidence interval approach with respective speckle pattern, using room temperature data at exposure time of 20,000  $\mu\text{s}$

Table 3.2 shows the  $Z_1$ ,  $Z_2$ , and  $\Delta$  for each of the 12 exposure times at RT and 1600°C, respectively. In general,  $Z_1$  and  $Z_2$  increase with higher temperature and higher exposure times until  $Z_2$  reaches 255 (saturation). Consequently,  $\Delta$  decreases at very high exposure times. The table also shows the percentage of pixels which are saturated in each of the images. Note that whenever this percentage is 5 or larger,  $Z_2$  is always 255.

Table 3.2. Raw data of  $\Delta$  calculation at RT and 1600°C

Exposure time	Room temperature				1600°C			
	$Z_1$	$Z_2$	$\Delta$	% of saturated pixels	$Z_1$	$Z_2$	$\Delta$	% of saturated pixels
500 $\mu$ s	8	12	4	0	9	12	3	0
2,500 $\mu$ s	15	28	13	0	19	31	12	0
5,000 $\mu$ s	23	49	26	0	30	55	25	0
10,000 $\mu$ s	38	89	51	0	53	103	50	0
20,000 $\mu$ s	70	170	100	0	99	196	97	0
30,000 $\mu$ s	100	249	149	3.57	144	255	111	20.00
40,000 $\mu$ s	131	255	124	31.41	190	255	65	56.10
45,000 $\mu$ s	146	255	109	41.45	213	255	42	73.83
50,000 $\mu$ s	161	255	94	49.86	236	255	19	88.28
55,000 $\mu$ s	176	255	79	57.81	255	255	0	95.85
58,000 $\mu$ s	185	255	70	62.81	255	255	0	97.92
61,000 $\mu$ s	194	255	61	67.96	255	255	0	98.93



### 3.5. Results

#### A. Change of exposure time during isothermal testing (Room temperature)

Figure 3.4 shows all pairs in which images at room temperature are able to be correlated against each other. There are 27 pairs which are successfully correlated in the total of 144 pairs as introduced in Table 3.1 at room temperature. The blue dashed line indicates no change of exposure time. It can be seen that for low exposure times (10,000  $\mu\text{s}$  and below in this paper), exposure time cannot be changed. However, for high reference exposure times, exposure time can be changed and higher reference exposure times give narrower ranges of alteration.

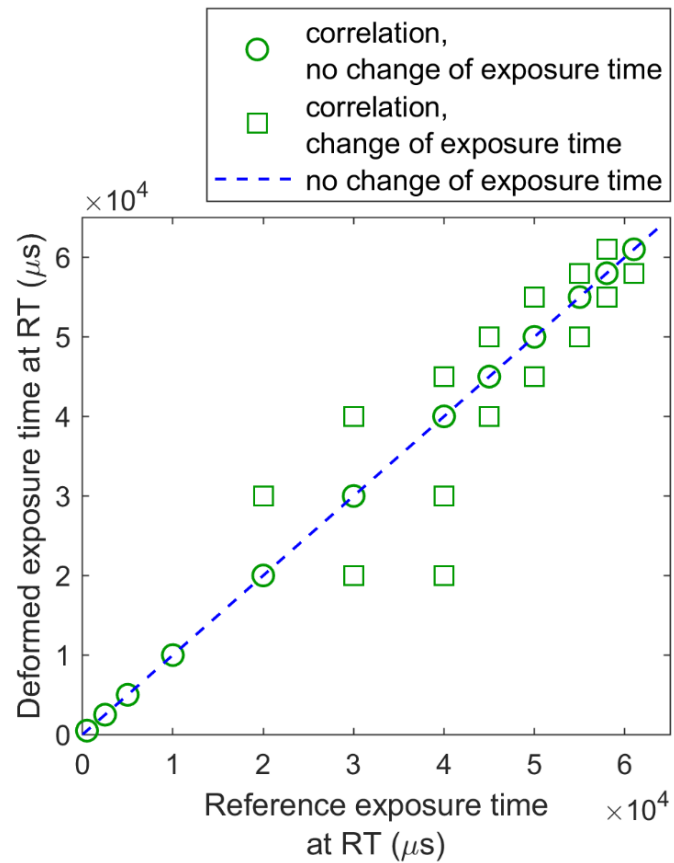


Figure 3.4. Image pairs which successfully correlated at room temperature

Figure 3.5 shows the (a) axial displacement  $u$  and (b) axial normal strain  $\epsilon_{xx}$  measured by DIC for each correlation pair from Figure 3.4, along with the 95% uncertainty band. Only the image pairs which successfully correlated are included in the figure. The legend indicates the reference exposure time while the horizontal axis indicates the exposure time of the deformed images. For any data points having the same value of exposure time, they are displaced slightly in order to avoid excessive overlapping of data markers. The experiment was purely static, therefore  $u$  displacement and strain  $\epsilon_{xx}$  should both nominally be zero. As can be confirmed from Figure 3.5, zero falls within the 95% uncertainty bands of about 95% of all displacement and strain measurements, which is in good agreement with no applied loading. Due to the similarity in results of  $u$  displacement and strain  $\epsilon_{xx}$ , only strain  $\epsilon_{xx}$  are presented in the subsequent figures to keep the writing to be more concise. Furthermore, as the mean strains are all nominally zero, subsequent figures will compare just the sizes of the uncertainty bands instead of showing full-range of the uncertainty bands.

In order to present results which can be generalized to other cameras, the exposure times of the deformed images have been converted into  $\Delta$  as shown in Figure 3.6. The vertical axis is the size of the 95% uncertainty band while the horizontal axis is  $\Delta$  of the deformed images. It can be inferred that of the image pairs studied, when  $\Delta < 50$  the exposure time is unable to change and still successfully correlate between two images. If  $\Delta > 50$ , it is possible to change exposure time, but the size of the uncertainty band always increases to result in V-shaped plots. In cases when there is no change of exposure time, higher  $\Delta$  generally gives lower uncertainty.

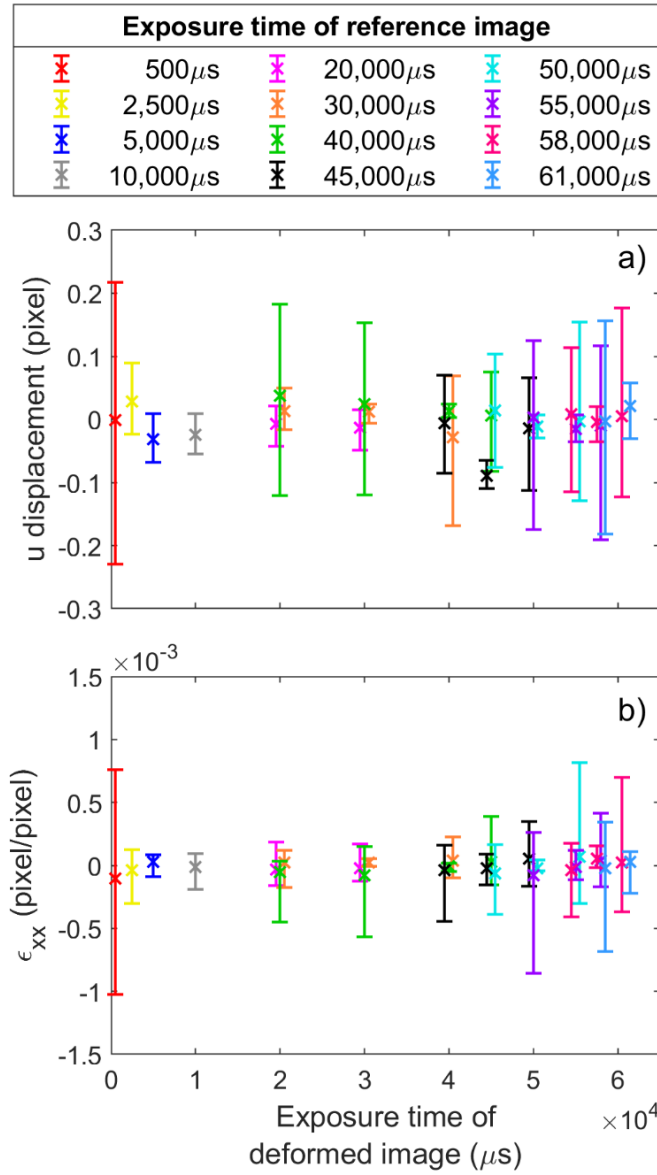


Figure 3.5. 95% uncertainty band when changing exposure time at room temperature

illustrated by (a) u displacement and (b) strain  $\epsilon_{xx}$

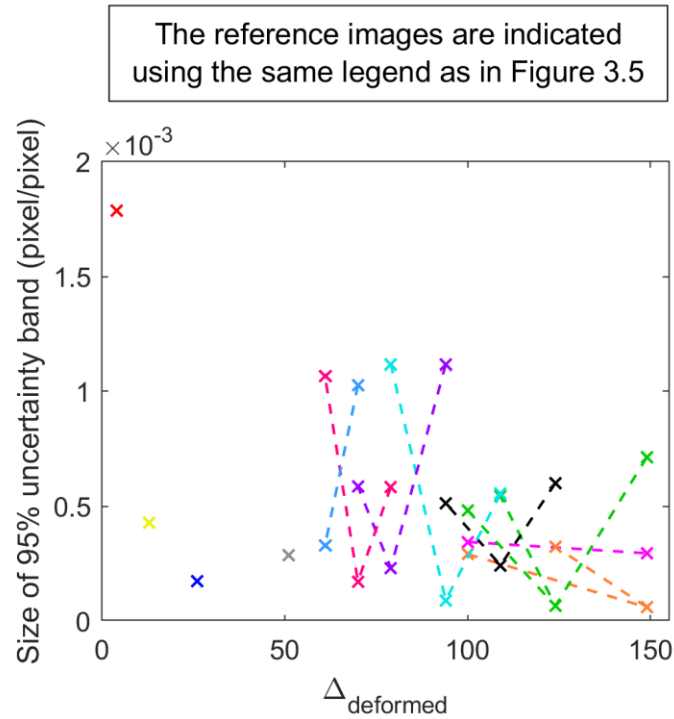


Figure 3.6. Influence of changing exposure time on uncertainty band at RT illustrated via  $\Delta$

Figure 3.7 shows the relationship between the size of the uncertainty band vs how far  $\Delta$  is changed. It can be deduced that at higher reference exposure times, a minor variation of  $\Delta$  results in a marked increase in uncertainty. This is demonstrated in Figure 3.7 thanks to the steeper slope of the dashed lines at longer reference exposure times.

Figure 3.8 is a further investigation where the slope of the data in Figure 3.7 is compared to  $\Delta$  of the reference images. Overall, once  $Z_2 = 255$ , longer reference exposure times lead to smaller  $\Delta$  and higher slope.

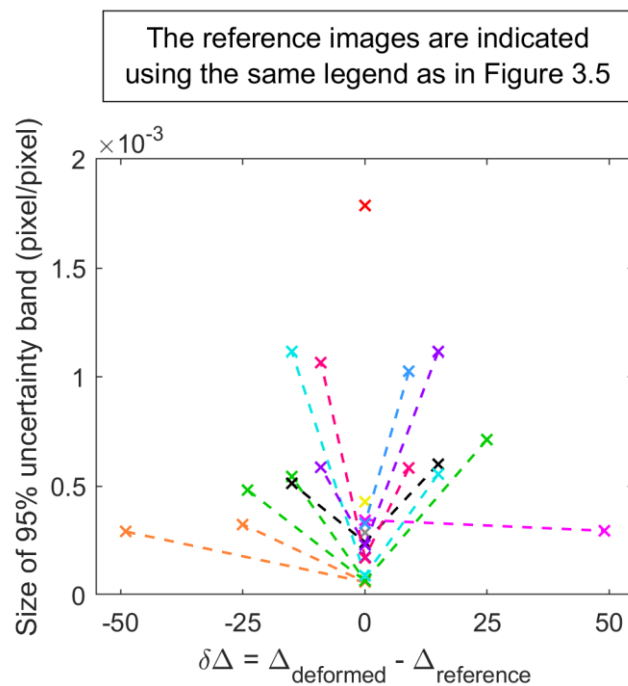


Figure 3.7. Relationship of 95% uncertainty band and  $\Delta$  variation at various exposure times

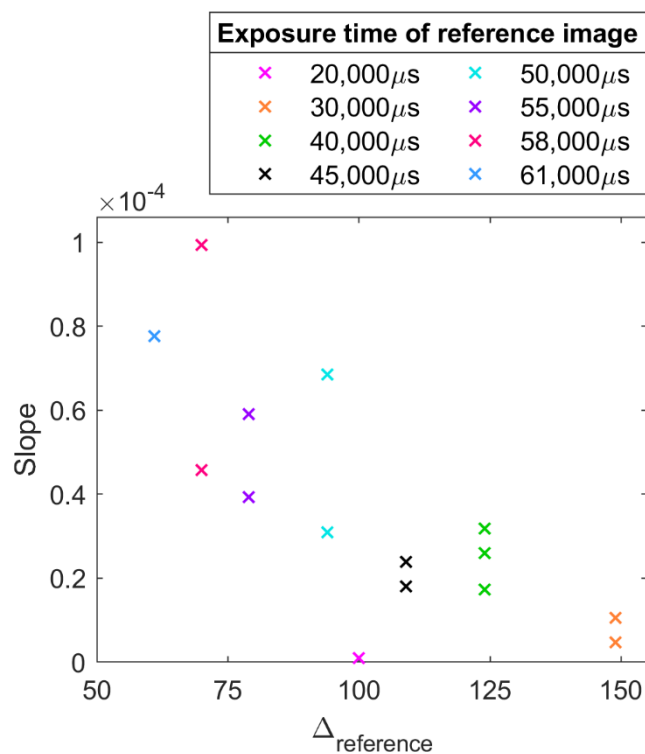


Figure 3.8. Investigation of slope with respect to  $\Delta$  of reference images

### B. Change of exposure time during isothermal testing (Extreme temperature – 1600°C)

The testing in this section is similar to Result A with the only difference being that the tests were performed at 1600°C. At such high temperatures, the specimen emits light in the form of blackbody radiation which can saturate the recorded images [18]. For this reason, there are 10 pairs which are successfully correlated in the total of 144 pairs as shown in Figure 3.9. This is lower when compared to the 27 successfully correlated pairs at room temperature. For the camera equipment and settings used in this study, images with exposure times above 45,000  $\mu\text{s}$  were too saturated to perform DIC, regardless of which other images they were correlated against as indicated by the red shaded region in Figure 3.9. Accordingly, only exposure times of 45,000  $\mu\text{s}$  and below are plotted in this section.

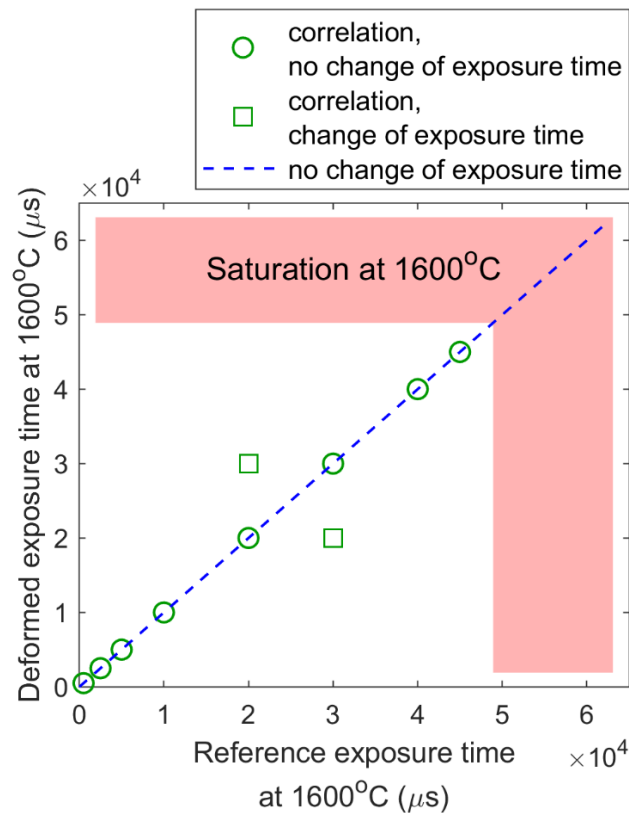


Figure 3.9. Image pairs which successfully correlated at 1600°C

Figure 3.10 presents the 95% uncertainty band of (a)  $u$  displacement and (b) strain  $\epsilon_{xx}$  during alteration of exposure time at 1600°C, comparable to Figure 3.5. The exposure time of the reference images are listed in the legend of the figure. In general, all displacements and strains are centered around zero which matches the condition of no applied loading. This is demonstrated that the 95% uncertainty bands cover zero in about 95% of all measurements which is in good agreement with the definition of 95% uncertainty band. Once again, only the size of the uncertainty bands in Figure 3.10(b) are reported in subsequent figures.

Figure 3.11 shows the conversion of the exposure time from the deformed image to  $\Delta$  at 1600°C, similar to the result of Figure 3.6 at room temperature. Once again, if the initial  $\Delta < 50$ , there is no chance for two images of different exposure times to be correlated. At high temperature, there is less chance for two images of different exposure times to be correlated due to the considerable decrease of how many images have  $\Delta > 50$ . In this data set, only two image pairs with differing exposure times are able to correlate, so no further examination of slopes is performed.

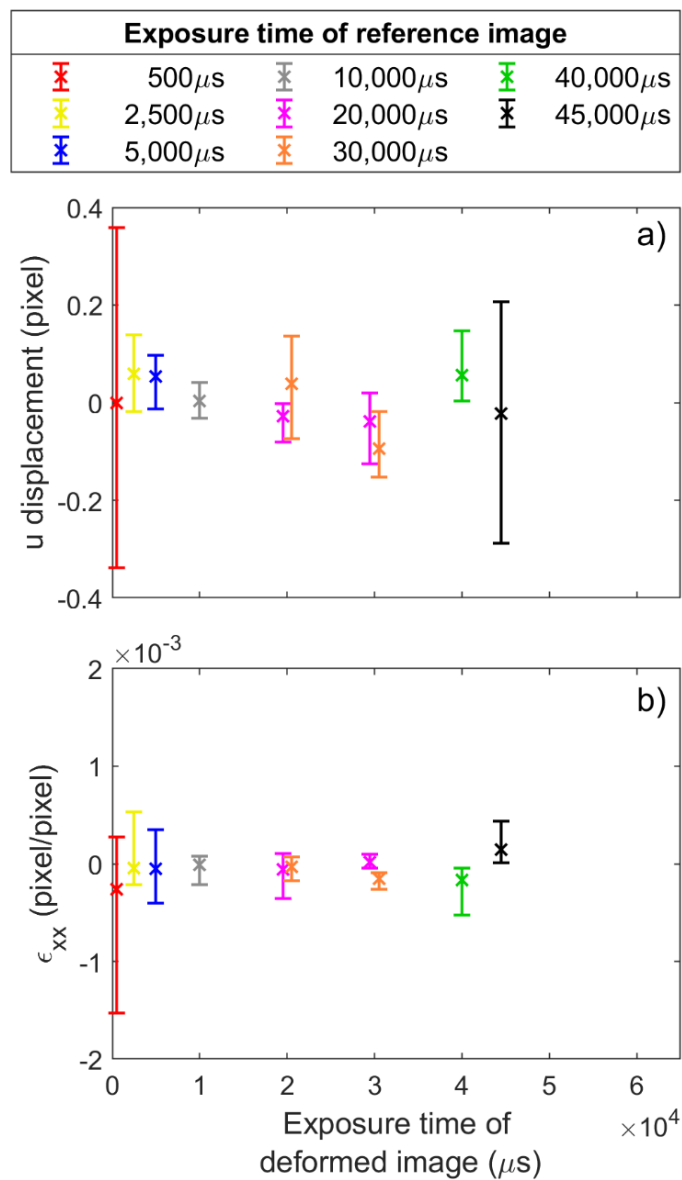


Figure 3.10. 95% uncertainty band when changing exposure time at 1600°C illustrated by

(a) u displacement and (b) strain  $\epsilon_{xx}$



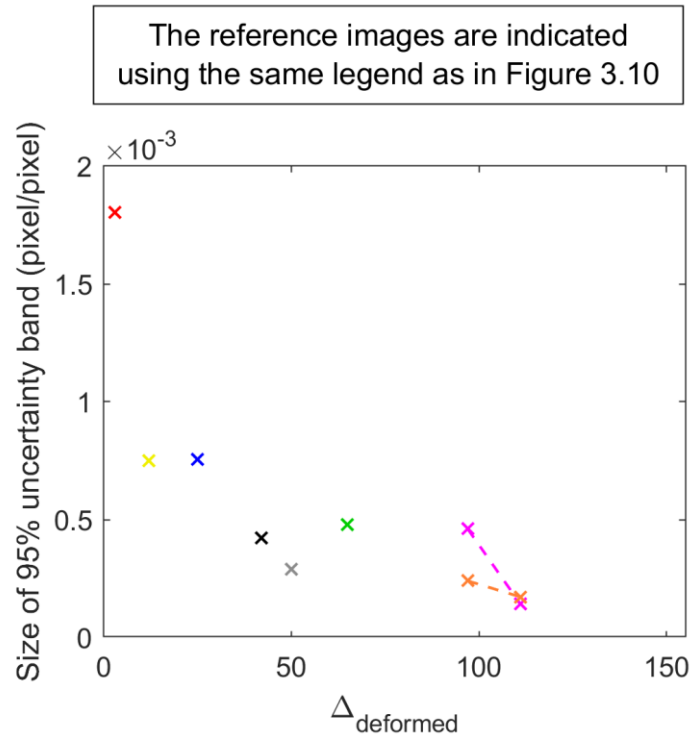


Figure 3.11. Influence of changing exposure time on uncertainty band at 1600°C illustrated via  $\Delta$

### C. Change of exposure time during mid test (i.e. different temperatures)

In this section, the analysis of the previous two sections is repeated again, using a reference image at room temperature and a deformed image at 1600°C. Compared to the previous high temperature result (Result B), in which all exposure times over 45,000  $\mu\text{s}$  failed to correlate, Figure 3.12 shows that exposure times of 50,000  $\mu\text{s}$  and 61,000  $\mu\text{s}$  at room temperature were able to correlate against images at 30,000  $\mu\text{s}$  and 40,000  $\mu\text{s}$ , respectively. Similarly, initial exposure times of 30,000, 40,000, and 45,000  $\mu\text{s}$  at room temperature were unable to correlate against images at the same exposure time at high temperature, but were able to correlate with other images at reduced exposure times. For

the cameras used in this paper, all initial exposure times exceeding 20,000  $\mu\text{s}$  at room temperature are required to reduce at high temperature in order to get successful correlation. Otherwise, they lose correlation due to saturation as indicated by the red shaded region in Figure 3.12.

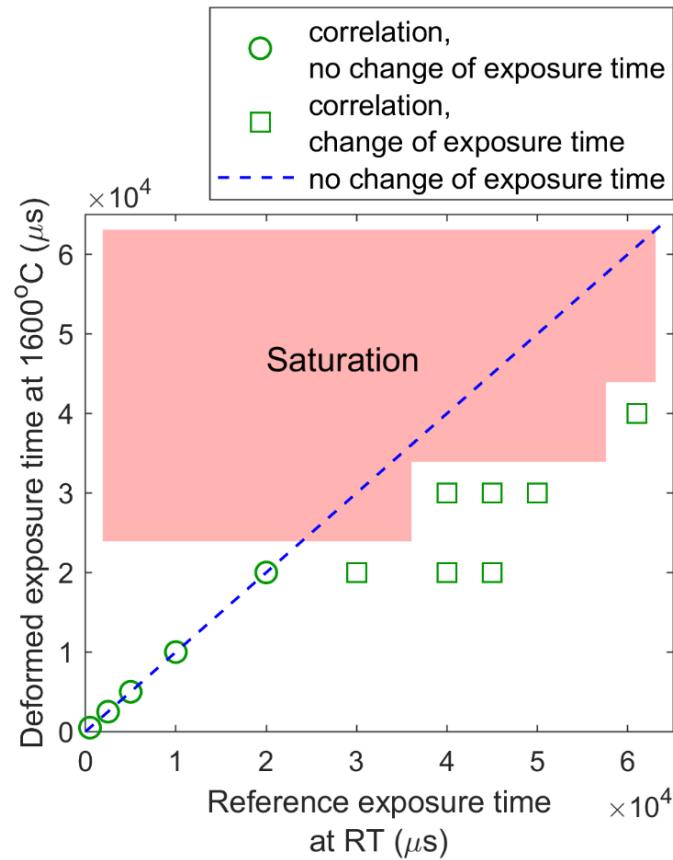


Figure 3.12. Image pairs which successfully correlated at RT vs 1600°C

Figure 3.13 adopts the identical approach of Figure 3.5 at room temperature as well as Figure 3.10 at high temperature. However, the mean displacement and strain are no longer zero indicating non-uniform thermal expansion which takes place between the reference and deformed images. Consequently, the size of the uncertainty band is no longer a meaningful metric of measurement uncertainty, so no analysis of slopes is performed.

Instead, Figure 3.14 shows the non-uniform thermal strain due to the non-uniform temperature gradients as demonstrated in Figure 3.2.

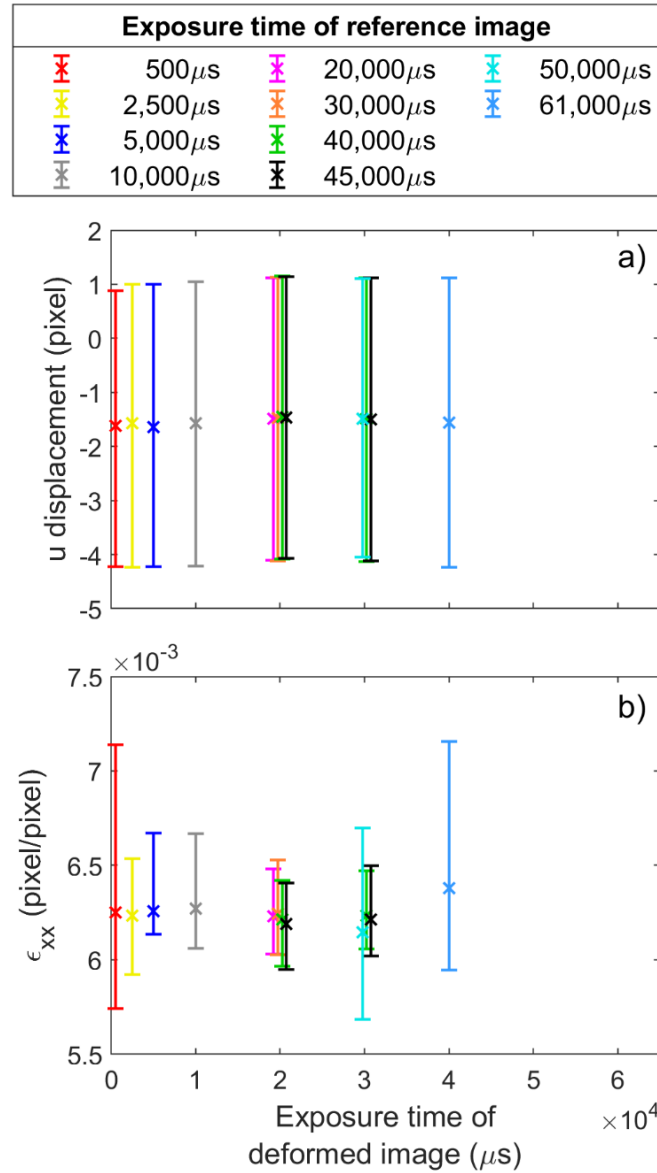


Figure 3.13. 95% uncertainty band when changing exposure time during mid test

illustrated by (a) u displacement and (b) strain  $\epsilon_{xx}$

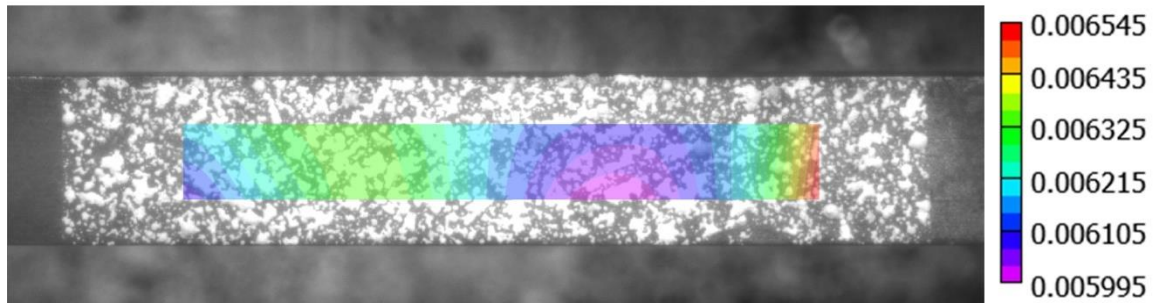


Figure 3.14. Non-uniform thermal strain from correlation of 45,000  $\mu\text{s}$  at room temperature against 30,000  $\mu\text{s}$  at 1600°C

### 3.6. Discussion

In our previous paper [19], we recommended two criteria for good contrast when performing DIC at extreme temperature. First, at room temperature the exposure time should be kept as small as possible while maintaining  $\Delta > 50$ , leaving the most room for  $Z_1$  and  $Z_2$  to increase as the images brighten at high temperature. Second, we recommended avoiding any images in which  $Z_2$  equals the maximum value of the sensor (255 for an 8-bit camera), as this would indicate that over 5% of all pixels have already saturated at the start of the test, and contrast can only worsen with increasing temperature. In that study, exposure time remained constant for each image pair.

It can be inferred from Figure 3.4 and Figure 3.5 that there is no possibility of changing exposure time even at RT when initial exposure time is set too low ( $\leq 10,000 \mu\text{s}$  for the camera in this paper). The reason comes from the excessive darkness of the images, as is demonstrated at low values of  $\Delta$  in Figure 3.6. This confirms that, of the image pairs studied, there is no chance to alter exposure time if  $\Delta < 50$ . When  $\Delta > 50$ , it becomes possible to change exposure time within a limited range from the reference exposure time, but the

uncertainty band becomes larger as demonstrated by the V-shaped plots in Figure 3.6. This is reasonable since varying the exposure time of the correlated images leads to a change of contrast which results in higher uncertainty of the DIC algorithm. In general, higher  $\Delta$  gives a smaller uncertainty and allows for modest changes in exposure time.

Figure 3.7 and Figure 3.8 further explore how far exposure time can be changed from the initial value at a fixed temperature. In general, larger initial values of  $\Delta$  have more space to change exposure time and show a smaller increase of uncertainty when exposure time is changed. Additionally, when changing exposure time, it is advised to change by small amounts. Larger changes result in higher uncertainty (as presented in Figure 3.7). Moreover, it is interestingly noted from Figure 3.8 that even at the same  $\Delta$ , higher slopes (i.e. higher sensitivity of error) take place at higher reference exposure times (when comparing 20,000  $\mu\text{s}$  to 45,000  $\mu\text{s}$  and 50,000  $\mu\text{s}$ ). This can be explained using Table 3.2, which shows that the images with exposure times of 45,000  $\mu\text{s}$  and 50,000  $\mu\text{s}$  have  $Z_2 = 255$ . Such images have more than 5% of their pixels already saturated and thus are more likely to add more errors into DIC when exposure time is changed.

When it comes to high temperature, it is once more observed that when  $\Delta < 50$  exposure time cannot be changed at a fixed temperature, and in all cases when exposure time can be changed  $\Delta > 50$ . Also, it is noted that since images get brighter at high temperature due to thermal radiation, it is advised to set the initial exposure time low at room temperature in order to avoid saturation at high temperature.

In the event when images glow brightly at high temperatures, camera settings which produced sufficient contrast at low temperature may produce saturated images at high

temperatures. For those situations, in order to salvage some data, it may be better to reduce the exposure time rather than lose all data due to saturation. To illustrate, Figure 3.12 shows all pairs in which an image at room temperature (horizontal axis) successfully correlated against an image at high temperature (vertical axis). The blue dashed line indicates no change of exposure time. It can be seen that for low exposure times (green circle data points), it is not necessary to change exposure time at high temperatures. However, for high initial exposure times (green square data points), the only successful correlations involved reducing exposure time at high temperature. Thus, by reducing exposure time at high temperature, a DIC user can salvage some data rather than no data, but should expect higher uncertainty as a trade-off.

Figure 3.15 shows  $Z_1$ ,  $Z_2$ , and  $\Delta$  for all 144 image pairs between room temperature and high temperature. The data are sorted into four quadrants depending on whether  $Z_2 = 255$  in the room temperature image, high temperature image, neither, or both. Additionally, the image pairs which correlated in Figure 3.12 are plotted as circles or squares. Each plot also includes a red dashed line, indicating no change of  $Z_1$ ,  $Z_2$ , or  $\Delta$ ; and a blue dashed line, indicating no change of exposure time. The dashed lines include image pairs which did not successfully correlate.

Figure 3.15(a) shows that when neither image saturates ( $Z_2 = 255$ ), no change of exposure time is needed; but if one or both images saturate, successful correlations occurred when the exposure time was reduced to maintain similar values of  $Z_1$  in both images. Figure 3.15(b) contains many overlapping points in which one or both images have  $Z_2 = 255$ , but in general the successful correlations also occur when  $Z_2$  of both images

remain similar. Figure 3.15(c) is much messier than parts (a) or (b), but generally agrees with Figure 3.15(a) that when neither image saturates no change of exposure time is needed, but when one or both images saturate  $\Delta$  can only change and still result in successful correlation if it started relatively large (on the order of 100). Figure 3.15(c) also shows that changes of exposure time must be relatively small to maintain correlation.

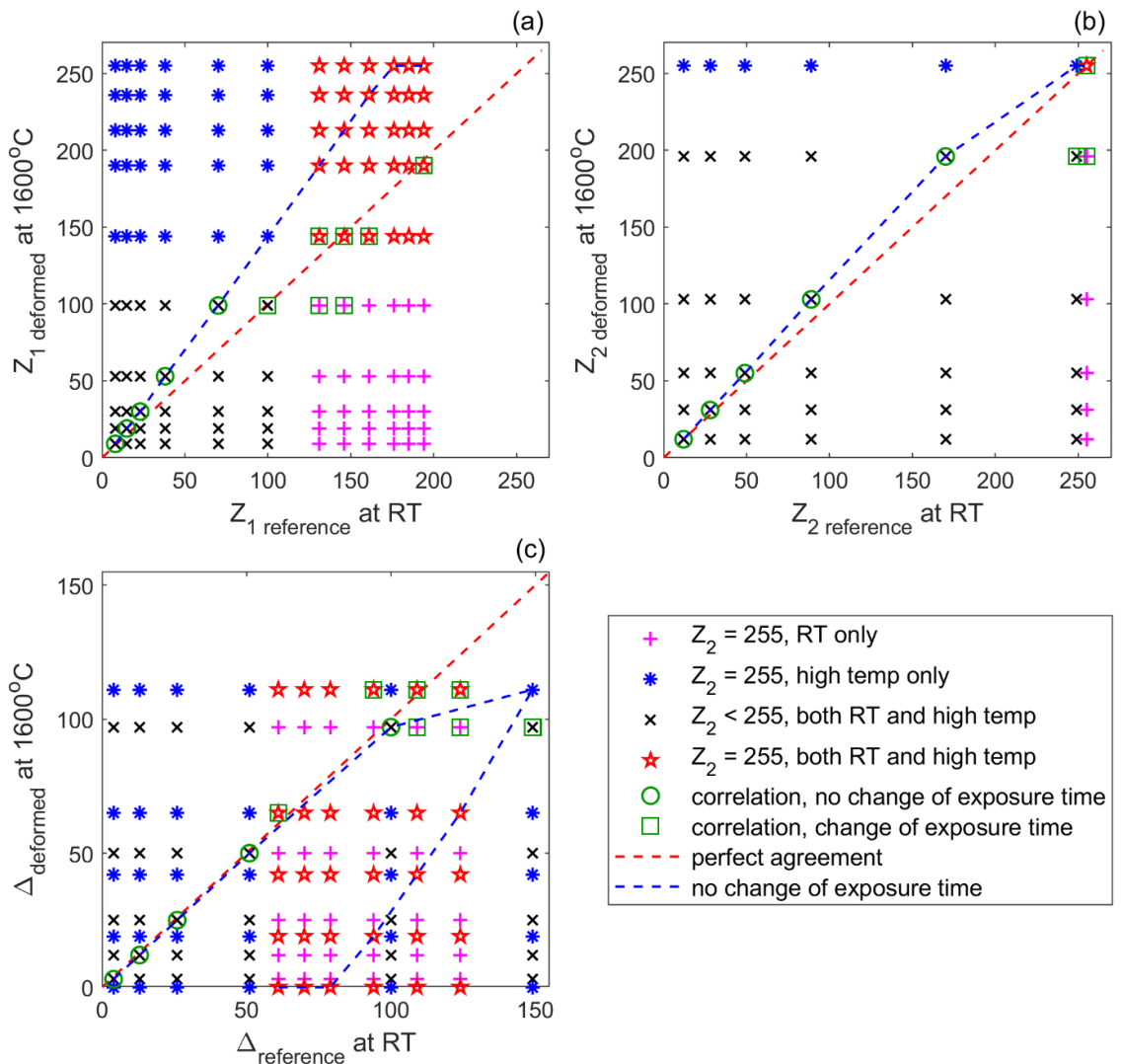


Figure 3.15. Correlation of image pairs at RT vs 1600°C when investigating via

(a)  $Z_1$ , (b)  $Z_2$  and (c)  $\Delta$

It is known that there are other ways to manipulate brightness besides exposure time and the findings from this paper can potentially apply to most of them. In this paper, exposure time was manipulated since the tests were quasi-static. In other cases like a dynamic test, exposure time must be kept short to prevent motion blur. In that case, by using the metric of  $\Delta$ , similar results are expected by (i) increasing or decreasing the amount of externally supplied light, (ii) broadening or narrowing the aperture on the lens, or (iii) increasing or decreasing the gain on the camera sensor – though it should be noted that the Vic-3D documentation strongly advises against using gain as a source of brightness [23].

### **3.7. Conclusions**

This paper investigated the effect of changing exposure time during the use of Digital Image Correlation (DIC) in (A) isothermal testing at room temperature, (B) isothermal testing at high temperature, and (C) variable temperature testing from room temperature to 1600°C. In summary, the contrast of an image can be quickly judged by the metric of delta ( $\Delta$ ), which takes the difference between a typical dark pixel ( $Z_1$ ) and a typical bright pixel ( $Z_2$ ), spanning 90% of all pixels in the image. As long as  $\Delta > 50$  and  $Z_2$  does not equal 255 (for an 8-bit camera), exposure time can be changed in the middle of test, although it results in higher uncertainty. In order to minimize uncertainty and maximize the ability to correlate with different exposure times,  $\Delta$  should be as high as possible in the room temperature image. Although changes to exposure time should be minimal in order to minimize uncertainty, in some cases it may be better to change exposure time in order to salvage some data rather than lose the data completely.



### 3.8. Acknowledgements

This work was funded in part by a grant from NASA's Marshall Space Flight Center (award # 80MSFC18M0009) and by the Utah State University Office of Research and Graduate Studies.

### 3.9. References

- [1] Sutton M A, Orteu J J and Schreier H 2009 *Image Correlation for Shape, Motion and Deformation Measurements: Basic Concepts, Theory and Applications* (Springer US)
- [2] Pan B 2018 Digital image correlation for surface deformation measurement: historical developments, recent advances and future goals *Meas. Sci. Technol.* **29** 082001
- [3] Pan B, Qian K, Xie H and Asundi A 2009 Two-dimensional digital image correlation for in-plane displacement and strain measurement: a review *Meas. Sci. Technol.* **20** 062001
- [4] Gradl P R 2016 Digital Image Correlation Techniques Applied to Large Scale Rocket Engine Testing *52nd AIAA/SAE/ASEE Joint Propulsion Conference AIAA Propulsion and Energy Forum* (American Institute of Aeronautics and Astronautics)
- [5] Wang X, Pan Z, Fan F, Wang J, Liu Y, Mao S X, Zhu T and Xia S 2015 Nanoscale Deformation Analysis With High-Resolution Transmission Electron Microscopy and Digital Image Correlation *J. Appl. Mech.* **82** 121001-121001-9
- [6] Sabaté N, Vogel D, Gollhardt A, Marcos J, Gràcia I, Cané C and Michel B 2006 Digital image correlation of nanoscale deformation fields for local stress measurement in thin films *Nanotechnology* **17** 5264
- [7] Li L-G, Liang J, Guo X, Guo C, Hu H and Tang Z-Z 2014 Full-field wing deformation measurement scheme for in-flight cantilever monoplane based on 3D digital image correlation *Meas. Sci. Technol.* **25** 065202
- [8] Rizo-Patron S and Sirohi J 2017 Operational Modal Analysis of a Helicopter Rotor Blade Using Digital Image Correlation *Exp. Mech.* **57** 367-75
- [9] Yoneyama S 2016 Basic principle of digital image correlation for in-plane displacement and strain measurement *Adv. Compos. Mater.* **25** 105-23

- [10] Thai T Q 2018 *Importance of Exposure Time on Digital Image Correlation (DIC) at Extreme Temperatures* All Graduate Theses and Dissertations. 7067 (Utah State University)
- [11] Reu P 2013 Calibration: A good calibration image *Exp. Tech.* **37** 1–3
- [12] Grant B M B, Stone H J, Withers P J and Preuss M 2009 High-temperature strain field measurement using digital image correlation *J. Strain Anal. Eng. Des.* **44** 263–71
- [13] Chen X, Xu N, Yang L and Xiang D 2012 High temperature displacement and strain measurement using a monochromatic light illuminated stereo digital image correlation system *Meas. Sci. Technol.* **23** 125603
- [14] Novak M D and Zok F W 2011 High-temperature materials testing with full-field strain measurement: Experimental design and practice *Rev. Sci. Instrum.* **82** 115101
- [15] Pan B, Wu D, Wang Z and Xia Y 2011 High-temperature digital image correlation method for full-field deformation measurement at 1200 °C *Meas. Sci. Technol.* **22** 015701
- [16] Blaber J, Adair B S and Antoniou A 2015 A methodology for high resolution digital image correlation in high temperature experiments *Rev. Sci. Instrum.* **86** 035111
- [17] Wang W, Xu C, Jin H, Meng S, Zhang Y and Xie W 2017 Measurement of high temperature full-field strain up to 2000 °C using digital image correlation *Meas. Sci. Technol.* **28** 035007
- [18] Berke R B and Lambros J 2014 Ultraviolet digital image correlation (UV-DIC) for high temperature applications *Rev. Sci. Instrum.* **85** 045121
- [19] Thai T Q, Hansen R S, Smith A J, Lambros J and Berke R B 2019 Importance of Exposure Time on DIC Measurement Uncertainty at Extreme Temperatures *Exp. Tech.* **43** 261–71
- [20] OMEGA Engineering, Inc. Thermocouple Type K Reference Table *Thermocouple Types*
- [21] Reu P 2015 All about speckles: Contrast *Exp. Tech.* **39** 1–2
- [22] Reu P 2013 Stereo-rig Design: Lighting—Part 5 *Exp. Tech.* **37** 1–2
- [23] Simonsen M Vic-3D Application Note: Using Gain in Vic-Snap

CHAPTER 4  
SPECKLE PATTERN INVERSION IN HIGH TEMPERATURE  
DIC MEASUREMENT

#### **4.1. Prologue**

This chapter presents a paper which is in preparation to be submitted to a peer-reviewed journal. The experiment and data were performed and processed at Utah State University, Logan, UT. The entire paper is presented below.

#### **4.2. Abstract**

During hot fire rocket engine testing, non-contacting measurements are superior to bonded gauges because they are immune to burning, shaking loose, or damage due to the harsh testing conditions. Additionally, when compared to instruments which register at single points, Digital Image Correlation (DIC) has the added benefit in that it collects full-field displacement and strain maps over the duration of the test. However, for certain materials and paints under some circumstances of temperature and camera sensitivity, portions of the speckle pattern which were darker at room temperature may emit more light compared to the initially lighter portions of the pattern, resulting in a high temperature pattern which is inverted in comparison with that at room temperature. To address this inversion, a post-processing method is introduced wherein an inverted image containing only emitted light is subtracted from an image containing both emitted and reflected light, thereby generating an un-inverted image. The artificial high temperature image is subsequently correlated against the room temperature image to obtain full-field strains. The

subtraction technique is then validated using optical bandpass filters to prevent significant amounts of emitted light from reaching the camera sensor.

Keywords: DIC, high temperature, inversion, ultraviolet light, graphite, Gleeble.

### **4.3. Introduction**

High temperature applications create an extremely demanding environment for which engineered components must survive [1]. One such application is for liquid rocket engine combustion device components, such as nozzles and combustion chambers [2, 3]. As components are developed for these applications, validated test data is required to understand performance and predict life in these extremely challenging environments for continued operation. Strain gauges are a common traditional technique to obtain the response to surface stresses and attached with an adhesive or through spot welding [4]. There are a few challenges with strain gauges in these high temperature environments. The first challenge with this contact instrumentation method is the durability in the environment and rarely survives more than a few seconds. The second challenge is that strain gauges measure only a discrete and local response. A third challenge is the selection of orientation through uni, bi, or triaxial applications. This limits the directional response of which the strains are measured and could also result in inaccurate predictions.

One such solution to resolve the issues with strain gauges is the use of non-contact methods, such as Digital Image Correlation (DIC) [5]. DIC offers full two-dimensional or three-dimensional line of sight non-contact measurement technique to obtain surface strain independent of location. DIC uses a single camera for 2D or a pair of digital cameras for 3D along with a stochastic speckle pattern on the surface being measured to obtain full surface

strain measurements and deflections of the surface [6, 7]. This provides significantly more data than traditional methods using contact instrumentation.

DIC techniques have been successfully demonstrated through a host of aerospace applications. For example, the National Aeronautics and Space Administration (NASA) demonstrated the use of DIC during J-2X engine development testing on components that had surface temperatures greater than 200°C [8]. For high temperature uncooled nozzle extensions on liquid rocket engines, DIC techniques have been successfully applied to Carbon-Carbon (C/C) and Ceramic Matrix Composite (CMC) materials in laboratory testing [9]. Additionally, NASA and commercial partners have demonstrated their use during hot-fire testing at elevated temperatures above 1370°C [10, 11]. More recently, DIC is reported to measure strains at 2000°C [12] or even up to 3000°C [13] in laboratory environments by using a blue filter and blue optics to mitigate the powerful glowing due to radiation.

Recently, NASA attempted to collect DIC data during hot-fire testing, but discovered a challenge that was not previously observed [10]. The nozzle extensions were speckled with the black and white stochastic pattern per standard methods. Visibly at room temperature, the white paint had good contrast with the black C/C composite material. During heating of the nozzle extension, a majority of the elevated temperature was saturated and the contrast inverted where the C/C material was high intensity and the paint was low intensity. This data was collected in the visible spectrum with no filtering.

In this paper, we investigate the physical principle behind the speckle pattern inversion. It is well known that objects at high temperature emit light to the black body radiation of Planck's law [14, 15]. Due to the difference in emissivity of the light speckle

paint and the dark background material, then at high temperatures the background can emit more light than the speckle. Thus, the inverted pattern is due only to emitted light, while the initially un-inverted pattern is due only to reflected light. If the camera sensitivity is high enough, the inverted pattern emitted by the specimen can overwhelm the non-inverted pattern reflected by the specimen. Two methods are presented to mitigate this inversion: (A) subtracting an inverted image which contains only emitted light from an inverted image which contains both emitted and reflected light, thereby artificially producing an un-inverted image; and (B) using an ultraviolet (UV) bandpass filter to prevent the emitted light from ever reaching the camera sensor. The UV-DIC technique was first presented by Berke and Lambros at 1125°C [16] and later extended by Thai et al. to 1600°C [17]. Compared to the subtraction technique, UV-DIC is preferable because the subtraction technique requires two images which could potentially have applied motion between them, although both techniques are sufficient under quasi-static conditions.

#### **4.4. Methods**

A series of thermo-mechanical experiments were performed using the equipment and procedures previously established in references [18, 19]. The specimens were graphite rods with diameter of 12.7 mm (0.5 in) purchased from Graphtek LLC. Graphite rods were then machined with a length of 152.4 mm (6 in) and a square cross-section gauge length of 7.62 mm (0.3 in) in the middle as depicted in Figure 4.1(a). The speckle is created by applying the white paint of Pyro-Paint 634-AL on the naturally dark background of graphite. The paint was cured according to the manufacturer's manual prior to starting the experiment. The specimens were monitored throughout testing by a UV camera (JAI CM-

140GE-UV) equipped with a 60 mm optical lens (Nikon AF Micro Nikkor) and a UV bandpass filter (XNite 330C M58 from LDP LLC) as shown in Figure 4.1(b). The filter was fixed to a swivel mount such that it could be repositioned without disturbing the camera. The specimen was additionally illuminated by a pair of UV LED ring lights purchased from CCS Inc. that emit at a peak wavelength of 365 nm. The specimen was then heated by a direct current using a Gleeble 1500D shown in Figure 4.1(c), which includes a vacuum chamber to prevent oxidation. The Gleeble chamber also features a window of sufficient size and transparent material through which to take camera-based measurements. More details can be found in references [19].

The speckle pattern recorded by the camera can be described as the superposition of reflected and emitted light. Specifically, at room temperature, the light coming to the camera sensor comes totally from the external light reflected off the surface of the specimen. At high temperature, the specimen emits light in addition to the light supplied from external light sources. However, due to the difference in emissivity of the white paint and the dark graphite background, the intensity of the light emitted from the dark background is brighter than the intensity of the light emitted from the lighter paint pattern. Under the right circumstances, this can result in images at high temperature which appear inverted when compared to images at low temperatures.

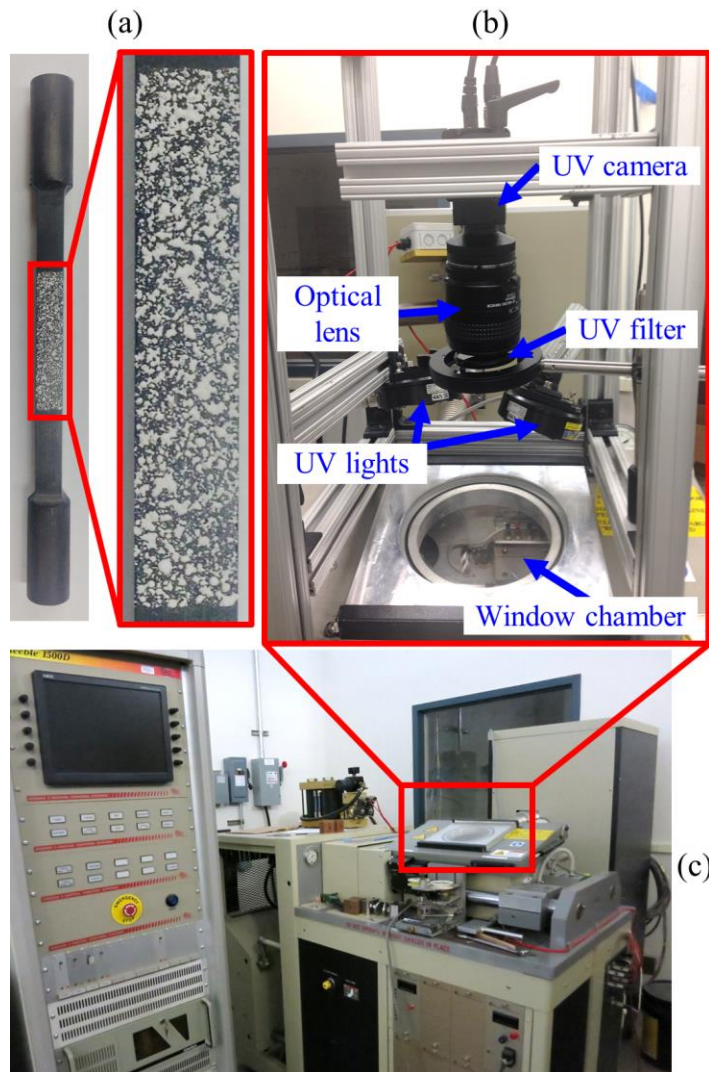


Figure 4.1. (a) Graphite specimen used in the experiments including a magnification of the speckle region (right), (b) a photograph of the experimental setup and related optics and (c) a photograph of the Gleeble 1500D system

To account for the relative contributions of reflected and emitted light, a series of four images were collected as summarized in Table 4.1. First, an image is recorded at room temperature with no externally applied light, producing a uniformly dark image which contains no reflected or emitted light. Second, the external lights are turned on, resulting



in an image composed solely of reflected light. Third, the specimen is heated to a temperature of  $\sim 1100^{\circ}\text{C}$  at which the specimen glows visibly brightly by eye, producing an image which contains both reflected and emitted light. Fourth, the external lights are turned off to produce an image which contains only emitted light. The four images were recorded twice: first with no UV bandpass filter, then with a UV bandpass filter, producing a total of 8 images. The camera settings for all 8 images were as follows: the UV light intensity was set to around 60%, the aperture of the lens was 11, the exposure time of the camera was  $61,000\ \mu\text{s}$  (maximum for this camera model) and the gain was 125.

Table 4.1. Test matrix with an explanation of light coming to the camera sensor

	Low temperature		High temperature		Post-Processing
	Lights Off	Lights On	Lights On	Lights Off	
Test A (No UV bandpass filter)	(A.1) No light	(A.2) Reflected only	(A.3) Reflected + Emitted	(A.4) Emitted only	(A.5) = (A.3) – (A.4) Reflected + Thermal strain
Test B (UV bandpass filter)	(B.1) No light	(B.2) Reflected only	(B.3) Reflected + Emitted (restricted by filter)	(B.4) Emitted only (restricted by filter)	

From the explanation of light sources in Table 4.1, it is recognized that in order to convert high temperature images to an un-inverted state, the emitted light should be

somehow removed from the images while preserving the displacement and strain to be computed from the images. Therefore, to exclude the emitted light but still keep the displacement, the high temperature images with no reflected light (A.4 and B.4) are subtracted from the high temperature images with both reflected and emitted light (A.3 and B.3) to produce new high temperature images that contain only reflected light. The new subtracted images are numbered A.5 and B.5, respectively. However, as the UV filter is very good at eliminating emitted light, B.4 is almost entirely dark, and thus B.5 is indistinguishable from B.3.

Images A.5 and B.3 are then correlated against the reference images A.2 and B.2 in order to compute full-field displacements and strains due to heterogeneous thermal expansion. The correlation is performed using Vic-2D (version 2009) from Correlated Solutions Inc. The subset size was 41x41 pixels, the step size was 19 pixels, and the strain window was 15 subsets. MATLAB was then used for post-processing and comparison purposes.

Although the images in Tests A and B are both recorded by the same test setup viewing the same specimen, the UV bandpass filter in test B has a finite thickness, which causes the field of view in Test B to shift when compared to that in Test A due to the light bending. To assess the agreement between Test A and Test B, the computing procedure presented in Figure 4.2 ensures that both tests use the same region of interest in Vic-2D. In particular, all images are correlated against Image A.2 (i.e. the same reference image for all correlations), Correlated B.2 are then subtracted from Correlated B.3 to get thermal expansion only. With this computation process, results from Test A and Test B are

guaranteed to be plotted in exactly the same coordinates hence making good conditions for comparison of consistency. Results of the subtracted images are subsequently compared to Correlated A.5 to give the agreement of two separate methods.

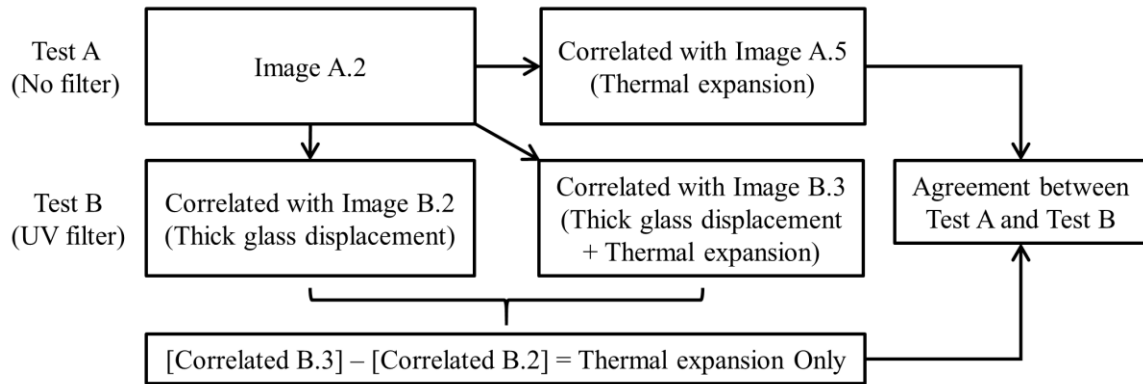


Figure 4.2. Flowchart to map Test A and Test B

#### 4.5. Results

Figure 4.3 shows the speckle images from Test A (No UV bandpass filter) and Test B (UV bandpass filter) as defined in Table 4.1. The images are recorded at low temperature ( $\sim 60^{\circ}\text{C}$ ) and high temperature ( $\sim 1100^{\circ}\text{C}$ ) with conditions of UV external lights on or off, respectively. Images A.1 and B.1 are uniformly dark and are thus omitted from the figure. As can be seen from Figure 4.3, inversion is visibly present in images A.3 and A.4 when there is no UV bandpass filter (Test A) whereas in image B.3, a UV bandpass filter (Test B) visibly eliminates the inversion at high temperature. Although Image A.3 is a superposition of reflected and emitted light, in the case of this test, the emitted light far outweighs the reflected light. Image B.4 is uniformly dark since its light source is only from emitted light which is effectively eliminated by the UV bandpass filter.

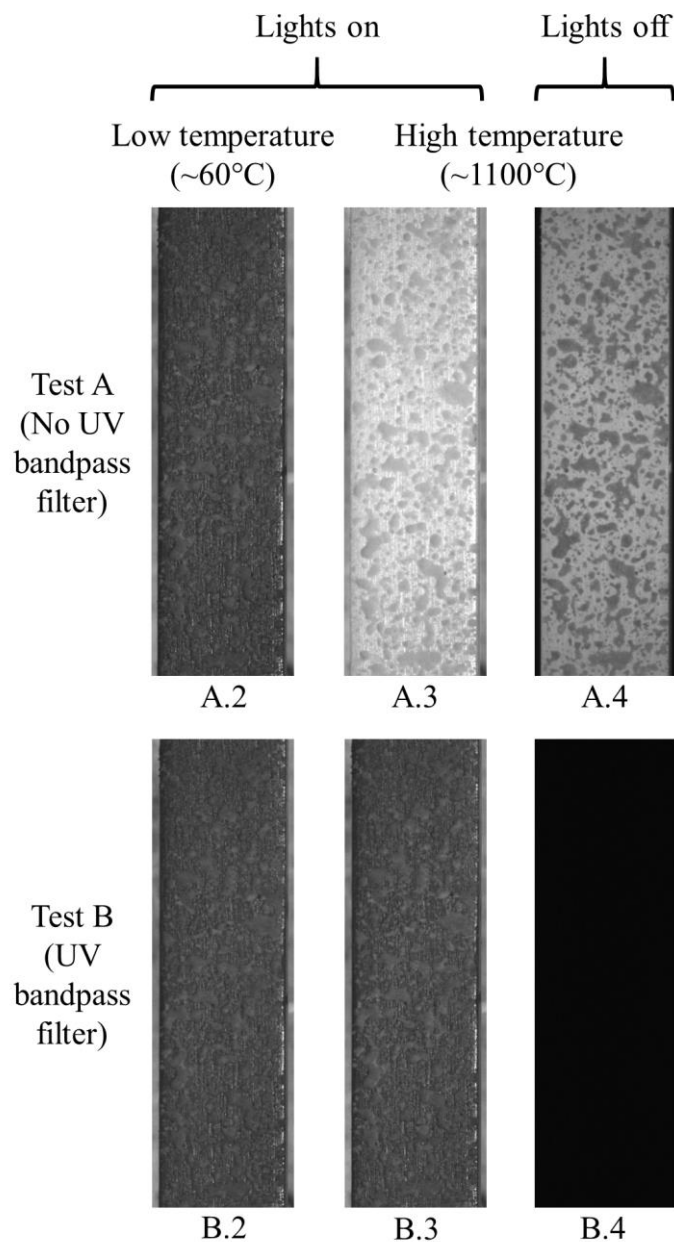


Figure 4.3. Speckle images recorded at low temperature and high temperature when there is no UV filter and a UV filter, respectively. For legibility, the images from test B in this figure have been artificially brightened by multiplying all pixel values by 2, but image B.4 still remains uniformly dark. No artificial brightening was used in DIC calculations

As mentioned in the above Methods section, the speckle inversion is observed to occur when not using a UV filter. In such cases, a method is needed to remove inversion in post-processing. Figure 4.4 presents a method to remove inversion by subtracting images. As shown in the figure, images A.3 and A.4 are at the same temperature and thus show the same deformed state of the specimen, but in A.3 the external lights are turned on while in A.4 the external lights are off. The emitted light is then removed by subtracting A.4 from A.3, resulting in image A.5. Compared to the room temperature image A.2, both A.2 and A.5 get all their light from reflected light but not emitted light, and thereby, image A.5 is able to correlate against image A.2 in order to detect full-field displacement and strain.

Figure 4.5 presents validation of the subtraction method by comparing the two results from Test A and Test B, respectively. The difference is calculated directly (i.e. comparison of subset-by-subset) with the following formula:

$$\text{Difference (\%)} = \frac{|\text{Strain from Test A} - \text{Strain from Test B}|}{\text{Average of Strain from Test A and Strain from Test B}} \quad (4.1)$$

It can be seen that between the two methods, most subsets agree within 10%. The most notable exceptions are near the corners of the region of interest, where strains are computed using fewer subsets [20]. The differences might also be explained by thick glass distortions due to the UV filter.

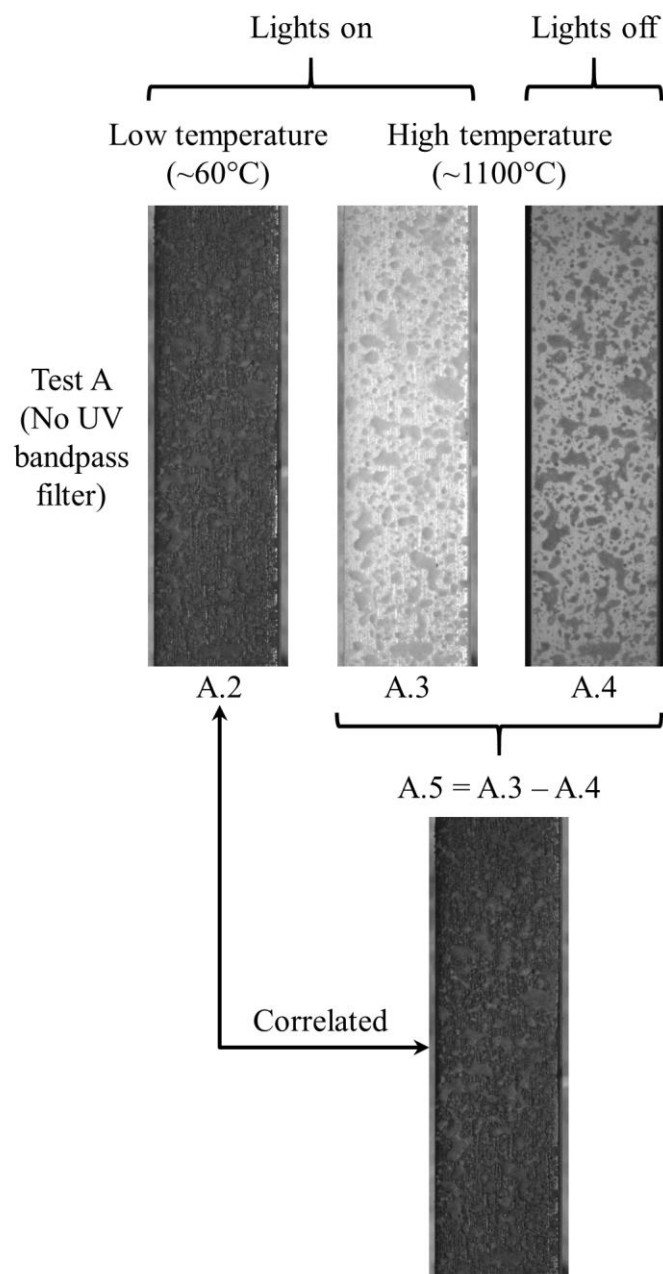


Figure 4.4. Graphical depiction of the subtraction-based method for excluding inversion at high temperature when a UV bandpass filter has not been used

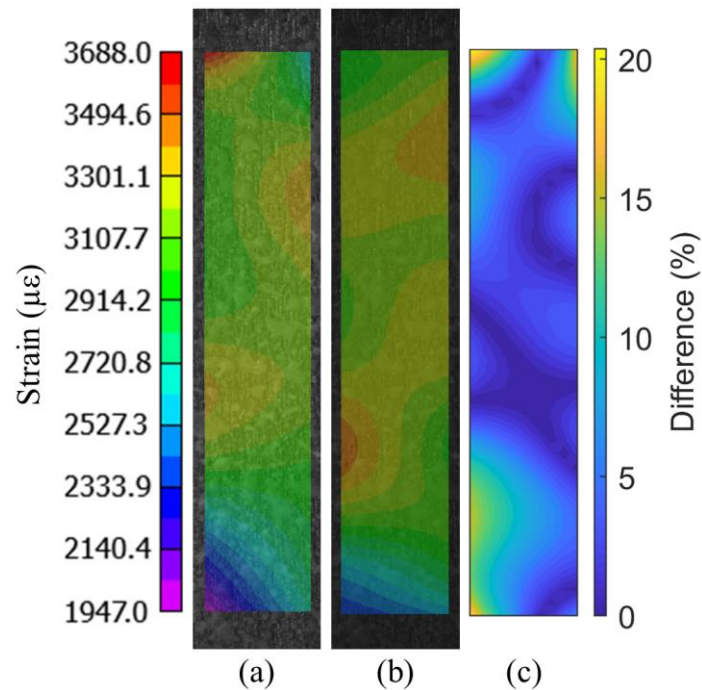


Figure 4.5. Thermal strain map from Vic-2D of Test A (a) and Test B (b) along with its differences (c)

#### 4.6. Discussion

As stated previously, each speckle pattern detected by a camera is a superposition of reflected and emitted light. The reflected speckle pattern depends on the reflectivity of the sample surface while the emitted speckle pattern is affected by emissivity. Given the right combination of materials which compose the dark and light speckles, a material which appears darker at room temperature may emit more light at high temperature and thus produce speckle patterns which are inverted. This is evidenced by images A.2 and A.4, in which all light is either reflected at room temperature or emitted at high temperature, respectively.

It is advised to avoid speckle pattern inversion in high temperature DIC measurements since it confuses the correlation algorithm, thus corrupting the measurement output. Since high temperature testing is often time-consuming and expensive, it is desirable to salvage any data possible after such inversion occurs. One idea to salvage data is to develop a computer algorithm which artificially converts the inverted images back to the un-inverted stage. Archer et al [21] presented one such method based on the known emissivities of their two speckle materials, but this needs to be performed very carefully as it involves the direct manipulation of raw image data. If the emitted light is removed improperly, it can directly corrupt the results by introducing artificial strain into the measurement. The subtraction-based method presented in our study makes no assumptions about the emissivities of the speckle materials, and thus all post-processing is performed from images recorded during the experiment itself. However, this method remains significantly limited because (1) the camera sensitivity must be set sufficiently low so that the combinations of emitted and reflected light (e.g. image A.3) do not saturate the camera sensor, and (2) the subtraction only works in quasi-static cases where there is no motion between the “lights on” and “lights off” images (A.3 and A.4, respectively).

As an alternative to the subtraction method, utilization of a UV bandpass filter is preferable since it can be applied to in-situ experiments without interruption of the test. According to the black body radiation of Planck’s law, it is well known that higher temperature objects emit more powerfully at longer wavelengths. As evidenced by Test B, the inversion is effectively prevented at high temperature by performing the test using cameras and optics which monitor at shorter wavelengths. It remains likely that the



inversion may reassert itself at temperatures high enough to evade the bandpass filter. However, by reducing camera sensitivity (e.g. by reducing the aperture on the lens or the exposure time on the camera) the upper temperature limit of UV-DIC can be effectively extended to higher temperatures [17, 19].

Although UV cameras and filters were used in this paper, in principle this approach should also work with visible cameras and blue filters if the temperature and camera sensitivity are set sufficiently low. The superiority of UV is that it works to higher temperatures [16, 17] thanks to its shorter wavelength compared to blue lights. The advantage to blue is that it can be paired with high speed cameras, which do not tend to inherently detect UV light. Additionally, UV optics is less popular than blue one due to its more hazardous testing condition and the common availability of blue optics devices.

Although temperature is assumed to be a primary factor which produces speckle inversion, there is no one specific temperature at which inversion occurs. The inversion further depends on the specific cameras, lights, optics, and testing conditions. Overall, the speckle pattern inversion is determined by (1) the emissivities of the dark and light speckle materials; (2) the temperature at which light is emitted; (3) the light sensitivity of the camera system (specifically, aperture, exposure time and gain amplification) to detect the emitted pattern; and (4) the relative brightness of the initial reflected pattern.

It is also worth noting that the emitted and reflected speckle patterns were observed to have slightly different focal lengths. Additional results which demonstrate this finding are presented in Figure 4.6 and Figure 4.7.

In Figure 4.6, images are collected using a lens with a larger aperture (i.e. smaller depth of field). The lens is initially focused at room temperature (image (a)), when the speckle pattern results only from reflected light. The specimen is then heated to high temperature to produce image (b) which contains both reflected and emitted light. The external lights are then switched off to produce an image (c) with only emitted light. Images (b) and (c) are both visibly blurry compared to image (a). The lens is then re-focused to produce image (d) which contains only emitted light. The external lights are then switched back on to produce image (e) which contains both emitted and reflected light. The specimen is subsequently cooled back room temperature to produce image (f). Having refocused the lens between images (c) and (d), although image (d) now appears more in-focus compared to image (c), image (f) appears to be less in-focus compared to image (a). This indicates that the emitted and reflected speckle patterns have different focal lengths, which produce blurry image if the focal plane is not within the depth of field.

In Figure 4.7, the same general procedure is repeated with a smaller aperture (i.e. larger depth of field) with the change in brightness offset by a longer exposure time. In this case, the emitted light remains in focus in all images, and thus there is no need to re-focus the lens at high temperature. Thus, when encountering speckle inversion at high temperature, it is critical to ensure that the measurement be performed with a sufficiently large depth of field such that both the reflected and emitted patterns remain in focus.

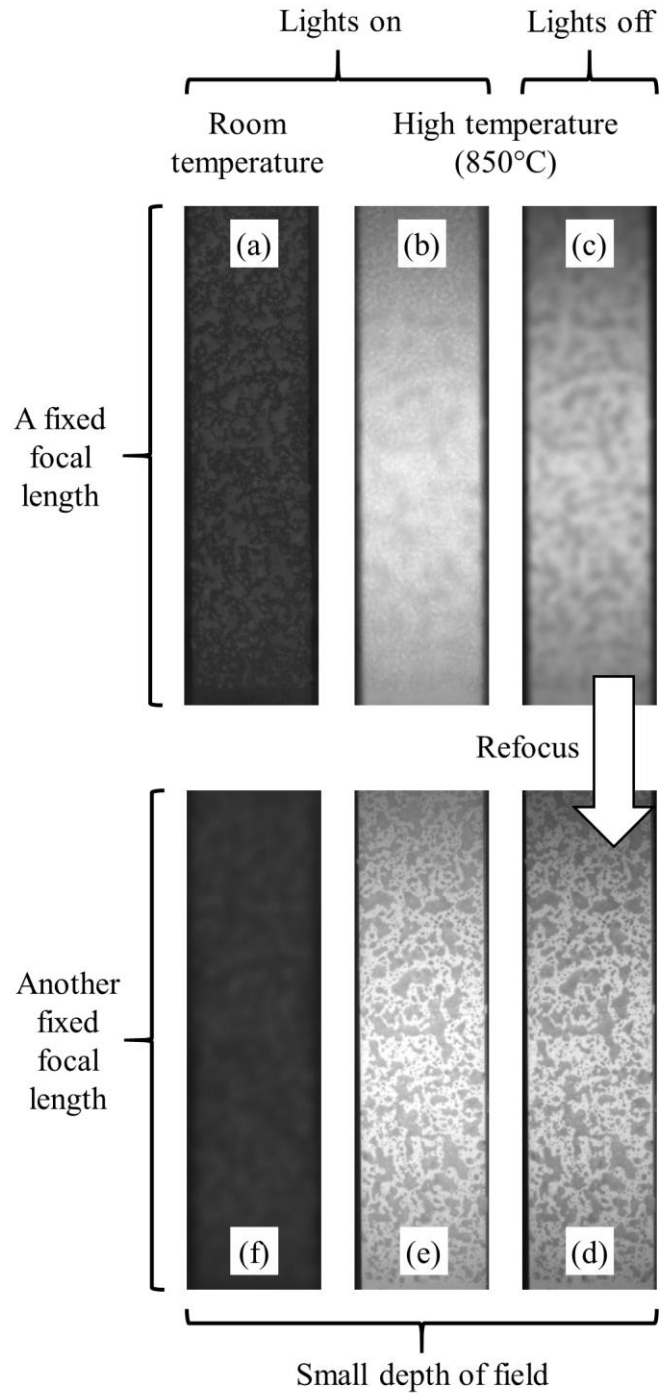


Figure 4.6. Reflected and emitted speckle patterns at low and high temperature under small depth of field. The lens is initially focused based on the reflected pattern (top row), and re-focused based on the emitted pattern (bottom row)

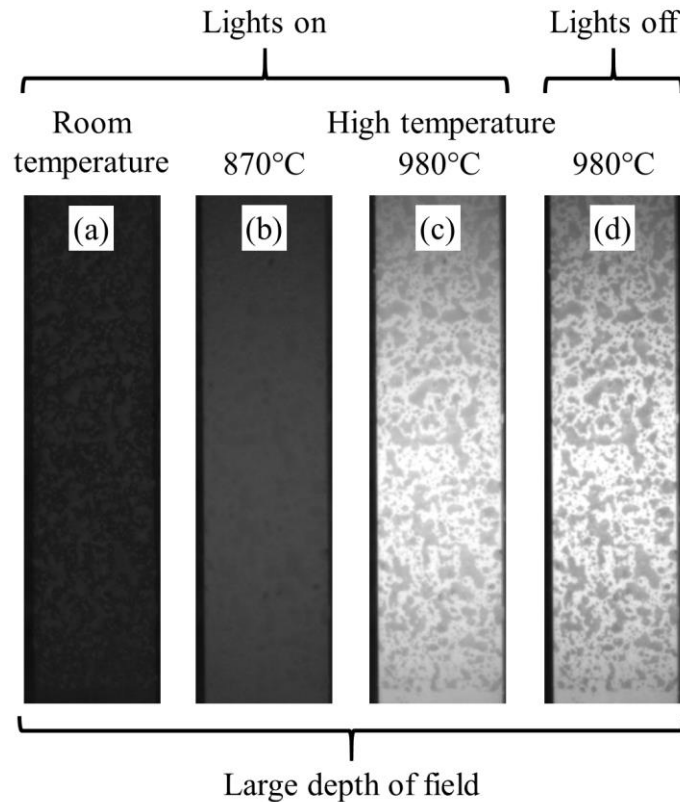


Figure 4.7. Reflected and emitted speckle patterns at low and high temperature under large depth of field. All images are captured in a fixed focal length. Refocus of the lens is not necessary since the difference of focal length is negligible when compared to the large depth of field

#### 4.7. Conclusions

In summary, this study investigated the phenomenon of speckle pattern inversion which is occasionally reported at high temperature. The physical principle behind the inversion comes from the superposition of reflected and emitted light. Under the right circumstances of temperature and camera sensitivity, the inversion occurs when the emitted light is significantly bright in comparison to the reflected light. Additionally, this paper

introduced a method to isolate the reflected speckle pattern at high temperature by subtracting two images with the external lights on and off, respectively, thereby eliminating the emitted light. Having eliminated the emitted light, the reflected speckle pattern at high temperature successfully correlates against the reflected speckle pattern at room temperature. However, there are two limitations of the subtraction-based method as follows: (1) camera sensitivity must be set low enough that the “lights on” image at high temperature can contain a superposition of both the emitted and reflected pattern without saturating; and (2) the subtraction only works in quasi-static cases where no motion occurs between the “lights on” and “lights off” images. For this reason, the best solution to avoid speckle pattern inversion is to prevent the inversion from reaching the camera sensor in the first place, which can be achieved with optical bandpass filters.

#### **4.8. Acknowledgements**

This work was funded by a grant from NASA’s Marshall Space Flight Center (award # 80MSFC18M0009) and by the Utah State University Office of Research and Graduate Studies.

#### **4.9. References**

- [1] Tenney DR, Starke EA, Newman JC, et al (2019) Structural Framework for Flight II: NASA’s Role in Development of Advanced Composite Materials for Aircraft and Space Structures. NASA Langley Research Center, Hampton, VA, United States
- [2] Lacoste M, Lacombe A, Joyez P, et al (2002) Carbon/Carbon extendible Nozzles. *Acta Astronaut* 50:357–367. [https://doi.org/10.1016/S0094-5765\(01\)00178-3](https://doi.org/10.1016/S0094-5765(01)00178-3)

- [3] Potapov A, Shtefan Y, Lichman E (2009) Research of material for uncooled nozzle extensions of liquid rocket engines. *Acta Astronaut* 64:22–27. <https://doi.org/10.1016/j.actaastro.2008.06.016>
- [4] Ajovalasit A (2011) Advances in Strain Gauge Measurement on Composite Materials. *Strain* 47:313–325. <https://doi.org/10.1111/j.1475-1305.2009.00691.x>
- [5] Sutton MA, Orteu JJ, Schreier HW (2009) *Image Correlation for Shape, Motion and Deformation Measurements: Basic Concepts, Theory and Applications*, 1st ed. Springer US
- [6] Pan B, Qian K, Xie H, Asundi A (2009) Two-Dimensional Digital Image Correlation for In-Plane Displacement and Strain Measurement: A Review. *Meas Sci Technol* 20:062001. <https://doi.org/10.1088/0957-0233/20/6/062001>
- [7] Pan B (2018) Digital image correlation for surface deformation measurement: historical developments, recent advances and future goals. *Meas Sci Technol* 29:082001. <https://doi.org/10.1088/1361-6501/aac55b>
- [8] Gradl PR (2016) Digital Image Correlation Techniques Applied to Large Scale Rocket Engine Testing. In: *AIAA Propulsion and Power 2016 Conference*. Salt Lake City, UT, United States
- [9] Mao WG, Chen J, Si MS, et al (2016) High temperature digital image correlation evaluation of in-situ failure mechanism: An experimental framework with application to C/SiC composites. *Mater Sci Eng A* 665:26–34. <https://doi.org/10.1016/j.msea.2016.04.021>
- [10] Gradl PR, Valentine PG (2017) Carbon-Carbon Nozzle Extension Development in Support of In-Space and Upper-Stage Liquid Rocket Engines. In: *53rd Annual AIAA/SAE/ASEE Joint Propulsion Conference 2017*. Atlanta, GA, United States
- [11] Valentine PG, Gradl PR (2019) Extreme-Temperature Carbon- and Ceramic-Matrix Composite Nozzle Extensions for Liquid Rocket Engines. In: *70th International Astronautical Congress*. Washington, DC, United States
- [12] Wang W, Xu C, Jin H, et al (2017) Measurement of high temperature full-field strain up to 2000 °C using digital image correlation. *Meas Sci Technol* 28:035007. <https://doi.org/10.1088/1361-6501/aa56d1>
- [13] Pan Z, Huang S, Su Y, et al (2020) Strain field measurements over 3000 °C using 3D-Digital image correlation. *Opt Lasers Eng* 127:105942. <https://doi.org/10.1016/j.optlaseng.2019.105942>

- [14] Grant BMB, Stone HJ, Withers PJ, Preuss M (2009) High-temperature strain field measurement using digital image correlation. *J Strain Anal Eng Des* 44:263–271. <https://doi.org/10.1243/03093247JSA478>
- [15] Novak MD, Zok FW (2011) High-temperature materials testing with full-field strain measurement: Experimental design and practice. *Rev Sci Instrum* 82:115101. <https://doi.org/10.1063/1.3657835>
- [16] Berke RB, Lambros J (2014) Ultraviolet digital image correlation (UV-DIC) for high temperature applications. *Rev Sci Instrum* 85:045121. <https://doi.org/10.1063/1.4871991>
- [17] Thai TQ, Smith AJ, Rowley RJ, et al (2020) Change of exposure time mid-test in high temperature DIC measurement. *Meas Sci Technol*. <https://doi.org/10.1088/1361-6501/ab7bbf>
- [18] Thai TQ (2018) Importance of Exposure Time on Digital Image Correlation (DIC) at Extreme Temperatures. All Graduate Theses and Dissertations. 7067, Utah State University
- [19] Thai TQ, Hansen RS, Smith AJ, et al (2019) Importance of Exposure Time on DIC Measurement Uncertainty at Extreme Temperatures. *Exp Tech* 43:261–271. <https://doi.org/10.1007/s40799-019-00313-3>
- [20] Simonsen M (2016) Strain Calculation in Vic-3D. *Appl. Notes*
- [21] Archer T, Beauchêne P, Huchette C, Hild F (2019) Global digital image correlation up to very high temperatures with grey level corrections. *Meas Sci Technol* 31:024003. <https://doi.org/10.1088/1361-6501/ab461e>

## CHAPTER 5

### DISCUSSION

This chapter presents a short further discussion about the relationship of  $\Delta$  with respect to exposure time and temperature. The discussion mainly results from my first two papers (Chapter 2 and Chapter 3).

Table 5.1 is an extension of Table 3.2 which includes 1300°C and 1450°C. As can be seen in the first 5 or 6 rows, under fixed temperatures,  $\Delta$  scales linearly with exposure time – for example, at room temperature and an exposure time of 10,000  $\mu\text{s}$ ,  $\Delta = 51$  and if exposure time increases to 20,000  $\mu\text{s}$  (i.e. double) or 30,000  $\mu\text{s}$  (i.e. triple)  $\Delta$  is scaled linearly to 100 and 149, respectively.

The table also shows that for a given exposure time,  $Z_1$  and  $Z_2$  shift rightward as temperature increases (i.e. the histogram shifts rightward too), such that  $\Delta$  remains constant with respect to temperature for a given exposure time. This result is valid as long as  $Z_2$  is lower than 255 (i.e. there is no occurrence of saturation). For example, at a fixed exposure time of 10,000  $\mu\text{s}$ ,  $\Delta$  is 51, 51, 49 and 50 corresponding to RT, 1300°C, 1450°C and 1600°C respectively.  $Z_1$  and  $Z_2$  in these cases increase gradually to keep  $\Delta$  unchanged.

Based on the relationship of  $\Delta$  with respect to exposure time and temperature, it is concluded that we can get a rough prediction of  $\Delta$  in absence of saturation (i.e. if camera sensors could detect  $Z_2 > 255$ ). In other words, we can predict and have initial assessment of histogram if saturation is assumed to not occur when we have camera with higher dynamic range. For example, at exposure time of 30,000  $\mu\text{s}$  and room temperature,  $\Delta = 149$ . The camera used in this dissertation is 8-bit monochromatic which has limit of 255 counts.



For this reason, if we increase exposure time to 40,000  $\mu\text{s}$  at room temperature,  $\Delta = 124$  as shown in Table 5.1. If we use a high dynamic range camera (e.g. 10-bit with the limit of 1023 counts),  $\Delta$  is expected to be  $149 \cdot 40000 / 30000 = 199$ . At 1600°C,  $\Delta$  is expected to be the same which is approximately 199, not 65 as 8-bit camera in this case.

Table 5.1.  $\Delta$  calculation of RT, 1300°C, 1450°C and 1600°C at multiple exposure times

Exposure time ( $\mu\text{s}$ )	Room temperature			1300°C			1450°C			1600°C		
	Z <sub>1</sub>	Z <sub>2</sub>	$\Delta$	Z <sub>1</sub>	Z <sub>2</sub>	$\Delta$	Z <sub>1</sub>	Z <sub>2</sub>	$\Delta$	Z <sub>1</sub>	Z <sub>2</sub>	$\Delta$
500	8	12	4	8	12	4	9	12	3	9	12	3
2,500	15	28	13	15	28	13	16	29	13	19	31	12
5,000	23	49	26	22	49	27	26	51	25	30	55	25
10,000	38	89	51	38	89	51	44	93	49	53	103	50
20,000	70	170	100	68	170	102	81	178	97	99	196	97
30,000	100	249	149	98	249	151	117	255	138	144	255	111
40,000	131	255	124	128	255	127	154	255	101	190	255	65
45,000	146	255	109	143	255	112	172	255	83	213	255	42
50,000	161	255	94	158	255	97	191	255	64	236	255	19
55,000	176	255	79	173	255	82	209	255	46	255	255	0
58,000	185	255	70	182	255	73	221	255	34	255	255	0
61,000	194	255	61	191	255	64	232	255	23	255	255	0

## CHAPTER 6

### CONCLUSIONS

In summary, this dissertation introduced a comprehensive and robust analysis of UV-DIC which facilitates DIC measurement at high temperature. With the contributions stated explicitly via a series of three journal articles, the UV-DIC technique is going to expand the application and robustness when performing DIC at extreme temperatures. Through my first two papers (Chapter 2 and Chapter 3), a simple and convenient metric was presented to help DIC users choose appropriate camera settings not only at the start of the test but also during mid-test. In brief, the metric of  $\Delta$  calculates the difference in the median 90% thresholds of the histogram. If  $\Delta > 50$ , it is considered as a good contrast since it covers most part of greyscale histogram which is likely to provide enough information for correlation. The metric was validated in both pre-testing conditions and on-going testing. That metric along with useful recommendations are expected to give DIC users more insights regarding the experimental setup of DIC measurement.

My third paper (i.e. Chapter 4) explained explicitly the physical principles behind the speckle inversion. Based on the principle, the paper showed an optical method which used the UV bandpass filter to evade or at least delay the inversion when performing DIC at high temperature. That paper also offered an alternative solution to modify the experimental setup in situations we have inversion data thereby excluding the inversion and obtaining a meaningful measurement.

Furthermore, all results from the dissertation have been presented through oral presentations or poster sessions in annual conferences of Society for Experimental

Mechanics (SEM) and American Society of Mechanical Engineers (ASME). Several posters have been presented during student events at Utah State University.

Based on my conclusions, I foresee three primary areas for future work:

1. The experimental mechanics community has demonstrated DIC across many temperature, time, and length scales, but so far UV-DIC has only been demonstrated at relatively slow speeds. Most high speed cameras are designed only to detect visible light, but our lab recently purchased UV amplifiers which effectively extend high speed imaging to UV wavelengths. This high speed UV-DIC is currently being investigated by my labmate, Robert Rowley, who expects to publish his findings to *Review of Scientific Instruments* with me as a co-author.

2. To extend UV-DIC capabilities to temperatures beyond 2000°C, it is especially challenging to develop new speckle patterns which can survive the harsh testing environment. All commercial refractory paints are reported to be discolored and damaged at that temperature. For this reason, it is required to develop a novel high temperature speckle pattern which is stable beyond 2000°C. An initial idea is to use a native speckle pattern produced via the surface roughness of the test specimen, which is assumed to work up to the melting point of the material.

3. For the inversion of speckle pattern, one of drawbacks of the subtraction method is that the method does not work if the object moves in between images when external lights are turned on and off. Accordingly, it is preferable to acquire both images at the same time. An initial idea is to use a color camera with a blue light source. The red and green sensors would detect minimal reflected pattern in comparison with the blue. Since the

emitted pattern is brighter at longer wavelengths, the red and green images would detect a brighter emitted speckle than the blue. An extrapolation scheme is needed to reproduce the blue image using only data from the red and green images. Thanks to that, we can produce a blue reflected image with no time in between.

## CURRICULUM VITAE

Thinh Quang Thai

(Last Updated March 2020)

**EDUCATION**

---

- **Ph.D. in Mechanical Engineering** 2016 - 2020  
Utah State University, Logan, Utah, USA
- **M.S. in Mechanical Engineering** 2016 - 2018  
Utah State University, Logan, Utah, USA
- **B.S. in Aerospace Engineering** 2010 - 2015  
Ho Chi Minh City University of Technology, Vietnam

**HONORS AND AWARDS**

---

1. **Outstanding Doctoral Graduate Scholar of the Year**, Mechanical & Aerospace Engineering, Utah State University, 2020
2. **The First Annual Paper Competition for Experimental Mechanics**, Finalist, ASME-IMECE 2019
3. **Michael Sutton International Student Paper Competition**, Finalist, SEM 2019
4. **Outstanding Master Student Researcher of the Year**, Mechanical & Aerospace Engineering, Utah State University, 2019
5. **PhD Student Travel Grant**, College of Engineering, Utah State University, 2018
6. **RGS Graduate Student Travel Award**, Utah State University, 2018
7. **RGS Graduate Research Assistantship**, Utah State University, 2016-2019

8. **University's Gold Medal**, Ho Chi Minh City University of Technology, 2015
9. **Department's Outstanding Student Award**, Ho Chi Minh City University of Technology, 2015
10. **Faculty Dean's Award** for the outstanding ranking, Ho Chi Minh City University of Technology, 2015
11. **Outstanding Student Scholarships** (i.e., Kanden-SS, Vallet, Safran, Holcim Talent, TIS Kitagawa & Lawrence S. Ting), 2012-2015
12. **Comprehensively Outstanding Student Award**, Ho Chi Minh City University of Technology, 2013-2014 academic year
13. **Faculty's Outstanding Student Award**, Ho Chi Minh City University of Technology, 2011-2012, 2012-2013 & 2013-2014 academic years
14. **Five-Strong Student Award**, Ho Chi Minh City University of Technology, 2012-2013 & 2013-14 academic years
15. **Third team place** in the 24<sup>th</sup> National Mechanics Olympiad, Vietnam, 2012
16. **Comprehensive Student Award**, Ho Chi Minh City University of Technology, 2010-2011 & 2012-2013 academic years

## **RESEARCH EXPERIENCE**

---

Graduate Research Assistant, Utah State University

2016 - 2020

- Heterogeneous Strain Measurement during Hot-Fire Testing of Carbon-Carbon Rocket Nozzles
- Materials Characterization at Extreme Temperatures for Advanced Aerospace Applications

## TEACHING EXPERIENCE

---

Graduate Teaching Assistant, Utah State University

- MAE 3040: Mechanics of Solids Fall 2016 & Fall 2017
- MAE 2165: Material Science Laboratory Spring 2017

## JOURNAL PUBLICATIONS

---

1. **T.Q. Thai**, J. Ruesch, P.R. Gradl, T.T. Truscott, R.B. Berke, “Speckle Pattern Inversion in High Temperature DIC Measurement,” (In preparation).
2. **T.Q. Thai**, A.J. Smith, R.J. Rowley, P.R. Gradl, R.B. Berke, “Change of Exposure Time Mid-Test in High Temperature DIC Measurement,” *Measurement Science and Technology* (2020). (Accepted, In press)
3. **T.Q. Thai**, R.S. Hansen, A.J. Smith, J. Lambros, R.B. Berke, “Importance of Exposure Time on DIC Measurement Uncertainty at Extreme Temperatures,” *Experimental Techniques*, **43**(3), pp. 261-271 (2019).
4. H.A. Ly, **T. Thai-Quang**, “Behavior of Sandwich Tubular-Hat Sections with Aluminum Foam Filler Subjected to Low Velocity Impact Load,” *Journal of Engineering and Technological Sciences*, **49**(1), pp. 144-162 (2017).
5. H.A. Ly, **T. Thai-Quang**, “Numerical Investigation of Circular and Square Tubes Subjected to Low Velocity Impact Load,” *International Journal of Mechanical Engineering and Applications*, **3**(1-3), pp. 54-62 (2015).
6. H.A. Ly, H.H. Nguyen, **T. Thai-Quang**, “Geometrical Optimization of Top-Hat Structure Subject to Axial Low Velocity Impact Load Using Numerical Simulation,”

*International Journal of Mechanical Engineering and Applications*, **3**(3-1), pp. 40-48 (2015).

7. H.A. Ly, V.N.V. Nguyen, **T. Thai-Quang**, H.H. Nguyen, “Structural Analysis of Sandwich Thin-Walled Hollow Cylindrical Tubes with Aluminum Foam Filler Subjected to Low Velocity Axial Load Using Numerical Simulation,” *ASEAN Engineering Journal Part A*, **5**(2), pp. 17-27 (2015).

#### **CONFERENCE PUBLICATIONS**

---

1. **T. Thai-Quang**, H.H. Nguyen, H.A. Ly, “Behavior of sandwich tubular-hat sections with aluminum foam filler subjected to low velocity impact load,” *Proceedings of the 3<sup>rd</sup> Symposium on Transportation Engineering for Young Scientists*, Faculty of Transportation Engineering, Ho Chi Minh City University of Technology, pp. 44-53. (May 2015)
2. H.A. Ly, V.N.V. Nguyen, **T. Thai-Quang**, H.H. Nguyen, “Structural analysis of sandwich thin-walled hollow cylindrical tubes with aluminum foam filler subjected to low velocity axial load using numerical simulation,” *The 7<sup>th</sup> AUN/SEED-Net Regional Conference in Mechanical and Manufacturing Engineering*, pp. 358-362, Hanoi, Vietnam. (Oct. 2014)

#### **CONFERENCE ABSTRACTS / PRESENTATIONS**

---

1. **T.Q. Thai**, J. Ruesch, P.R. Gradl, T.T. Truscott, R.B. Berke, “Competition of Reflected and Emitted Light in High Temperature DIC Measurement,” *ASME International Mechanical Engineering Congress & Exposition*, Salt Lake City, UT, Nov. 2019.



2. A.J. Smith, R.S. Hansen, **T.Q. Thai**, R.B. Berke, “Characterizing the Impact of Phase-Angle on Thermo-Mechanical Fatigue Behavior,” *ASME International Mechanical Engineering Congress & Exposition*, Salt Lake City, UT, Nov. 2019.
3. A.J. Smith, R.S. Hansen, **T.Q. Thai**, R.B. Berke, “The Effect of Phase-Lag on Materials Undergoing Thermo-Mechanical Fatigue,” *SEM Annual Conference and Exposition on Experimental and Applied Mechanics*, Reno, NV, June 2019.
4. **T.Q. Thai**, A.J. Smith, A. Dabb, R.B. Berke, “How Alteration of Exposure Time Mid-Test affects UV-DIC at Extreme Temperatures,” *SEM Annual Conference and Exposition on Experimental and Applied Mechanics*, Reno, NV, June 2019.
5. **T.Q. Thai**, “The Significance of Exposure Time in High Temperature DIC Measurements,” *SEM Annual Conference and Exposition on Experimental and Applied Mechanics*, Reno, NV, June 2019.
6. **T.Q. Thai**, R.S. Hansen, A.J. Smith, P.R. Gradl, R.B. Berke, “Effect of Exposure Time on Ultraviolet DIC at Extreme Temperatures,” *ASME International Mechanical Engineering Congress & Exposition*, Pittsburgh, PA, Nov. 2018.
7. **T.Q. Thai**, A.J. Smith, A. Dabb, R.B. Berke, “Speckle Pattern Inversion in DIC at Extreme Temperatures,” *SEM Annual Conference and Exposition on Experimental and Applied Mechanics*, Greenville, SC, June 2018.
8. **T.Q. Thai**, A. Ding, J. Lambros, R.B. Berke, “Full-Field Strain Measurements up to 1700°C with Ultraviolet Digital Image Correlation,” *SEM Annual Conference and Exposition on Experimental and Applied Mechanics*, Indianapolis, IN, June 2017.

9. **T.Q. Thai**, E.K. Nickerson, R.B. Berke, "Full-Field Thermal Strain Measurements on Graphite at Extreme Temperatures," *ASME International Mechanical Engineering Congress & Exposition*, Phoenix, AZ, Nov. 2016.
10. **T.Q. Thai**, E.K. Nickerson, R.B. Berke, "Measuring Full-Field Strains on Graphite in Extreme Temperatures using Ultraviolet Digital Image Correlation (UV-DIC)," *SEM Annual Conference and Exposition on Experimental and Applied Mechanics*, Orlando, FL, June 2016.

#### **POSTER SESSIONS**

---

1. **T.Q. Thai**, A.J. Smith, R.S. Hansen, R.J. Rowley, R.B. Berke, "Set-Up of Camera Sensitivity in Non-Contacting Full-Field Strain Measurement up to 1600°C," *ASME International Mechanical Engineering Congress & Exposition*, Salt Lake City, UT, Nov. 2019.
2. **T.Q. Thai**, A.J. Smith, R.S. Hansen, R.J. Rowley, R.B. Berke, "Selection of Camera Sensitivity in High Temperature Optical Strain Measurement," *USU College of Engineering Research Week*, Logan, UT, Apr. 2019.